Thesis for the degree of Doctor of Philosophy

INVESTIGATIONS OF PLASMA-ENHANCED CVD GROWTH OF CARBON NANOTUBES AND POTENTIAL APPLICATIONS

MARTIN JÖNSSON

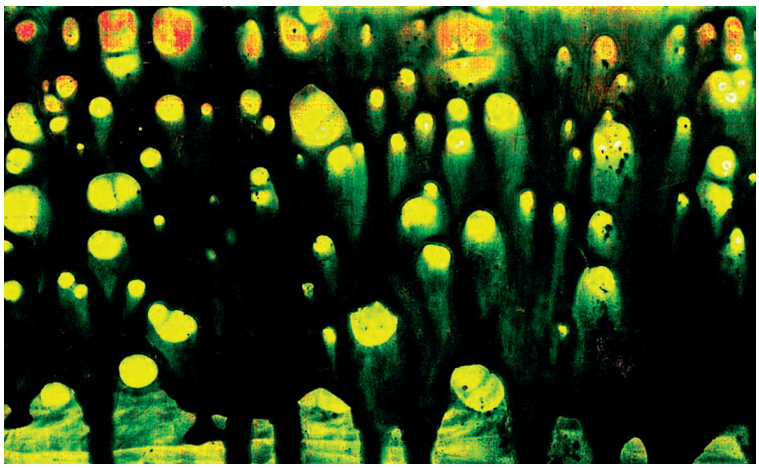

GÖTEBORG UNIVERSITY

Department of Physics

Göteborg 2007

Investigations of plasma-enhanced CVD growth of carbon nanotubes and potential applications

ISBN: 978-91-628-7082-9

Atomic Physics
Department of Physics
Göteborg Univeristy
SE-412 96 Göteborg
Sweden

Typeset using LaTeX.

Cover: Detail from the painting “It looks so exactly” by Bogdan Chorążuk. Used with kind permission of the artist.

Chalmers reproservice
Göteborg, Sweden 2007

INVESTIGATIONS OF PLASMA-ENHANCED CVD GROWTH OF CARBON NANOTUBES AND POTENTIAL APPLICATIONS

Martin Jönsson
Atomic Physics
Department of Physics
Göteborg University
SE–412 96 Göteborg, Sweden

Abstract

Carbon nanotubes and nanofibres are promising materials for many different applications. Their interesting electrical, thermal and mechanical properties have been attracting attention for their use in electronic circuits, thermal handling and as components in composites.

One method of producing carbon nanotubes is plasma-enhanced chemical vapour deposition (PE-CVD). This method allows control of length and position of vertically aligned carbon nanofibres (VACNFs), as well as the growth of forests of aligned multi-walled carbon nanotubes (MWCNTs). We have investigated PE-CVD growth of both VACNFs and MWCNT to elucidate what parameters are important in the control of the growth and to optimise the growth conditions. Optical emission spectroscopy was used to monitor the plasma composition *in situ*. It was found that the growth of CNTs and CNFs was strongly affected by the amount of atomic hydrogen in the plasma. Laser reflection was also used for *in situ* monitoring of the growth speed and the deposition of amorphous carbon on top of the MWCNT forests.

Investigations of some applications of the grown tubes and fibres are also presented. Emission spectroscopy was used to investigate light emission from carbon nanotubes used as electron field emitters. We also examined the possibility of using carbon nanotubes in microfluidic coolers. VACNFs embedded in a polystyrene membrane showed promising results as an anisotropic electric conductor.

Keywords: Carbon nanotubes, vertically aligned carbon nanofibres, plasma-enhanced CVD, optical emission spectroscopy.

Sammanfattning

Kolnanorör är lovande material för en rad olika tillämpningar. Tack vare sina intressanta elektroniska, termiska och mekaniska egenskaper är de attraktiva t ex som komponenter i elektroniska kretsar, inom värmeöverföring och som del i olika kompositmaterial.

En metod för tillverkning av kolnanorör är kemisk ångdeposition med hjälp av plasma (PE-CVD). Det är en metod som ger god kontroll över såväl position som längd vid växt av vertikala kolnanofibrer (VACNF) och som möjliggör växt av skogar av flerväggiga kolnanorör (MWCNT). I den här avhandlingen har vi studerat PE-CVD för att ta reda på vilka parametrar som är viktiga vid växt av kolnanorör och -fibrer och för att optimera tillverkningen av dessa. Optisk emissionsspektroskopi användes för att undersöka plasmats sammansättning *in situ*. Vi fann att mängden atomärt väte i plasmat starkt påverkade växten av MWCNT och VACNF. Laserreflektion användes för att mäta växthastigheten *in situ* och tillväxten av amorft kol ovanpå MWCNT-skogarna.

Även undersökningar av en del applikationer av de växta nanotuberna och -fibrerna presenteras. Emissionspektroskopi användes för att undersöka ljusemission från kolnanorör som används som fältemissionsspetsar. Vi har också tittat på möjligheten att använda kolnanorör i mikrofluidkylare. VACNF inbäddade i en polystyrenfilm visar lovande resultat som anisotrop elektrisk ledare.

Preface

This thesis is a summary of the work I've done during the last two years in the field of carbon nanotubes. Two years do not make a full PhD term, so this thesis is best enjoyed in the company of my licentiate thesis from 2005 about endohedral fullerenes [1].

The layout of this thesis is such that after a general introduction, a background chapter will provide an overview of the properties of carbon nanotubes. This is intended to serve as a short introduction to the field of nanotubes for the uninitiated, as well as placing the current work in perspective. The main equipment used for the thesis work will be presented in chapter 3. In chapter 4 a short introduction to plasmas will be given, needed for some understanding of the vibrational temperature measurements. Chapter 6 and 7 are the most important part of the thesis as they contain the results and a discussion about these. Those who feel they want to skip directly to the acknowledgements will find them on page 73.

Appended Papers

This thesis is partly based on work reported in the following papers, referred to by Roman numerals in the text:

I. M. Jönsson, O. A. Nerushev, and E. E. B. Campbell, "DC plasma-enhanced chemical vapour deposition growth of carbon nanotubes and nanofibres: *in situ* spectroscopy and plasma current density dependence" Submitted to Applied Physics A.

II. M. Jönsson, O. A. Nerushev, and E. E. B. Campbell, "*In situ* growth rate measurements during plasma enhanced chemical vapour deposition of vertically aligned multiwall carbon nanotube films" Submitted to Nanotechnology.

III. M. Sveningsson, M. Jönsson, O. A. Nerushev, F. Rohmund, and E. E. B. Campbell, "Blackbody Radiation from Resistively Heated Multi-Walled Carbon Nanotubes During Field Emission", Appl. Phys. Lett. **81**, pp. 1095-1097, 2002.

IV. T. Wang, M. Jönsson, E. Nyström, Z. Mo, E. E. B. Campbell, and J. Liu, "Development and Characterization of Microcoolers using Carbon Nanotubes," in Proceedings of the 1st IEEE CPMT Electronics Systemintegration Technology Conference (ESTC2006), **8**, pp. 881-885, 2006.

These papers are printed in the Appendix.

The following scientific publications are not included in the thesis:

- O. A. Nerushev, R.-E. Morjan, D. I. Ostrovskii, M. Sveningsson, M. Jönsson, F. Rohmund, and E. E. B Campbell, "The temperature dependence of Fe-catalysed growth of carbon nanotubes on silicon substrates", Physica B **323**, pp. 51-59, 2002.
- A. Lassesson, A. Gromov, M. Jönsson, A. Taninaka, H. Shinohara, and E. E. B. Campbell, "Oxygen reactivity of La@C_{82} investigated with laser desorption mass spectrometry", Int. J. Mass Spectrom., **228**, pp. 913–920, 2003.

- A. Gromov, D. Ostrovskii, A. Lassesson, M. Jönsson, and E. E. B. Campbell, "Fourier Transform Infrared and Raman Spectroscopic Study of Chromatographically Isolated Li@C_{60} and Li@C_{70}", J. Phys. Chem. B, **107**, 2003, pp. 11290–11301.

- V. N. Popok, I. I. Azarko, A. V. Gromov, M. Jönsson, A. Lassesson, and E. E. B. Campbell, "Conductance and EPR study of endohedral fullerene Li@C_{60}", Solid State Commun., **133**, pp. 499–503, 2005.

- A. Lassesson, K. Hansen, M. Jönsson, A. Gromov, E. E. B. Campbell, M. Boyle, D. Pop, C. P. Schulz, I. V. Hertel, A. Taninaka, and H. Shinohara, "A femtosecond laser study of the endohedral fullerenes Li@$C_{60}$and La@C_{82}", Eur. Phys. J. D, **34**, pp. 205-209, 2005.

- T. Wang, M. Jönsson, E. E. B. Campbell, and J. Liu, "Development of Carbon Nanotube Bumps for Ultra Fine Pitch Flip Chip Interconnection," in Proceedings of the 1st IEEE CPMT Electronics Systemintegration Technology Conference (ESTC2006), **8**, pp. 881–885, 2006.

- V. N. Popok, M. Jönsson, and E. E. B. Campbell, "Conductance and polarisability of C_{60} films", J. Nanosci. Nanotechn., (in press).

Contents

Preface **v**

Contents **ix**

1 Introduction **1**

2 Background **5**
2.1 History of carbon nanotubes 5
2.2 Structure of carbon nanotubes 6
2.3 Properties of carbon nanotubes 9
2.4 Growth of carbon nanotubes 11

3 Equipment for nanotube production **17**
3.1 PE-CVD for nanotube/nanofibre growth 17
3.2 Thermal CVD for nanotube growth 20
3.3 Preparation of the substrates 22
3.4 Characterisation of grown tubes 22
3.5 Spectroscopy during electron field emission 23
3.6 Raman spectrometry of CNTs 23

4 Plasma **27**
4.1 Glow discharge plasma 28
4.2 Vibrational temperature and the sum rule 31

5 Experimental procedures **37**
5.1 T-CVD growth of MWCNT 37
5.2 PE-CVD growth of nanotubes and nanofibres 38
5.3 Spectroscopy during field emission 43

6 Results and discussion **45**
6.1 Optical emission spectroscopy 45
6.2 *In situ* growth rate measurements 55
6.3 Blackbody radiation from MWCNTs during field emission 60

7 Nanotubes for applications **65**
7.1 Using MWCNTs as microcoolers 65
7.2 Anisotropic conduction in nanofibre composites 67

8 Conclusions and outlook **71**

Acknowledgements **73**

Bibliography **75**

1

Introduction

"Nano" has become the catch phrase of the century. In terms such as nanoscience and nanotechnology it embodies our hopes for the technology of the future that will bring us faster computers, new materials, cures for diseases and so on. Addressing issues like mass-production and commercialisation as well as people's concern [2–5], e.g. for our health and the environment, and downright fear [6], will promise to make nanotechnology no more mysterious tomorrow than the microprocessors of today. The proverbial man on the street talks freely about Gigahertz, RAM and ROM without bothering about all the "micro" on the inside. On the other hand, the word nano printed on your tennis racket is enough to double its price. All the interest and the money invested in the field is causing the nanotechnology community to grow with mindnumbing speed. The number of articles with the word "nano" has been doubling roughly every 4 years since 1990, see figure 1.1. A search on Google for the word "nanotechnology" gives 15.4 million[1] hits [7].

At the centre of much of this attention is the carbon nanotube (CNT). A remarkable molecule made all of carbon, a thin tube, sometimes a million times longer than its diameter, described as "stronger than steel", yet light-weight and ductile. It's one of only a handful of carbon allotropes, i.e. forms of pure carbon, as shown in figure 1.2. Carbon itself is arguably the most studied element of all. More than

[1] Up from 14.5 million on the same search in the beginning of Dec. 2006.

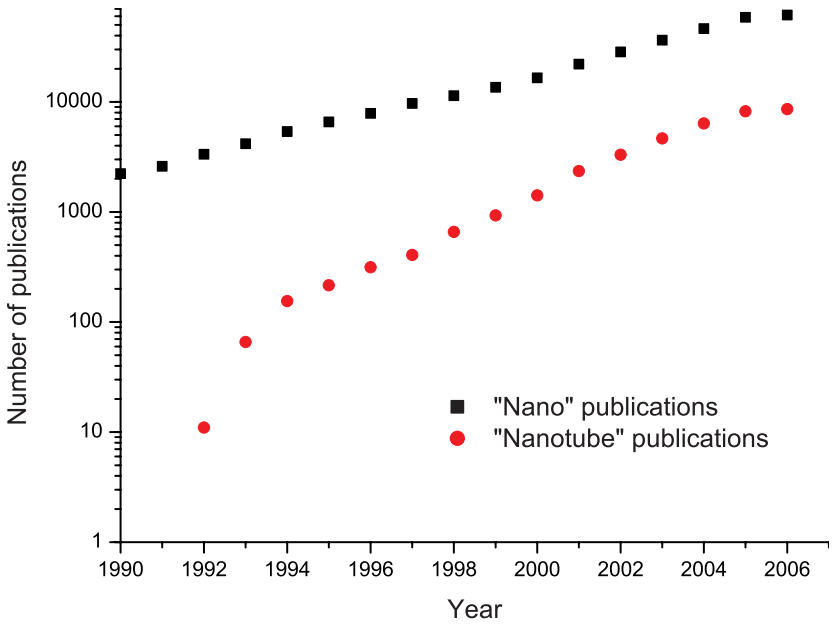

Figure 1.1: Number of articles found in CAS using the search words “nano” and “nanotube”. Sorted according to year of publication.

6.5 million carbon-containing chemical compounds are known, since it’s essential for life as we know it and one of the most abundant elements in the universe, everyone from astronomers to biologists are studying carbon. But until recently only two forms of pure crystalline carbon were known, the greyish graphite and the dazzling diamond. That all changed in 1985 when Kroto, Curl and Smalley tuned their apparatus, used for studying the formation of long carbon chains in stars, to find a molecule consisting of 60 carbon atoms beautifully arranged like on the vertices of the seams of a normal football [9]. The molecule was named the Buckminsterfullerene after the American architect, inventor and author R. Buckminster Fuller. The fullerenes, and especially C_{60}, were quickly adopted as the physicists’ pet molecule. The theoreticians loved it because of the remarkable symmetry, the experimentalists for its stability, versatility and that enticing hollow space where “stuff” could be hidden [10]. This was the material of the future! So far not much has come out of all the lofty speculations. However, the fullerenes are still ranked among the most interesting topics in physics [11] and fullerene derivatives are still drawing attention, especially in the field of plastic photovoltaic cells [12]. When it comes to that futuristic material that carries the great hope of nanotechnology, the torch has been passed on to the carbon nanotube. The research in nanotubes is exploding, as can be seen from the yearly number of publications in figure 1.1. In

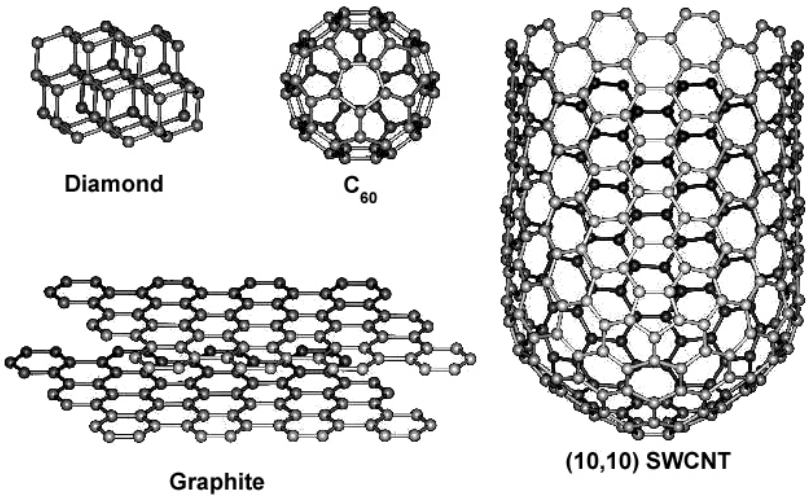

Figure 1.2: A schematic picture of the known crystalline forms of carbon. The family of fullerenes is represented by the C_{60} and the nanotubes by a (10,10) single walled CNT. Picture adapted from [8].

the Nature article about hot topics in physics [11], nanotubes top the list and are described thusly

> Super-strong materials and blisteringly fast electronic circuits: the potential applications of these tiny carbon tubes [. . .] are so enticing that everyone is pouring money into the field.

However, whether the nanotube passes the test and fulfills the hopes pinned on it, or stays an interesting compound with few applications like so many predecessors, remains to be seen. In the next chapter carbon nanotubes, their properties and how they are produced will be covered in some detail.

2

Background

As was mentioned in the previous chapter, the carbon nanotube is a material of pure carbon. The tubes come in two main flavours, with a single carbon wall, as depicted in figure 1.2, or with many single-walled tubes stacked within each other in a Russian doll fashion. In this chapter some of the properties of carbon nanotubes will be described, along with a few potential applications. It should also serve as an attempt to put the present work into context. For more about the general properties of CNTs and their potential applications the book "Carbon nanotubes: Science and applications" [13] is recommended.

2.1 History of carbon nanotubes

The history of carbon nanotubes is a complex story. It could have started already in 1952 when Radushkevich and Lukyanovich published transmission electron microscope (TEM) images of $\sim 50\,\mathrm{nm}$ tubes of carbon in the Russian Journal of Chemical Physics [14]. However, no one, including the authors, seem to have realised the importance of the find so the paper, written in Russian in a journal not easily accessible outside the Soviet Union, went unnoticed. A lot of work continued to be done in the field that was not yet called carbon nanotubes. Another shot for fame came in 1976 with a paper by Oberlin *et al.* [15] showing clear TEM

images of what might be the first single-walled, or at least few-walled, nanotubes. But alas, also this time the hype did not come off. What was to be the real breakthrough came in 1985 with the already mentioned discovery of the fullerenes [9] that lead to the Nobel prize being awarded to Kroto, Curl and Smalley in 1996 and a lot of interest in the new field of nano-carbon materials. A patent for the production of "carbon fibrils with a constant diameter [...] an outer region of multiple essentially continuous layers of ordered carbon atoms and a distinct inner core" was issued to Howard G. Tennent of Hyperion Catalysis International, Inc. in 1987 [16]. Still, large scale production of neither fullerenes, nor nanotubes was possible. In 1990 Krätschmer *et al.* managed to build a machine that, by burning graphite rods by an electric discharge in a helium atmosphere, created macroscopic amounts of C_{60} [17]. The article that really made the field of carbon nanotubes take off was the 1991 article by Sumio Iijima [18] (see fig. 1.1) announcing his discovery that carbon "microtubules" can be produced using a Krätschmer-Huffmann apparatus. Inside the hard carbon shells that grew on the cathode he found carbon nanotubes. The first solid proofs of single-walled CNTs were published in 1993 in two back-to-back articles in Nature. Independently Iijima and Ichihashi [19] and Bethune *et al.* from IBM [20] reported the discovery of SWCNT. Both groups had hoped to fill MWCNTs with transition metals by incorporating it into the graphite rods, but instead the metal acted as a catalyst for the formation of SWCNT. By this time CNT research was an established field that is growing by the day.

An interesting editorial was recently published in the journal Carbon [21] on the controversies regarding the discovery of the carbon nanotubes.

2.2 Structure of carbon nanotubes

The six electrons in a carbon atom are arranged as two strongly bound core, $1s$, electrons and four valence electrons. The valence electrons are arranged into linear combinations of the $2s$ and the three $2p$ atomic orbitals. Through this hybridisation it is possible for carbon to form many types of bonds that makes the difference between materials as diverse as graphite and diamond. In the latter the hybridisation is between the s and all the p orbitals forming four sp^3 orbitals. These are arranged in a tetrahedral configuration as can be seen in figure 2.1A. Each carbon atom forms strong covalent σ-bonds with four neighbours forming a rigid three-dimensional structure. In graphite the s orbital mixes with two p to forms three sp^2 orbitals. These are in one plane and allow the carbon to bond to three other carbon atoms forming a sheet. The remaining p_z orbital is perpen-

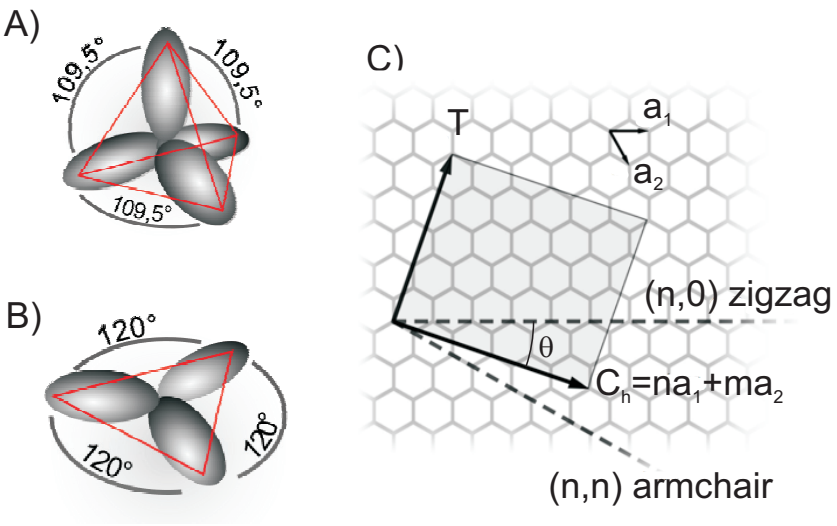

Figure 2.1: A schematic image of the A) carbon sp^3 orbitals and B) sp^2 orbitals. C) illustrates the rolling of a graphite sheet into a nanotube. The chiral vector, $\mathbf{C}_h$, is the circumference of the tube and the vector T lies along the tube axis. The vectors $\mathbf{C}_h$ and $\mathbf{T}$ span the unit cell of the tube. The unit vectors of graphite, $\mathbf{a}_{1,2}$, are also indicated. Pictures from [22].

dicular to the sp^2 orbitals and forms a π-bond with the neighbouring atoms. The different graphite sheets are held together by weak van der Waals forces.

A SWCNT is formed by rolling a sheet of graphite into a cylinder. The graphite can be rolled in different directions leading to tubes with different physical properties. To describe the direction of rolling one defines the chiral vector

$$\mathbf{C}_h = n\mathbf{a}_1 + m\mathbf{a}_2 \equiv (n, m), \tag{2.1}$$

that goes around the circumference of the tube so that the point (n, m) rolls onto the origin $(0, 0)$. $\mathbf{C}_h$ is defined in terms of the unit vectors of graphite $\mathbf{a}_1$ and $\mathbf{a}_2$ and m and n are integers. Tubes are commonly described just using the shorthand notation (n, m). Tubes with $n = m$ are called armchair tubes and $(n, 0)$ type tubes are known as zigzag. These tubes have mirror symmetry planes. All other tubes with $n \neq m \neq 0$ lack such planes and are thus known as chiral tubes. Given a certain chiral vector the diameter of the nanotube can simply be calculated as

$$d_t = \frac{|\mathbf{C}_h|}{\pi} = \frac{a}{\pi}\sqrt{n^2 + m^2 + mn} \tag{2.2}$$

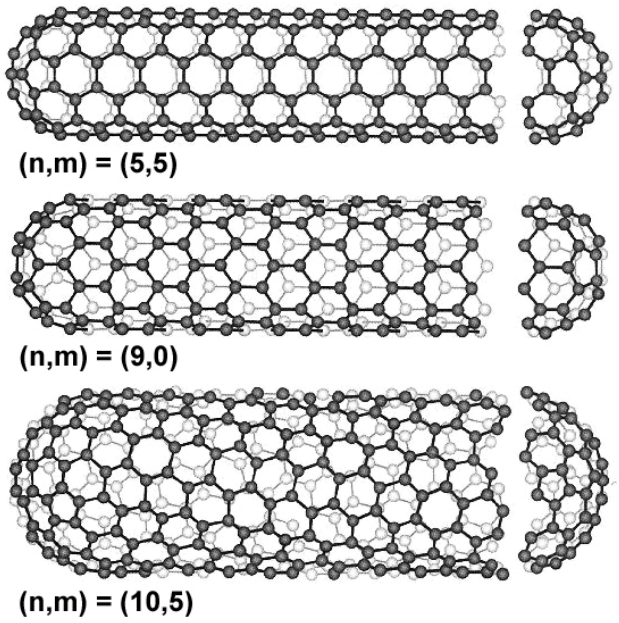

Figure 2.2: Three examples of SWCNT with different geometries. Top is a $(5, 5)$ armchair tube, middle a $(9, 0)$ zigzag tube and bottom is a $(10, 5)$ chiral tube. Picture from [8].

and the chiral angle, θ, is given by

$$\cos\theta = \frac{\mathbf{C}_h \cdot \mathbf{a}_1}{|\mathbf{C}_h|\, a} = \frac{2n+m}{\sqrt{n^2+m^2+mn}}, \tag{2.3}$$

where $a = |\mathbf{a}_1| = |\mathbf{a}_2| = 2.461$Å. Due to the hexagonal symmetry of the graphite lattice only angles $0^\circ \leq \theta \leq 30^\circ$ need to be considered.

Multi-walled carbon nanotubes are made by stacking SWCNT concentrically inside one another. The separation between the layers in a MWCNT is roughly the same as the between the layers of graphite ~ 3.4Å [23].

The diameter of SWCNTs is typically 0.4–4 nm [24, 25]. It was long claimed that the smallest energetically stable nanotube is the 4 Å $(5, 0)$ tube, but a paper by Zhao *et al.* [26] from 2005 shows a 3 Å $(2, 2)$ tube as the innermost shell in a MWCNT. The MWCNT usually are much thicker than the SWCNT with outer diameters up to several tens of nanometres. The length of the tubes vary greatly, from a few hundred nanometres up to centimetres [27]

2.3 Properties of carbon nanotubes

2.3.1 Electronic properties

The electronic structure of a SWCNT is closely related to that of graphite. Graphite is a semi-metal or a zero-band-gap semiconductor. The band structure is such that the valence and conduction bands meet at a single point in $\mathbf{k}$-space called the K-point. This is the corner point of the hexagonal Brillouin zone. This makes graphite an electric conductor at finite temperatures. However, whereas a graphite sheet stretches out to macroscopic distances in all directions, a nanotube has a very different geometry. Along the tube axis it can be considered as infinite, but the very small distance around the circumference leads to confinement effects. Along the $\mathbf{C}_h$ vector periodic boundary conditions must be imposed. This leads to a quantisation of the energy levels and only a limited number of wave vectors are allowed. If any of these allowed vectors cross the K-point in the graphite lattice the tube is conducting otherwise it is semiconducting. Whether a tube is metallic is determined by the (n, m) values. A tube where

$$n - m = 3i, \tag{2.4}$$

and i is an integer, displays a metallic behaviour at room temperature. All other tubes are semiconductors. Armchair tubes, with $n = m$ are always metallic, whereas tubes fulfilling the condition in eq. 2.4 but where $n \neq m$ have a small curvature induced bandgap of about 2-50 meV [28]. At low temperatures these tubes are semiconductors. They are also known to sometimes show ambipolar transport characteristics [29].

An interesting aspect on the conductivity of metallic CNT is that they act as one-dimensional quantum wires. The quantized energy levels lead to observation of phenomena such as Coulomb blockade [30] and Fabry-Perot interference [31]. Nanotubes also act as ballistic conductors. In a metallic SWCNT only two levels cross the Fermi level, and only these two contribute to the electric conductance. Each level can carry one conduction quantum $G_0 = 2e^2/h$, where e is the fundamental charge and h Planck's constant. Thus an ideal SWCNT can have a resistance no lower than $h/4e^2 = 6.45\,\mathrm{k}\Omega$. This also means that the conductivity is independent of the tube length as long as they are shorter than the mean free path of the electrons due to scattering [32].

In the case of multiwalled nanotubes the electrical properties are more difficult to elucidate. The complex structure makes calculations difficult and they are mainly

limited to two or a few wall tubes [33]. The weak contact between the different layers ensures that mainly the outer layer carries the current if the tubes are contacted from the side. However, a certain interaction between the walls does exist at finite temperatures leading to a higher conductance for MWCNTs than the $2G_0$ limit for SWCNTs [34]. It is also possible that the electrodes make contact with many layers, dramatically decreasing the resistance [35]. Since 1/3 of all nanotubes are metallic and there is no correlation between the structure of tubes in different shells of MWCNTs, these almost always show a metallic behavior. MWCNTs also show ballistic conductance, with a mean free path longer than for SWCNT (see ref. [36] for a comprehensive discussion.). The (quasi-)ballistic transport dissipates little energy in the tube, so a nanotube, both single- and multiwalled, can carry a very high current. Current densities $> 10^7\,\mathrm{A/cm^2}$ have been measured [37].

2.3.2 Mechanical properties

Carbon nanotubes are among the stiffest materials known, meaning that they have a high Young's modulus (E) . The Young's modulus is defined as stress divided by strain, or the force per cross-sectional area divided by the relative elongation, i.e.

$$E = \frac{F/A}{\Delta L/L} \tag{2.5}$$

Nanotubes are strong because they are bound together solely by strong σ-bonds. These bonds also hold together diamond and the carbon atoms within graphite planes. Calculations show that SWCNTs have a Young's modulus of roughly $1\,\mathrm{TPa}$, which is the same as that for diamond and the in-plane stiffness of graphite [38]. MWCNTs have a slightly higher modulus than SWCNTs. These values correspond to experiments measuring the electrostatic deflection of vibrating tubes [39,40]. These measurements also show that, in agreement with calculations [38], thin tubes are stiffer than thick.

It was mentioned in the introduction that carbon nanotubes are "stronger than steel". That usually means that they have a higher tensile strength than steel . The tensile strength is the highest force per area that a material can withstand before it breaks. Perfect carbon nanotubes are predicted to have a tensile strength up to $150\,\mathrm{GPa}$ [41], but experimental results on MWCNTs have so far managed to reach less than half of that, $64\,\mathrm{GPa}$ [42]. This should be compared with the strength of steel at $1.8\,\mathrm{GPa}$. Macroscopically, $20\,\mathrm{cm}$ ropes of MWCNT have been measured to a strength of $2.2\,\mathrm{GPa}$, rivalling that of high strength fibres such as Kevlar at $3.3\,\mathrm{GPa}$. However, given the extremely high theoretical strength of CNTs hope

is for super-strong fibres in the future. A limiting factor is the crystalline structure of CNTs. The strength is dramatically decreased by the presence of defects. Recent calculations suggest that macroscopically, defects will always limit the maximal strength to $\lesssim 30\,\mathrm{GPa}$ [35]. One advantage though for nanotubes is their low density. The density adjusted strength of CNT is unrivalled and may lead to interesting applications in the future.

Another area where nanotubes hold great promise due to their mechanical properties is in the field of nanoelectromechanical systems (NEMS) where the combination of mechanical and electrical properties make nanotubes extremely interesting for e.g. high speed relays [43, 44].

2.3.3 Thermal properties

Unlike most dielectrics, diamond in an excellent thermal conductor due to the strong bonds in the lattice that make the phonon conduction very efficient. Carbon nanotubes also have very strong lattice bonds and are therefore expected to be equally good conductors. Calculations show that CNTs have a thermal conductance of $2000 - 6000\,\mathrm{Wm^{-1}K^{-1}}$ at room temperature, increasing from low T up to about $T = 300 - 350\,\mathrm{K}$ where it starts decreasing due to the onset of Umklapp phonon scattering. [45, 46]. This should be compared with that of copper at $\sim 400\,\mathrm{Wm^{-1}K^{-1}}$ and diamond at $\sim 2000\,\mathrm{Wm^{-1}K^{-1}}$. However, as with mechanical strength, experiments show very disparate results, ranging from about $20\,\mathrm{Wm^{-1}K^{-1}}$ [47] to more than $3000\,\mathrm{Wm^{-1}K^{-1}}$ [48].

Carbon nanotubes can also withstand high temperatures. In an oxygen-rich atmosphere they start decomposing around 500°C [49], but in vacuum they are stable well above $2000\,\mathrm{K}$ [50].

The excellent thermal and electrical properties, and the high aspect ratio between length and width makes nanotubes excellent candidates as e.g. field emitters [51].

2.4 Growth of carbon nanotubes

Carbon nanotubes, just like their sister compound the fullerenes, cannot be synthesised in the normal chemical fashion[1]. Instead they need to be produced using other methods, like laser ablation, arc discharge or chemical vapour deposition.

[1] That is: Add A to B; stir, heat, stir and heat; cool; wait; add C; stir some more; wait, wait, wait … distill and voilà.

2.4.1 Arc discharge and laser vaporisation

Arc discharge was the method used in Iijima's 1991 Nature paper [18] for nanotube growth and was used before that to produce fullerenes [17]. The method is basically simple; in a helium atmosphere burn a graphite rod by passing a high current (up to several hundred Ampere) across a small gap in an arc discharge. In the arc the temperature is extremely high, creating a carbon vapour plasma. When the plasma cools the carbon arranges itself into fullerenes and multi-walled nanotubes, as well as lots of amorphous and graphitic soot. Adding a catalyst such as Co, Ni or Fe to the graphite rod leads to the production of SWCNTs, mainly in the form of nanotube ropes. A big disadvantage of the arc method is the amount of soot and encapsulated metal particles in the product necessitating purification before the tubes can be used for anything.

A method similar to the arc method is laser ablation or laser vaporisation (LV). In this method, pioneered by the Smalley group [52], a carbon/metal composite target, placed in a furnace heated to about 1200°C and flushed by a stream of helium or argon, is hit by a focussed laser beam, either pulsed or cw. In the focal spot of the laser a plasma plume is formed with a temperature of 6000 K. As the plume expands supersonically it rapidly cools off. In the cooling process catalyst metal particles are formed that interact with the condensing carbon vapour producing a large amount of SWCNTs, with length up to 10 μm, on a timescale of a few μs. The laser ablation method provided a breakthrough in NT science, as the nanotubes produced were very pure, with little amount of amorphous carbon, and of good quality with very few defects. Most of the early work on electric characterisation etc. was performed on tubes from this method. Many nice studies of the growth mechanisms have been performed, e.g. [53]. Still the laser vaporisation offers only limited control of the growth process, by varying a few parameters such as furnace temperature, target composition and so on.

More about these methods can be found in e.g. ref. [13].

2.4.2 Chemical vapour deposition

A method for growing carbon nanotubes that gives a somewhat greater measure of control is chemical vapour deposition (CVD). In CVD growth of nanotubes a gaseous carbon precursor is allowed to interact with a catalyst particle. The precursor needs to be activated in some way, and the different CVD-methods are categorised according to their energy source. The most common methods, and the

ones used in this thesis are thermal CVD (T-CVD) and plasma-enhanced CVD (PE-CVD).

Thermal CVD

In thermal CVD gaseous precursors are introduced into a furnace with a temperature between $700 - 1200°$C, often together with an inert carrier gas. The system is often a home-built tubular furnace where the gases are introduced into one end of a quartz tube, pass through the hot zone and are pumped out at the other end. As the gases flow through the hot zone the precursor gases react with a catalyst, either in the gas phase or on a substrate, and carbon nanotubes start to grow. The exact mechanism will be discussed briefly below. The growth rate varies a lot from a few nm/min to several $\mu\mathrm{m/min}$.

The T-CVD method offers a vast range of variability with different carbon precursors, different catalysts, temperature and so on. The catalysts can be introduced either in gas phase, the so-called floating catalyst method, or be deposited on a substrate. Depending on the catalyst and precursors nanotubes can be grown either in bulk amounts in the gas phase [54], as vertically aligned dense forests on a substrate or as single tubes from predefined catalyst dots. Suspended nanotubes have been grown from pillars [55] and electric field directed growth has been used to make crossed CNT-CNT junctions [56].

Many different types of nanotubes are grown in T-CVD, from high-quality SWCNTs, to MWCNTs, bamboo-like MWCNTs and structures resembling stacks of ice-cream cones. The list of different catalysts is long. Pure Fe is often used deposited on substrates in predefined patterns. Other catalysts used include ferrocene [57], ferritin [58] and $Fe(CO)_5$ [59]. Similarly the range of carbon precursors is huge. Virtually every gaseous hydrocarbon seems to have been tried, such as methane, acetylene, ethylene, xylene, benzene and so on. Recently the so-called HiPCO (High Pressure CO) method [60] has become popular for producing large amounts of high-quality single walled nanotubes in the gas phase. The HiPCO method uses disproportionation of CO ($2\mathrm{CO} \rightarrow \mathrm{C}(s) + \mathrm{CO}_2$) catalysed on the surface on clusters of iron formed by the dissociation of $Fe(CO)_5$. High-quality SWCNTs can also be formed using alcohol as a carbon feedstock [29]. Adding a small amount of water to the ethylene flow can also produce arrays of mm-long high-quality SWCNT [61], so-called “super-growth”.

T-CVD, and maybe in particular the HiPCO method, shows promise for being the method that can be used for scaling up the production of quality nanotubes to industrial scale, meaning several tons per year.

Plasma enhanced CVD

Plasma enhanced CVD (PE-CVD) is a method commonly used in the semiconductor industry for some processes that cannot tolerate the high temperatures of thermal CVD. The advantage of PE-CVD is that the high-temperature electrons available in the otherwise cold plasma help dissociate the precursor gases in the gas phase without the need for elevated temperatures. During PE-CVD the substrate is usually kept at a much lower temperature, room temperature to $\sim 300°$C, than in T-CVD. However, during nanotube production the dissociation mainly takes place at the surface of the catalyst particle, and not in the gas phase. Just heating methane to 900°C without any catalyst present would lead to very little self-thermolysis of the methane [62]. Indeed the temperature must be kept below the decomposition temperature of the carbon feedstock to prevent the production of a large amount of soot. There is thus no guarantee that PE-CVD will work for nanotube synthesis at much lower temperatures than in T-CVD. If a certain catalyst temperature is needed for the catalysed decomposition of the precursor to work the gas phase processes in the plasma might not do much for enhancing the decomposition rate at low temperatures. However, processes in the plasma produce a range of different radicals, as will be seen in chapter 6. This can considerably change the chemistry involved.

Like in T-CVD the carbon feedstock is in the form of a gaseous precursor, commonly a hydrocarbon such as acetylene. Since the plasma processes leads to a decomposition of the hydrocarbon precursor that can lead to a large amount of non-catalytic amorphous carbon deposition the carbon feedstock is usually diluted in an inert gas like argon or a reactive gas like hydrogen or ammonia. There are then two competing processes in the gas-surface interaction, deposition of carbon on the substrate, and etching by the reactive gases. What the result will be depends on the competition between the two.

One of the advantages of PE-CVD over T-CVD is that the electric field helps create well aligned vertically growing nanotubes. This can also happen in T-CVD, but is then a result of crowding. Nanotubes growing next to each other are held together by van der Waals forces and support each other. In PE-CVD it is possible to grow free-standing single structures such as vertically aligned carbon nanofibres (VACNFs) or nanotubes.

In 1998 Ren *et al.* [63] reported the growth of aligned MWCNTs on glass. The substrate temperature was estimated to be less than 660°C. Later articles have reported growth of nanotubes at substrate temperatures estimated at 450°C [64,65] and some reports at even lower temperature than that [66].

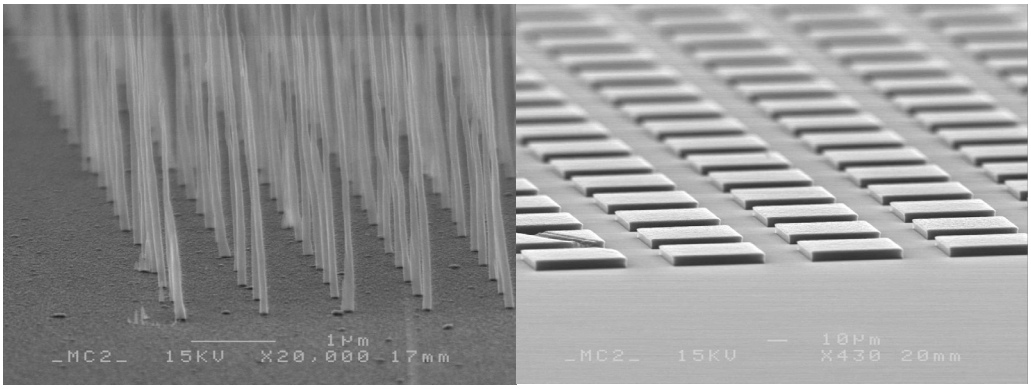

Figure 2.3: Examples of samples grown using PE-CVD. (left) VACNFs from pre-patterned Ni-dots. (right) Forests of $5\,\mu\mathrm{m}$ long MWCNTs grown from squares of Fe catalyst film.

The growth mechanisms of CNTs in general are not quite clear, but the standard model is the so-called VLS (Vapour Liquid Solid) model see figure 2.4. It basically consists of 5 steps. 1) First a catalyst particle is formed. 2) Then the carbon precursor gas is dissociated on the catalyst surface, forming carbon atoms. 3) The carbon atoms are dissolved into the catalyst. 4) Some of the carbon atoms precipitate to the surface. 5) The precipitated atoms lift off, forming a carbon nanotube. This is the basic idea, however the details are still a bit hazy. Some theories say that the supersaturated carbon in the particle precipitates to the surface and forms a carbon cap on the surface of the particle that lifts off [67] forming SWCNTs or MWCNTs whose diameters correspond to the size of the catalyst particle. Others claim that in CVD the dissolution into the catalyst is not necessary. The hydrocarbons can be dissociated and assemble directly on the particle surface [68]. Another theory explaining the discrepancy between the nanotube diameters and the catalyst particles, as well as the formation of SWCNT ropes implies that 2D graphitic clusters form on the catalyst surface. These clusters attach to other clusters. The formation of a heptagon-pentagon defect leads to out of plane bonds that makes the cap lift off instead of just forming a graphitic shell around the particle [69, 70]. However the VLS model has also been the subject of some criticism, especially in the case of laser vaporisation growth. In a recent review, and references therein the current state of affairs regarding solid state growth is summarised [71]. The growth and potential applications of VACNFs is summarised in an exhaustive review by Malechko *et al.* [72].

Depending on the interaction between the catalyst and the surface one can have either tip growth or base growth, as illustrated in figure 6.2. In the case of base

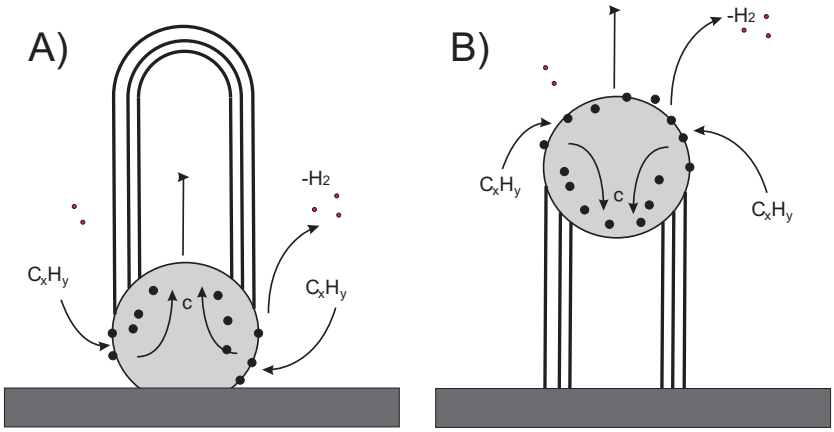

Figure 2.4: A schematic image of A) base growth and B) tip growth of a MWCNT.

growth the catalyst particle stays on the substrate and the nanotube grows upwards like a leaf of grass. In tip growth the catalyst lifts off the surface and is pushed up by the nanotube growing under it.

Summary

At the nanotube conference NT06 in Nagano in June 2006 Alan Windle gave an introduction to the poster session about CNT growth that underscored the uncertainty regarding this topic today [73]. Even if some of the main traits of CNT growth may be known, there are still many things that are unclear. There is e.g. no consensus about what factors are affecting the growth rate controlling steps, or even if some factors are important at all, and results from different groups are often incongruous. Windle continued to give examples of at least seven different process variables that are relevant in floating catalyst T-CVD. “We are doing technology in multidimensional parameter space”, he said. Each group continues to probe a small region in this space. It is the purpose of this thesis to boldly go where no-one has gone before in this parameter space. Specifically to examine some of the parameters that might be important in PE-CVD growth of MWCNTs and VACNFs. It is also the aim to use some of the growth techniques available in our labs to explore potential applications.

3
Equipment for nanotube production

There are, as was mentioned earlier, a number of ways of producing CNTs, each with their particular advantages and disadvantages. At the University of Göteborg we have several systems for growing nanotubes and nanofibres, both thermal and plasma enhanced chemical vapour deposition. In this thesis most work has been done with the PE-CVD system and it will be described in detail below. Some work was also made using thermally grown tubes, so also this system will be described.

In addition, some of the equipment available for characterisation of the grown tubes will be briefly described.

3.1 PE-CVD for nanotube/nanofibre growth

The plasma enhanced CVD is available in many different configurations, e.g. with an rf plasma [74], microwave plasma [75], inductively coupled plasma (ICP) [76], triode plasma [77], DC plasma with hot filament [78] and so on. In our lab we're using a stable DC glow discharge plasma. With this system we grow vertically aligned CNTs and CNFs. The main difference between the different plasmas is the way the power source is connected to the reaction volume. In a DC or rf plasma two electrodes are used, an anode and a cathode. One of them is also usually used as sample holder, but remote plasmas are possible. The electrodes

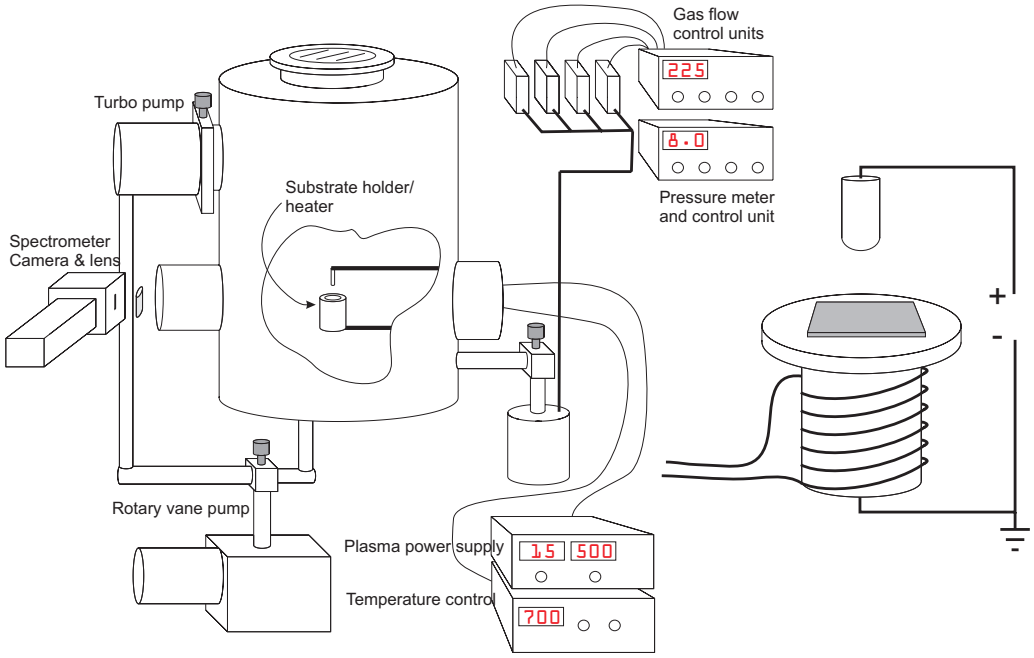

Figure 3.1: A schematic drawing of the PE-CVD system used for growing carbon nanotubes and nanofibres.

are biased by the power source, through a matching network for high frequency plasmas, and this bias sustains the plasma. In an ICP or a microwave plasma one instead couples the power through an inductive coil or a microwave source. The sample -holder can be biased independently. This can help to reduce damage to the substrate through bombardment of ions accelerated by the bias voltage, but at the same time limits the aligning effect of the electric field. A discussion of plasma processes in general is given in section 4.

The set-up is a homebuilt machine consisting of two cylindrical metal vacuum chambers, see figure 3.1. The larger part is the growth chamber with a volume of 75 litres, and attached to it is a 4-litre pre-mixing chamber used for achieving the correct gas mixture to be let into the growth chamber. The two chambers are connected via a valve. The gas flow into the mixing chamber is controlled via mass flow controllers from MKS. With this scheme we have the possibility of working both with static pressure or with a continuous gas flow. The gases are taken directly from the gas supply without any additional purification.

The sample holder, which is also the cathode in the plasma discharge, consists of a resistively heated molybdenum core, housed in a ceramic body and isolated

with quartz foam. A thermocouple is embedded into the heater body and the temperature is kept stable using a thermocontrol-unit. The temperature gradient across the heater surface is only a few K, and heat loss from the surface leads to a substrate temperature 10–15K lower than the temperature of the body. Heating of the substrate due to plasma irradiation is deemed to be negligible given the low power of the plasma.

The substrates are mounted on the heater and attached using a small clamp. Care must be taken to ensure that the clamp is close to the surface to prevent the creation of a hollow cathode discharge under the clamp. Preparation of the substrates will be detailed in section 3.3.

After insertion of the substrate the chambers are pumped using a turbo molecular pump (TMP) with a rotary vane fore-vacuum pump. The ultimate pressure is on the order of $10^{-6}\mathrm{mbar}$. During growth with continuous gas flow the valve to the turbopump is closed and the system is pumped using only the rotary vane pump. Constant pressure is maintained either by manually adjusting the output valve, or using an automatic valve controlled via the pressure meter.

As mentioned above the sample holder also functions as cathode for the plasma. The holder and the chamber walls are grounded. An anode consisting of an M6 steel screw is fixed from a ceramic rod 10–15 mm above the cathode surface. The anode is connected to a power supply via a $100\,\Omega$ ballast resistor. The plasma current is controlled by setting the current limitation on the power supply. The voltage is set to its maximal value of $1250\,\mathrm{V}$. When the gases are let into the chamber the breakdown voltage is $\sim 500\,\mathrm{V}$ depending on gas composition, pressure and current density. Unfortunately we have no way of directly controlling the current density at the sample surface. The area of the cathode is $7\,\mathrm{cm}^2$. However, a setting of less than $10\,\mathrm{mA}$ leads to only a part of the cathode surface covered by the plasma. In this case the current density in the plasma covered part remains constant even as the total current changes [79]. At currents higher than $\sim 50\,\mathrm{mA}$ the discharge becomes unstable and there are discharges to different parts of the chamber or the development of a hollow cathode with a very high local current density leading to a lowering of the current density at the substrate surface.

A telescope was constructed for collecting the optical emission spectra from the plasma comprising a $150\,\mathrm{mm}$ focal length lens inside the PE-CVD growth chamber and a cylindrical lens outside the chamber focussing the emitted light onto the entry slit of a SpectraPro 150 spectrometer. The optical set-up was aligned using a photodiode attached to the sample holder. The diameter of the photodiode was $\sim 3\,\mathrm{mm}$, which puts a limit on the spatial accuracy of the light collection. The telescope was mounted parallel to the cathode surface. The spectra

were recorded using a thermoelectrically cooled ICCD-camera (PI-MAX, Princeton Instruments) connected to a computer. The spectral sensitivity of the system is $350 - 900\,\mathrm{nm}$ with the window to the vacuumchamber responsible for the lower cut-off.

The optical set-up was calibrated using a broad band light source (LSK100 Halogen lamp, L.O.T. Oriel) with known spectrum.

For in situ monitoring of the CNT growth a small $3\,\mathrm{mW}$ diode laser ($\lambda = 670\,\mathrm{nm}$) was mounted on the growth chamber shining on the sample through a view-port in the chamber ceiling. The laser was focussed onto the sample surface and the reflected light was collected with a photodiode on the outside of the chamber through a side view-port as can be seen in the sketch in figure 3.2. A band-pass filter was placed in front of the photo-diode to limit the influence of the emission from the plasma. The incident angle of the light is $35°$. The photocurrent was recorded using an Agilent 3410A multimeter connected via GPIB to a computer using LabVIEW.

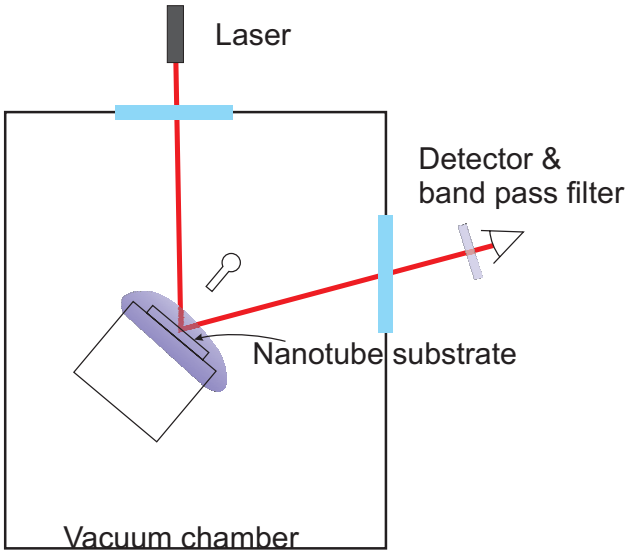

Figure 3.2: A schematic sketch of the laser reflection measurement.

3.2 Thermal CVD for nanotube growth

A schematic drawing of the thermal CVD system can be seen in figure 3.3. It consists of a furnace that can be heated to 1200 °C, gas flow controllers as in

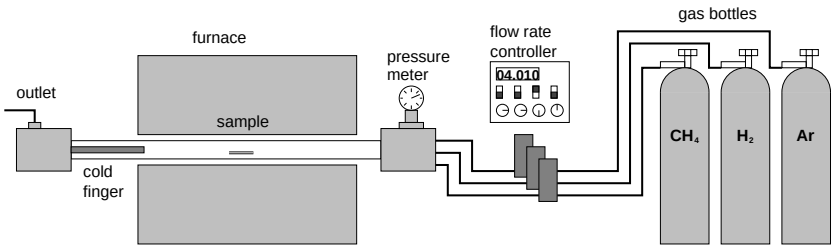

Figure 3.3: A schematic drawing of the thermal CVD set-up.

the PE-CVD set-up and a thermal control unit. The hot zone of the furnace is about 40 cm. A roughly 1 m long quartz tube with a diameter of either 20 or 40 mm serves as reaction vessel. The tube's ends extend outside the furnace and are connected to water cooled housings for gas in- and outlet as well as electrical feedthroughs. The quartz tube is connected to a rotary vane vacuum pump that allows the tube to be evacuated to a pressure $< 1\,\mathrm{mbar}$. During this thesis work growth of CNTs is exclusively taking place on chips with predefined catalysts. See section 3.3 for details on the preparation of the substrates. Previously a water cooled Cu finger was inserted into the furnace to collect nanotubes grown in the gas phase, but it is presently disused.

The Si-substrate prepared with catalyst is placed inside the quartz tube in the centre of the hot zone. The tube is sealed and evacuated. After purging with argon, the tube is filled to ambient pressure with a mixture of Ar and H_2 and heated to growth temperature, 700–1000 °C. During annealing in the Ar:H_2 mixture small catalyst particles are formed on the substrate surface [80]. As the carbon feedstock, prevalently in the form of acetylene (C_2H_2), is introduced the carbon is decomposed at the catalysts and nanotubes are grown. The manner of growth is dependent on many of the parameters , but most importantly the temperature. At a furnace temperature of 750 °C thick forests of multiwalled CNTs are grown. A more detailed analysis is given in [81].

The group also has a small low temperature CVD system where the catalyst is heated resistively using a microelectrode. The system has not been used in the scope of this thesis. For a thorough description the reader is referred to refs. [82, 83].

3.3 Preparation of the substrates

The substrates used for growing carbon nanotubes are usually silicon (100) wafers. Historically the group did a lot of work using $Fe(CO)_5$ as a catalyst for CNT growth [84–86]. At the present, catalysts are prepared by evaporating a film of iron or nickel onto the substrate.

Using standard photo- or electron beam lithography techniques a mask can be created in a polymer resist layer through which the catalyst can be evaporated in a well-defined pattern. The evaporation system (AVAC HVC600) is an electron beam evaporator with a $4\,\mathrm{kW}$ e-gun. Up to four different evaporation sources can be used sequentially in a rotating pocket stage. There is also the possibility to use two resistively heated sources. The thickness of the evaporated layer is monitored with a quartz crystal oscillator. the evaporation is performed at a base pressure of $3 \times 10^{-6}\,\mathrm{mbar}$. The evaporation sources are $\geq 99.5\%$ Ni or Fe metal pieces.

For PE-CVD it is important to have a conducting substrate. Therefore the catalyst is deposited directly onto a Si-wafer with only native oxide. In the case where a wafer with oxide is needed it is necessary to lay down a metal support layer under the catalyst to provide a conducting surface. A metal underlayer is also used when the tubes are to be grown on electrical contacts etc. However, it was realised that it is crucial for adequate nanotube/nanofibre growth to include a thin ($\leq 10\,\mathrm{nm}$) Si or Al_2O_3 layer between the metal support and the catalyst. The inclusion of this intermediate layer is important for the wetting and morphological interaction between the catalyst and the metal. A thorough discussion on this issue is found in [87].

3.4 Characterisation of grown tubes

When it comes to characterising the grown nanotubes or nanofibres there are many different methods at hand. In the scope of this thesis, aside from spectroscopic methods of characterising the plasma itself, mostly scanning electron microscopy (SEM) has been employed. The SEM used is a JEOL JSM6301F with $10\,\mathrm{nm}$ resolution. Using SEM has advantages and a few disadvantages that can be severely limiting in certain cases, but as shall be seen, these limitations are of no great importance in the present work. The main advantage of SEM is that it's a fast and simple method of imaging the as grown nanotube films. In some cases it is possible that the tubes are destroyed when many slow scans are performed. However, as the present work focusses on the growth of nanotube forests the loss of

individual tubes is of no importance. When using single tubes in electronic devices care needs to be taken when using SEM as the imaging method. Also, due to the limited resolution of the SEM it is difficult to image SWCNTs. When it is necessary to look at an individual SWCNT other methods such as atomic force microscopy are preferable.

3.5 Optical emission spectroscopy during electron field emission

Measurements of the field emission properties of carbon nanotubes and spectroscopy of the light emitted during the field emission were performed in a specially dedicated vacuum chamber at pressure of $10^{-7}\,\mathrm{mbar}$. The sample was mounted on a stage and a hemispherical anode was placed at a distance of 100 $\mu\mathrm{m}$ from the surface of the nanotube film, see figure 3.4. The stage was connected with copper wires to a voltage source (Keithley 2410) and a picoamperemeter (Keithley 6485). In front of the vacuum chamber an optical set-up was built to collect the light emitted from the nanotube film. The set-up was very similar to the one described above for plasma-characterisation, consisting of a telescope, a $150\,\mathrm{mm}$ focal length spectrometer and a CCD camera. However, in this case no lens was placed inside the vacuum chamber. The camera and the spectrometer were controlled by a computer. A LABView program on the same computer also controlled the voltage source and the amperemeter.

3.6 Raman spectrometry of CNTs

Raman spectrometry is a powerful technique for analysing carbon nanotubes. Raman measures the excitation of vibrational levels in the tubes, and through this information one can draw conclusions about the overall quality of the sample, but also determine both the diameter and chirality (n, m) of single tubes [88].

As opposed to normal Rayleigh scattering, Raman scattering is an inelatic process in which an incident photon gets absorbed by the sample and scatters at a different wavelength. This is because the incident photon is absorbed by the sample and at the same time induces a vibrational transition and another photon is sent out at a slightly different energy. The difference in energy between the incident and outgoing photons tell us about the energy of the excited phonons. Of course the

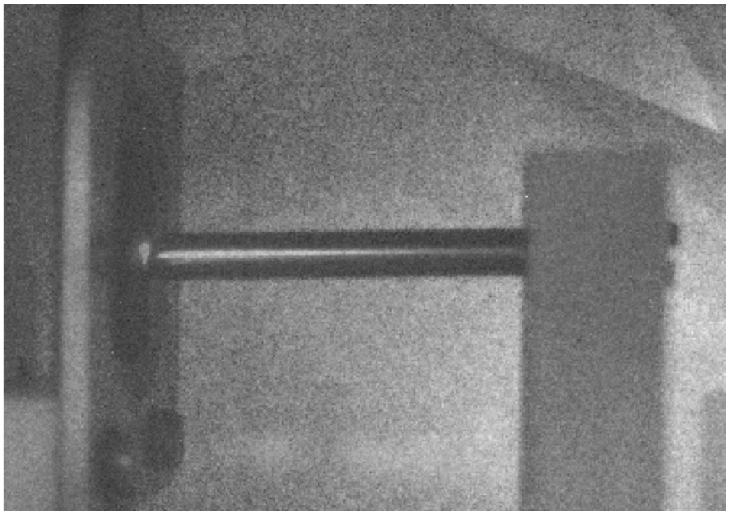

Figure 3.4: A composite image taken with the CCD camera of the stage for field emission measurements, and superimposed an image of the light emission during measurements.

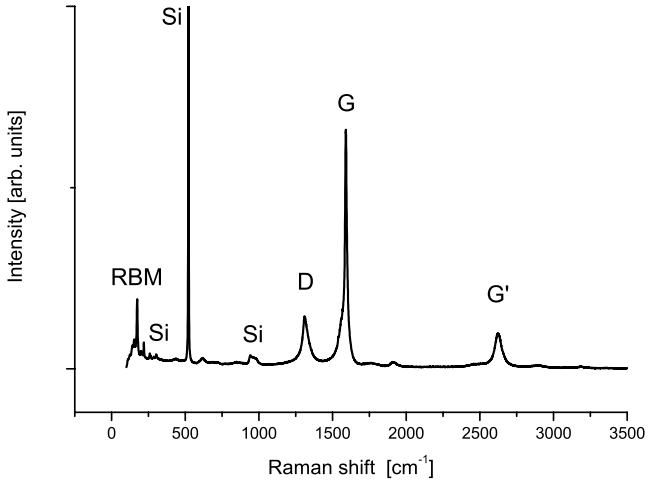

Figure 3.5: A typical Raman spectrum from SWCNTs. The marked features are the RBM modes, the D and G lines, The G' line and a number of lines from the silicon substrate

outgoing photon can also interact with the sample, we then get what is called second order Raman scattering.

In figure 3.5 a typical Raman spectrum from a SWCNT is shown. The region around $100 - 400\,\mathrm{cm}^{-1}$ shows the radial breathing modes (RBM) which is the vibration when the tubes expands and contracts radially in "breathing" motion.

This vibration is very sensitive to diameter and the frequency of the peak can be used to determine the tube diameter.

Other important peaks are the G and the D lines. The G (graphitic) line around $1570\,\mathrm{cm}^{-1}$ comes from in-plane vibrations of the graphite rings, whereas the D (disordered) line around $1370\,\mathrm{cm}^{-1}$ comes from the stretching vibration of $sp2$ clusters. The ratio between the G and D lines give an indication of the quality of the tubes. If the area of the G line is significantly larger than that of the D line the sample is well graphitised with few defects.

4

Plasma

Compared to vapour, liquid and solid, plasma is a much less known state of matter. However, it is by far the most abundant in the universe. Roughly 99% of the (light) matter in the universe is plasma. Stars are plasmas, as is most of the intergalactic gas, the solar corona and so on. Terrestrial, natural plasmas are seen as discharges such as lightning, the polar auroras and the spooky St. Elmo's fire. A plasma can loosely be described as a mixture of neutral gas species, ions and electrons. A plasma can be made from a gas by adding enough energy so that the neutral gas species start to ionise. Processes in the plasma lead to fragmentation of the original gas molecules into often very reactive radicals known as active species. If the energy supply is turned off the plasma species will recombine, again forming a neutral gas mixture. Plasmas are often categorised according to their energy supply, and the physical properties of different plasmas are vastly varying. The differences in size, density and temperature span many orders of magnitude. The intergalactic medium is an extremely rarified plasma consisting mostly of ionised hydrogen atoms with a temperature of ca $3\,\mathrm{K}$ and a density of a mere $10\,\mathrm{m}^{-3}$. A laser-driven inertial confinement plasma for fusion experiments in the other extreme end can have a temperature of $10^8\,\mathrm{K}$ and a density of $> 10^{30}\,\mathrm{m}^{-3}$.

4.1 Glow discharge plasma

In our lab the plasma is a stable direct current glow discharge plasma. The glow discharge is a self-sustaining discharge with a relatively cold cathode. The electrons are generated mainly by secondary emission due to ion bombardment of the cathode surface. At the cathode there is a region with a large positive space charge with a large potential drop on the order of hundreds of volts, see sketch in figure 4.1. Since plasmas are efficient electric conductors most of the voltage drop occurs here. This is known as the cathode fall. After the cathode fall comes a region with almost zero, or even negative, longitudinal field. This gives way to the positive column that stretches, with a constant field, all through the rest of the tube. If the gap between the cathode and the anode is small the positive column might disappear. This is the case in our setup. Close to the anode is a similar region to the cathode fall, with a negative space charge, called the anode fall.

In a long discharge tube, especially with low pressure, one can clearly distinguish several light emitting regions, as schematically depicted in figure 4.1. The description below basically follows the one by Raizer [79]. Closest to the cathode is the *Aston dark space*. The secondary electrons emitted from the cathode surface have a low energy of $< 1\,\mathrm{eV}$. Since this is insufficient to electronically excite the molecules/atoms in the plasma there is no emission and the region appears dark. As the electrons are accelerated in the cathode fall field they will gain sufficient energy to start exciting the plasma-species. A glowing region called the *cathode glow* appears. This can have two or even three layers representing different excitation levels. When the electron energy gets too high the excitation cross-section decreases and ionisation becomes the dominant reaction. Little light is emitted from the *cathode dark space*. The ionisation creates both positive ions and electrons. Since the ions have much lower mobility than the electrons a positive space charge is built up. At the end of the region, where the electron flux, and thus also the electron generation, is the largest, the field is very low. The electrons have a moderately high energy and again generate excitations. This is the *negative glow*. As the energy of the electrons is dissipated the excitations become rarer and the negative glow goes over into the *Faraday (dark) space*. The field increases in the Faraday space to a constant level in the *positive column*. The positive column is electrically neutral, and the electron energy is $1 - 2\,\mathrm{eV}$, with some higher energy electrons available. This gives the column its glow. Towards the anode the ions are repelled and the electrons accelerated, this creates the anode dark space and lastly the anode glow, which is not always present.

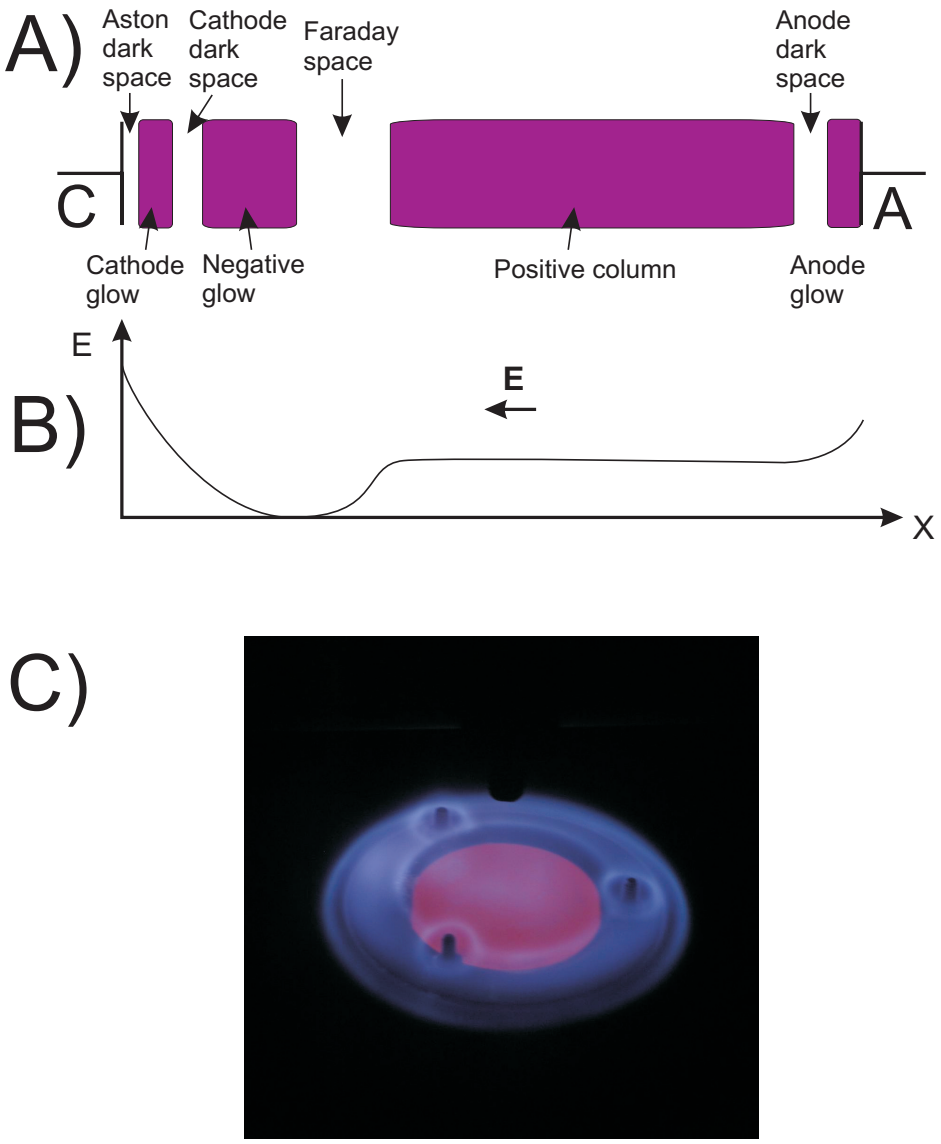

Figure 4.1: In A) a schematic image of the regions in a glow discharge, and in B) a sketch of the general behaviour of the longitudinal electric field in the the plasma. C) a photograph of our plasma during operation.

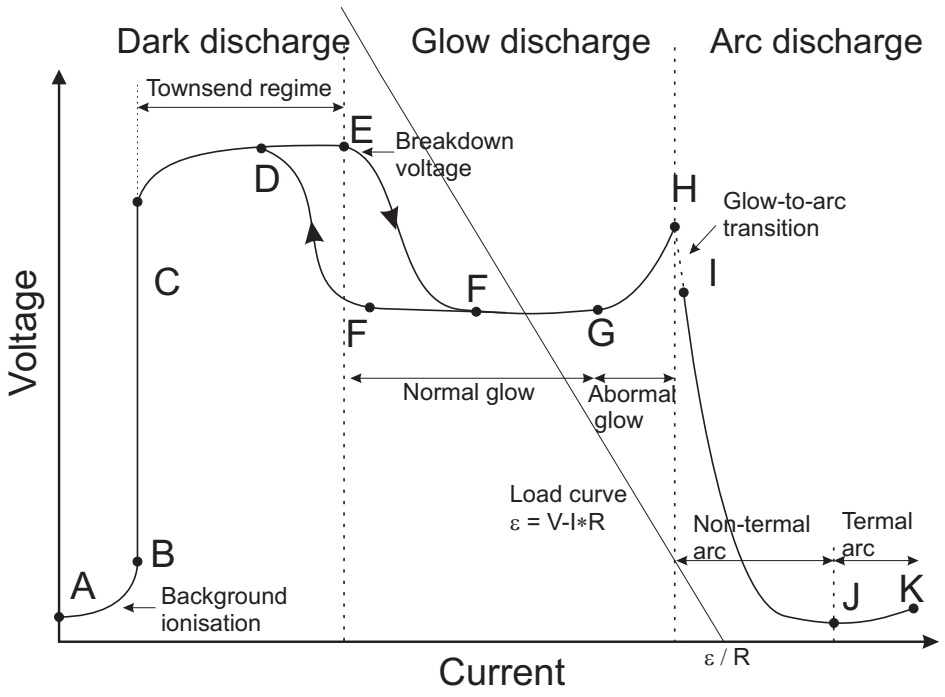

Figure 4.2: Typical voltage-current curve between electrodes in a plasma. For details see text.

4.1.1 Current-voltage characteristics of a glow discharge

The current-voltage characterisation of a discharge depends on many different parameters, such as the gas composition, the pressure, the cathode temperature, and so on. The circuit from the power supply over the discharge gap always has an ohmic resistance R. This can be either a specially introduced ballast resistor or just the resistance in the wires and the power supply. With ε being the electromotive force of the power supply, I the current and V the voltage over the gap the equation for the load line is given as

$$\varepsilon = V - I \times R. \tag{4.1}$$

The load line is plotted as a straight line in figure 4.2. The interception with the x-axis is the limiting current ε/R. The values that can be realised are the intersection points between the load line and the V-I curve of the plasma.

For a very small ε (or large R) the only current through the circuit comes from background ionisation (A–C). Once the voltage reaches the ignition potential V_t (at C) the discharge becomes self-sustaining. At V_t the number of electrons pulled

to the anode is balanced by the number extracted from the cathode. The ionisation is very low. The space charges in the gap are very weak, due to the low density of charged species, so the field is constant $E = V/L$ across the whole gap length L. As long as the charge density is low enough not to distort the field the voltage $V(I)$ will be roughly constant. The plasma emits almost no light at this low ionisation level, thus it is known as a Townsend dark discharge. As the voltage reaches the breakdown voltage appreciable ionisation occurs and a glow discharge develops. Initially the voltage drops with increasing currents (E–F), but it then reaches a level that is constant over a wide current range. This is the normal glow discharge region. This is where our growth plasma usually operates. In a normal glow discharge the current density remains constant. When the current increases only the area the current flows through changes. The plasma spreads out over all areas not covered by a dielectric to increase the current. When the whole cathode area is filled the current can only increase by increasing the voltage and thus extracting more electrons from the cathode. This is the abnormal glow (G–H). The high current heats the cathode surface, at point H the cathode is so hot that electrons are emitted thermionically. If the power supply has a sufficiently low resistance the discharge undergoes a sudden glow-to-arc transition (H–I). The region above I is the arc-discharge region.

Unfortunately the plasma isn't quite as predictable as described above. The glow discharge is quite often unstable, and small perturbations can grow catastrophically, especially at high currents. This can make the plasma contract into high current filaments. Another complicating factor is the hollow cathode. In a gap on the cathode with dimensions similar to the mean free path of the electrons $\lesssim 1\,\mathrm{mm}$ the sustainable current can be orders of magnitude higher than normally. This means that basically the whole plasma current will pass through the hollow cathode instead of filling out the whole cathode surface. One must therefore be careful not to create such gaps, e.g. under the clamp holding the substrate on the cathode surface.

As we now understand the basic workings of the plasma used to grow tubes we can turn our attention to how one can use optical emission spectroscopy to extract information of the species in the plasma. OES will be used for measuring the temperature of the C_2 molecule using the method described below.

4.2 Vibrational temperature and the sum rule

This section will explain how the vibrational temperature of a molecule can be measured from its optical emission spectrum.

This description is basically summarised from ref. [89]. The intensity of the emission bands in a molecular spectrum is largely determined by the Franck-Condon principle. According to this the transition between two electronic states happens so fast that the internuclear distance in the vibrational state does not have time to change. In a graph of potential curves like in figure 4.3 this means that the transition takes place vertically. Consequently the highest intensity transitions will be those with the "best" overlap between the initial and final states. This overlap, called the transition matrix element or transition moment, can be described by the integral

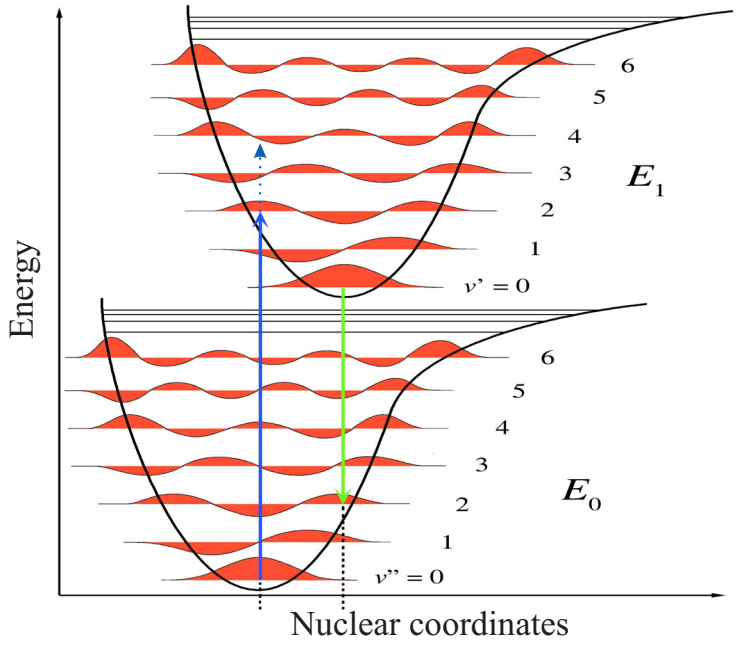

Figure 4.3: Potential curves illustrating the Franck-Condon principle. The left arrow marks an absorption event where the transition from $\upsilon'' = 0$ to $\upsilon\prime = 2$ is much more likely than e.g. to $\upsilon' = 4$ (dotted). The right arrow marks an emission event. Figure adapted from [90].

$$\mathbf{R} = \int \psi'^{*}\mathbf{M}\psi''\mathrm{d}\vec{r}, \tag{4.2}$$

where ψ'' and ψ' are the total eigenfunctions for the initial and final states respectively, and $\mathbf{M}$ is the electric moment. Using the Born-Oppenheimer approximation, the total eigenfunction can be divided into one vibrational part, ψ_υ, and one electronic part, ψ_e, so that $\psi = \psi_\upsilon\psi_e$. The same goes for the electric moment, $\mathbf{M} = \mathbf{M}_\upsilon + \mathbf{M}_e$. Rewriting the expression in 4.2 using the fact that $\mathbf{M}_\upsilon$ is independent of the electron coordinates and remembering that $\psi_\upsilon = \psi_\upsilon^*$ one gets the

transition moment from state υ'' to υ'

$$\begin{aligned}\mathbf{R}^{\upsilon''\upsilon'} &= \int \mathbf{M}_e \psi_e'^* \psi_\upsilon' \psi_e'' \psi_\upsilon'' \mathrm{d}\vec{r} + \int \mathbf{M}_\upsilon \psi_e'^* \psi_\upsilon' \psi_e'' \psi_\upsilon'' \mathrm{d}\vec{r} \\ &= \int \mathbf{M}_e \psi_e'^* \psi_\upsilon' \psi_e'' \psi_\upsilon'' \mathrm{d}\vec{r} + \int \mathbf{M}_\upsilon \psi_\upsilon' \psi_\upsilon'' \mathrm{d}\vec{r_\upsilon} \underbrace{\int \psi_e'^* \psi_e'' \mathrm{d}\vec{r_e}}_{=0} \\ &= \int \psi_\upsilon' \psi_\upsilon'' \mathrm{d}r \int \mathbf{M}_e \psi_e'^* \psi_e'' \mathrm{d}\vec{r_e}. \end{aligned} \tag{4.3}$$

The vibrational eigenfunctions ψ_υ depend only on the internuclear distance r. The last integral in eq. 4.3,

$$\mathbf{R}_e = \int \mathbf{M}_e \psi_e'^* \psi_e'' \mathrm{d}\vec{r_e} \tag{4.4}$$

is known as the electronic transition moment. Since the vibrational transitions are slow compared to electronic transitions $\mathbf{R}_e$ can be replaced with an average value $\overline{\mathbf{R}}_e$. Thus

$$\mathbf{R}^{\upsilon''\upsilon'} = \overline{\mathbf{R}}_e \int \psi_\upsilon' \psi_\upsilon'' \mathrm{d}r. \tag{4.5}$$

The intensity of an emission line relating two states n and m is given by

$$I_{\text{em}}^{nm} = N_n h c \nu_{nm} A_{nm}, \tag{4.6}$$

where ν_{nm} is the wave number of the photon emitted in the transition, and $hc\nu_{nm}$ its energy. N_n is the number of atoms in state N, and A_{nm} is the Einstein coefficient for spontaneous emission. It is related to the transition matrix element as

$$A_{nm} = \frac{64\pi^4 \nu_{nm}^3}{3h} |\mathbf{R}^{nm}|^2 \tag{4.7}$$

Thus, by combining 4.5 with 4.6 and 4.7, the intensity of an emission line between two vibrational levels can be written as

$$I_{\text{em}}^{\upsilon''\upsilon'} = \frac{64}{3}\pi^4 \nu^4 c N_{\upsilon'} \overline{\mathbf{R}}_e^2 \left[\int \psi_\upsilon' \psi_\upsilon'' \mathrm{d}r\right]^2. \tag{4.8}$$

For properly normalised vibrational eigenfunctions it can be shown using basic properties of orthogonal functions (e.g. [91]) that the square of the overlap integral summed over all upper or lower levels equals one, i.e.

$$\sum_{\upsilon''} \left[\int \psi_\upsilon' \psi_\upsilon'' \mathrm{d}r\right]^2 = \sum_{\upsilon'} \left[\int \psi_\upsilon' \psi_\upsilon'' \mathrm{d}r\right]^2 = 1. \tag{4.9}$$

Together with 4.8 this expression gives the the so called vibrational sum rule,

$$\sum_{\upsilon''} \frac{I_{\text{em}}^{\upsilon''\upsilon'}}{\nu^4} \propto N_{\upsilon'}. \tag{4.10}$$

In other words, summing over the band strengths[1] of all the bands with the same upper, or lower, level gives a value proportional to the population of that level. When deriving 4.10 the assumption was implicitly made that the electronic transition moment $\mathbf{R}_e$ is constant for all vibrational states that give an appreciable contribution to the total band strength. Also, depending on experimental conditions, it might be necessary to consider the self absorption of emitted light.

For a gas, or plasma, in (local) thermal equilibrium the population of the excited states is Boltzmann distributed, that is

$$N_\upsilon \propto \mathrm{e}^{G(\upsilon)hc/kT_{\text{vib}}}, \tag{4.11}$$

where k is Boltzmann's constant, T_{vib} is the effective vibrational temperature, and $G(\upsilon)$ is the term value corresponding to the state at hand. For diatomic molecules an approximation of G based on an anharmonic oscillator description of a vibrating rotator is often used (see [89] Chapter III,2). There G is given as a series expansion

$$G(\upsilon) = \omega_e \left(\upsilon + \frac{1}{2}\right) - \omega_e x_e \left(\upsilon + \frac{1}{2}\right)^2 + \omega_e y_e \left(\upsilon + \frac{1}{2}\right)^3 + \cdots \quad , \tag{4.12}$$

where ω_e, $\omega_e x_e$ and $\omega_e y_e$ are the vibrational frequencies of the anharmonic oscillator and can be found in tables. For the C_2 Swan band transitions of interest in this thesis the term value is plotted in fig. 4.4.

Combining eqs. 4.10 and 4.11 one obtains

$$\ln \sum_{\upsilon''} \frac{I_{\text{em}}^{\upsilon''\upsilon'}}{\nu^4} = C_1 - \frac{G(\upsilon')hc}{kT_{\text{vib}}}, \tag{4.13}$$

where C_1 is a constant. Therefore, plotting the logarithm of the sums of the band strengths against the term values of the transitions will give a straight line. The slope of the line will give the vibrational temperature of the molecule. This is a method used for analysis of plasmas under vastly differing conditions [92–94].

[1] The band strength is defined as $\frac{I_{\text{em}}^{\upsilon''\upsilon'}}{\nu^4}$ for emission, but as $\frac{I_{\text{abs}}^{\upsilon''\upsilon'}}{\nu}$ in absorption, where that expression goes into the sum instead. That is, summing over band strengths still is a true statement, only the definition of band strength is different.

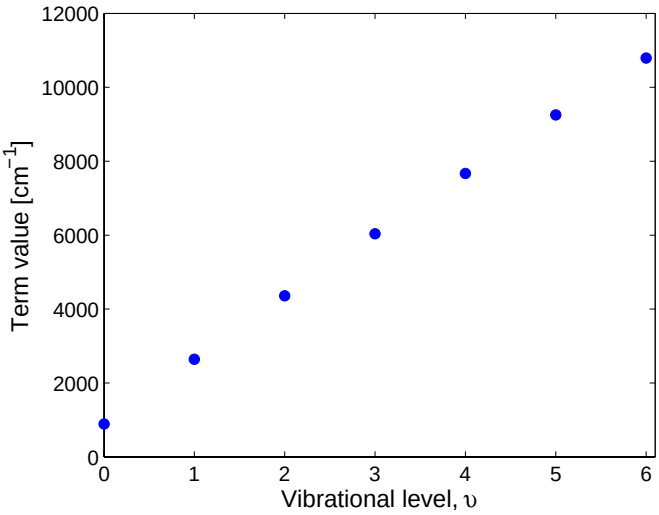

Figure 4.4: The term value $G(\upsilon)$ as a function of the vibrational level of the first excited state $\left(A\,^3\Pi_g\right)$ of the C_2 radical, responsible for the Swan band transitions. The values are calculated using eq. 4.12 with constants taken from [89].

Using similar methods it is possible to calculate the electron temperature in a plasma from the emission intensity of the atomic hydrogen lines. Assuming that the different levels have similar cross sections and collisional quenching rates the emission intensity from each level is proportional to the number density of electrons at that energy. The temperature of the electrons can then be determined by

$$\ln\left(\frac{I_{f\leftarrow i}\lambda_{f\leftarrow i}}{g_i A_{f\leftarrow i}}\right) = \frac{E_i}{kT_e}, \tag{4.14}$$

where $I_{f\leftarrow i}$ is the emission intensity, g_i the degeneracy of state i and $A_{f\leftarrow i}$ the emission coefficient [95]. A relative value for the electron temperature is given by the ratio of the H line intensities [96]. If the presumptions are valid a Boltzmann plot of the expression of the left hand side of

5

Experimental procedures

5.1 T-CVD growth of MWCNT

The substrates for thermal CVD growth of carbon nanotubes are prepared according to the description in section 3.3.

Thermal CVD growth of carbon nanotubes was used only occasionally for the work in this thesis. For a thorough discussion about growth conditions for different types of CNTs in our lab using T-CVD please refer to [97]. In this work the recipe used for tube growth was the same in all instances.

For the use of MWCNTs as microcooling fins, pre-patterned catalyst films evaporated onto a Si(100) wafer were used. The pattern was prepared by photolithography. A number of different strip patterns were prepared, with different strip widths and pitches. The catalyst consist of an evaporated $10\,\mathrm{nm}$ layer of Al_2O_3 under a $1\,\mathrm{nm}$ layer of Fe.

The growth was performed using acetylene as a carbon precursor and hydrogen and argon as buffer gases. The sample was placed in the centre of the quartz tube, at the centre of the furnace hot zone. After the tube was sealed it was pumped down to $< 1\,\mathrm{mbar}$ after which it was flushed with a mixture of Ar and H_2 to fill it to ambient pressure and heating was turned on. The growth temperature used

was 750°C. When the growth temperature was reached the acetylene was turned on. The flow rates of the gases were 5:200:500 for C_2H_2:H_2:Ar respectively. The growth time was varied between 10 and 45 min for different length of the tubes.

However, the efforts were often hampered by bad reproducibility of the growth process. Many times the growth was inhomogeneous over the samples and sometimes nothing grew at all, even under nominally similar growth conditions. The reason for this in not clear, but could be due to contamination of the chamber either by pump-oil or some contamination in the gas flow system. Other sources of error could be the iron source used for evaporation or some mistake in handling of the samples during lift-off and dicing. This underscores the sensitivity of the CNT growth process and the utmost importance of standardised handling of the samples during all stages of the process, from empty wafer to finished growth.

5.2 PE-CVD growth of nanotubes and nanofibres

What makes plasma-enhanced CVD of carbon nanotubes and nanofibres such an attractive growth method is the very good control of growth position and length that it offers. By pre-patterning small catalyst dots, that each grow only one VACNF, it is possible to have extremely good control of the exact position of the grown fibres. The goal for the PE-CVD growth in our group is to be able to grow CNTs or CNFs directly into pre-fabricated devices. The control of the growth positions also offers the possibility of using carbon nanotubes for e.g. photonic crystals, and many other applications.

Much of the work in this thesis is dedicated to analysing the effect of different growth conditions. For this reason the system for optical emission spectroscopy (OES) of the light from the plasma was set up, as well as the laser reflection measurement for in situ monitoring of CNT growth.

As was described in chapter 4 a plasma can exist in vastly different conditions, and even a small glow discharge plasma like in our set-up has a wide range of (more or less) stable operation. There are many parameters that control the way the plasma functions; the pressure, the gas composition, the current, the cathode temperature, just to mention the most important ones. These parameters are mutually interconnected, and it is unfortunately not possible to change one parameter and hold the rest constant, at least outside a narrow range. Instead only certain combinations lead to a stable plasma. Thus the parameter space one would need to map out is a strangely shaped body in a many-dimensional space. And of course, not all regions with stable plasma lead to good CNT growth. Instead of setting out on

the impossible quest of charting the parameter space described above, we try to investigate which factors are important by making short excursions from a point known to facilitate good conditions for CNT growth. This point, or rather these points, was found through a combination of laborious research, luck and instrumental constraints by my predecessors in the lab. Below will follow a description of the standard recipes for growth of MWCNTs and VACNFs. After that there will be a discussion about the experiments performed straying from those recipes.

MWCNT growth

The growth of vertically aligned MWCNTs in our PE-CVD system is limited to forests of tubes grown either on patterned substrates or substrates completely covered with catalysts. The width of the individual CNT pillars should be at least a few $\mu\mathrm{m}$ on each side. The MWCNTs remain standing by supporting each other through van der Waals interaction. When the width-to-height-ratio of the nanotube pillars become too small they usually topple. Forests of nanotubes with uniform height have been shown to be very good field emitters, especially very long tubes with thorn-like protrusions on the side walls [98].

MWCNTs are grown using Fe as a catalyst. A $1\,\mathrm{nm}$ layer is the normal catalyst thickness. The standard growth procedure is:

1. The substrate is place on the heated cathode surface and introduced into the chamber.
2. The chamber is pumped using a turbo molecular pump (TMP) to a pressure $< 10^{-5}$ Torr.
3. The heater is set to 700°C.
4. The premixing chamber is filled with a C_2H_2:H_2-mixture in the proportions 1:9. The filling pressure is 180 Torr.
5. A DC-voltage is applied to the anode.
6. The valve between the growth chamber and the TMP is closed.
7. The valve between the growth and the premixing chambers is opened releasing the gas mixture into the growth chamber. The final pressure is 8 Torr.
8. After the growth is finished, the voltage and heater are turned off and the chamber pumped out using the TMP.

9. The cathode and the substrate are allowed to cool down to room temperature in vacuum.

The applied DC-voltage is provided by a power supply with a maximum voltage of 1250 V and a maximum current of 250 mA. The voltage is set for the maximum value and the actual applied voltage is controlled by the current limitation setting and the I-V-characteristics of the plasma. The standard plasma current used is 15 mA. This corresponds to a current density at the cathode of $\sim 1-1.5\,\mathrm{mA cm^{-2}}$. The distance between the cathode and the anode is $13\mathrm{mm}$, but the interelectrode distance and the shape of the anode has no influence on the plasma close to the cathode.

The growth time was varied between 10 s and ca 1 h. When the desired growth time is reached the gas inlet is closed and the valve to the already running TMP is opened. The chamber is evacuated to below 10^{-3} Torr in a matter of seconds. The growth is brought to a halt within 5 s. For the shortest growth times, lower than 3 min static gas conditions were used, i.e. the correct gas amount is let into the growth chamber with all valves closed. For the longer times dynamic conditions were used. The combined inflow of acetylene and hydrogen is set to 250 sccm. The constant pressure is maintained by an automatic regulating valve on the pump-line. The ratio of C_2H_2 to H_2 is usually set to 1:9, but changing it between 1:3 and 1:20 results in no change of the nanotubes grown. Thus within a reasonable interval, the gas mixture has a small influence on the nanotube growth.

During the investigation of the current dependence, the current was changed between 7 mA and 70 mA. For a lower current than 7 mA it was not possible to get any stable plasma, just irregular flashing. Above 50 mA the plasma was well into the abnormal glow and started to discharge to other places of the chamber apart from the designated cathode.

VACNF growth

The procedure during growth of vertically aligned nanofibres is very similar to the MWCNT growth. The catalyst used for VACNFs is 10 nm Ni. If the fibres were to be grown on a metal underlayer an intermediate layer of 10 nm Si or Al_2O_3 was included. For VACNFs it is possible to grow either forests of fibres from a fully catalyst-covered substrate or individual still vertically aligned fibres from pre-patterned nanosized catalyst dots. The mechanism behind the alignment was discussed by Merkulov *et al.* [99].

In VACNF growth NH_3 is used instead of H_2 as a buffer gas. Since NH_3 is an electronegative gas this puts a limit on how little C_2H_2 can be mixed into the gas and still form a stable plasma. The standard procedure is:

1. The substrate is place on the heated cathode surface and introduced into the chamber.
2. The chamber is pumped using a TMP to a pressure $< 10^{-5}$ Torr.
3. The heater is set to 700°C.
4. The premixing chamber is filled with a C_2H_2:NH_3-mixture in the proportions 1:5. The filling pressure is 90 Torr.
5. A DC-voltage is applied to the anode.
6. The valve between the growth chamber and the TMP is closed.
7. The valve between the growth and the premixing chambers is opened releasing the gas mixture into the growth chamber. The final pressure is 4 Torr.
8. After the growth is finished, the voltage and heater are turned off and the chamber pumped out using the TMP.
9. The cathode and the substrate are allowed to cool down to room temperature in vacuum.

As with MWCNT growth, for the shorter growth times static gas conditions were used and for longer times dynamic conditions.

5.2.1 Laser reflection measurements

The laser reflection (LAR) measurements for *in situ* monitoring of CNT growth were installed as a late addition to the growth chamber. therefore it is unfortunately, due to geometric constraints not possible to perform the LAR measurement simultaneously with the OES.

The LAR measurements were used in connection with growth of MWCNTs from substrates fully covered with a catalyst film. The laser, which is located on the top of the chamber, is focussed through a view-port onto the Si-substrate. A photodiode is placed on the outside of the chamber. When the growth temperature has

been reached the detector is aligned so that the reflected laser spot hits the centre of the detector. This is because due to thermal expansion of the heater and the clamp the substrate moves slightly during heating which can shift the reflected spot as much as $2\,\mathrm{cm}$. Since the Si wafer is highly polished this marks the highest reflectivity. Before the growth starts the lights are turned off in the lab to limit the background signal and the data collection is started. The diode current is read by a multimeter and the data collection is controlled by a LABView program. The system collects 160 datapoints per second during the first stages of the growth. After the initial fast decrease in reflectivity when the readout has stabilised the data collection is switched to a lower rate, with significantly lower noise.

The thickness of the nanotube film can be determined by looking at the Fabry-Perot interference peaks that appear as oscillations in the reflection measurements [100]. These fringes appear at constant increments in the film thickness.The phase shift between the beam reflected at the top layer and the one going through the CNT film with thickness d and reflected at the substrate is given by

$$\delta = \frac{4\pi d}{\lambda_0}\left(n_{\text{eff}}^2 - n_{\text{amb}}\sin\vartheta_i\right)^{1/2}, \tag{5.1}$$

where λ_0 is the wavelength in vacuum, ϑ_i the incident angle, n_{eff} the effective refractive index of the CNT film and n_{amb} the refractive index of the surrounding medium, in this case ≈ 1. For constructive interference $\delta = 2\pi$, so solving for n_{eff} gives

$$n_{\text{eff}} = \sqrt{\left(\frac{\lambda_0}{2d}\right)^2 + \sin^2\vartheta_i} \tag{5.2}$$

The growth time and growth conditions were altered to investigate the effect on the CNT growth. The length of the tubes were measured independently with SEM.

5.2.2 Optical emission measurements

The studies of the emission spectra from the plasma during different growth conditions were performed in conjunction with growth measurements.

The collection of spectra from the plasma is done with a spectrometer and an ICCD-camera controlled by a computer. The control and data collection is done by the program WinSPEC (Roper Scientific). When the spectrometer is set for a central wavelength the CCD chip of the camera is illuminated by a roughly $50\,\mathrm{nm}$ wide spectral region. For collecting a full spectrum from $300 - 850\,\mathrm{nm}$

the program uses a stepping function collecting a number of spectral files that are subsequently glued together to a full spectrum. The time to take one spectrum is roughly 1 minute.

Since the spectral sensitivity of the optical system is not constant for all wavelengths the system was calibrated using a halogen lamp with known spectrum that was placed at the same position as the substrate-holder.

The growth parameters were kept the same during all experiments, except for the plasma current. The growth time was 15 minutes and the other parameters kept at their standard values as described above. Spectra were recorded for different plasma currents ranging from $7\,\mathrm{mA}$ to $70\,\mathrm{mA}$, and the results were correlated with SEM images of the grown tubes. As a control, spectra were recorded both at the beginning of growth and after about ten minutes to check if the plasma conditions changed over time. They did not, and neither was this expected since the growth was performed with a dynamic gas flow where there is a constant influx of gas at the same time as gas is pumped out of the system.

The intensities of the Swan band emission peaks were analysed using a peak-fit program (Wire2) to determine the vibrational temperature of the C_2 molecule in the dc plasma.

5.3 Spectroscopy during field emission

Much work has been done in the group concerning electron field emission from carbon nanotubes. For a thorough description of these experiments the interested reader is referred to the PhD-thesis of Martin Sveningsson [101]. This description is mainly concerning the OES measurements performed.

The field emission measurements were performed on films of MWCNTs grown with T-CVD on Si substrates. The substrate was attached to the holder with a conducting glue and inserted into the vacuum chamber. The voltage was increased stepwise and at each point the current and the light emission was measured. The relative emission intensity was measured using the zeroth-order diffraction peak in the spectrometer. Spectra in the range $400 - 900\,\mathrm{nm}$ were recorded using the step-and-glue procedure described above.

6

Results and discussion

6.1 Optical emission spectroscopy

The optical emission spectra from the plasma under our typical growth conditions are very rich as can be seen in figure 6.1. The spectra contain hundreds of peaks, most with very low intensity and some very prominent bands. The Swan bands from C_2 are clearly visible. The origin of the Swan bands is the transition between the $\mathrm{d}^3\Pi_g$ and the $\mathrm{a}^3\Pi_u$ electronic levels of the C_2 molecule. The transition to different vibrational states leads to the division of the emission into bands. In the spectra, the emission bands with $\Delta\upsilon = -1, 0, 1, 2$ are observed, where $\Delta\upsilon$ denotes the difference in vibrational level between the upper and the lower electronic levels. The band with $\Delta\upsilon = -2$ is only weakly visible. Other prominent bands are from CH and, in the case of the C_2H_2:NH_3 plasma, CN. Also clearly visible are the atomic hydrogen peaks of the Balmer series. However, many small peaks remain unidentified. The spectra were analysed in two ways. First the Swan band transitions were analysed to find the vibrational temperatures of the C_2 molecules according to the method described in section 4.2. Unfortunately it is not possible to do the same analysis for the CH and CN species. The bands from these species appear in the very peak rich region of the spectra below $450\,\mathrm{nm}$ so the peaks overlap with peaks from other bands from other species. Secondly the relative emission intensity of chosen CH, C_2, CN and H were analysed at different

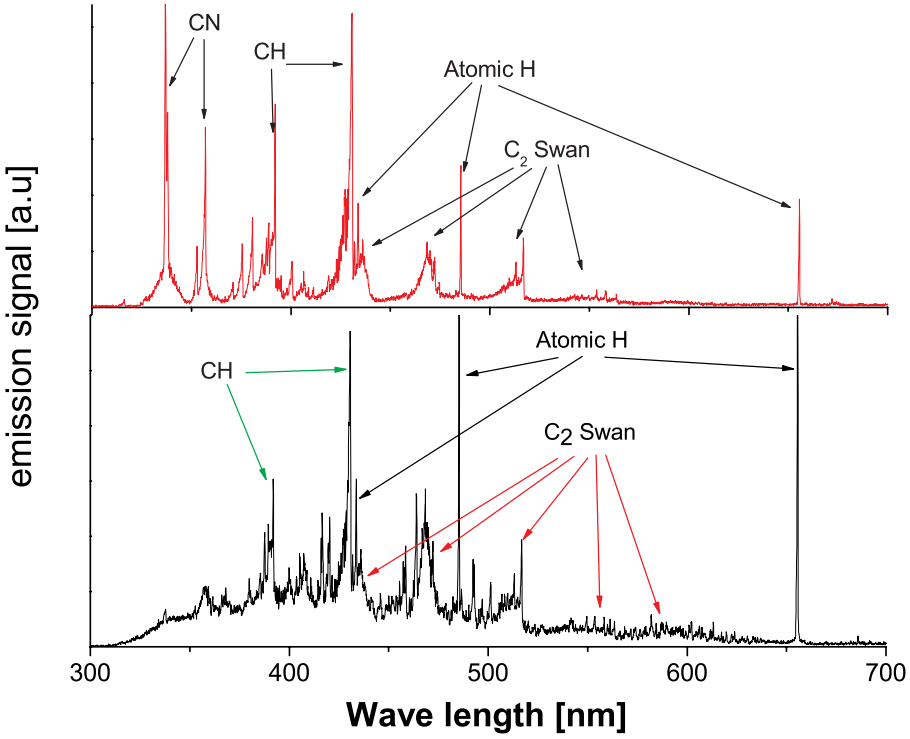

Figure 6.1: Typical optical emission spectra from the cathode layer of a C_2H_2:NH_3 plasma in the upper panel and a C_2H_2:H_2 plasma in the lower panel. Arrows mark the most prominent emission bands.

plasma currents. This was done to get an idea of whether the plasma composition is changing with varying conditions. The emission intensity for a particular peak might change with changing conditions and the intensity can therefore not be directly related to the abundance of the species. However, the changes of the relative emission intensities give an indication of the changes in plasma composition.

The reason for the OES measurements was the marked change in CNT/CNF growth that occurs when the plasma current is changed. In figure 6.2 the effect of changing the plasma current can be seen on the growth of VACNFs under otherwise similar conditions. There is a clear tendency for thickening of the fibres at higher currents. At 10 mA the fibres grow slowly. The longest fibres are found for a plasma current of 30 mA. At 50 and 70 mA the fibres are covered with a thick layer of carbon material. This is most likely amorphous, although no analysis, other than SEM, has been performed to confirm this. A similar behaviour was observed for MWCNTs grown from Fe catalyst as is seen in figure 6.3. Here

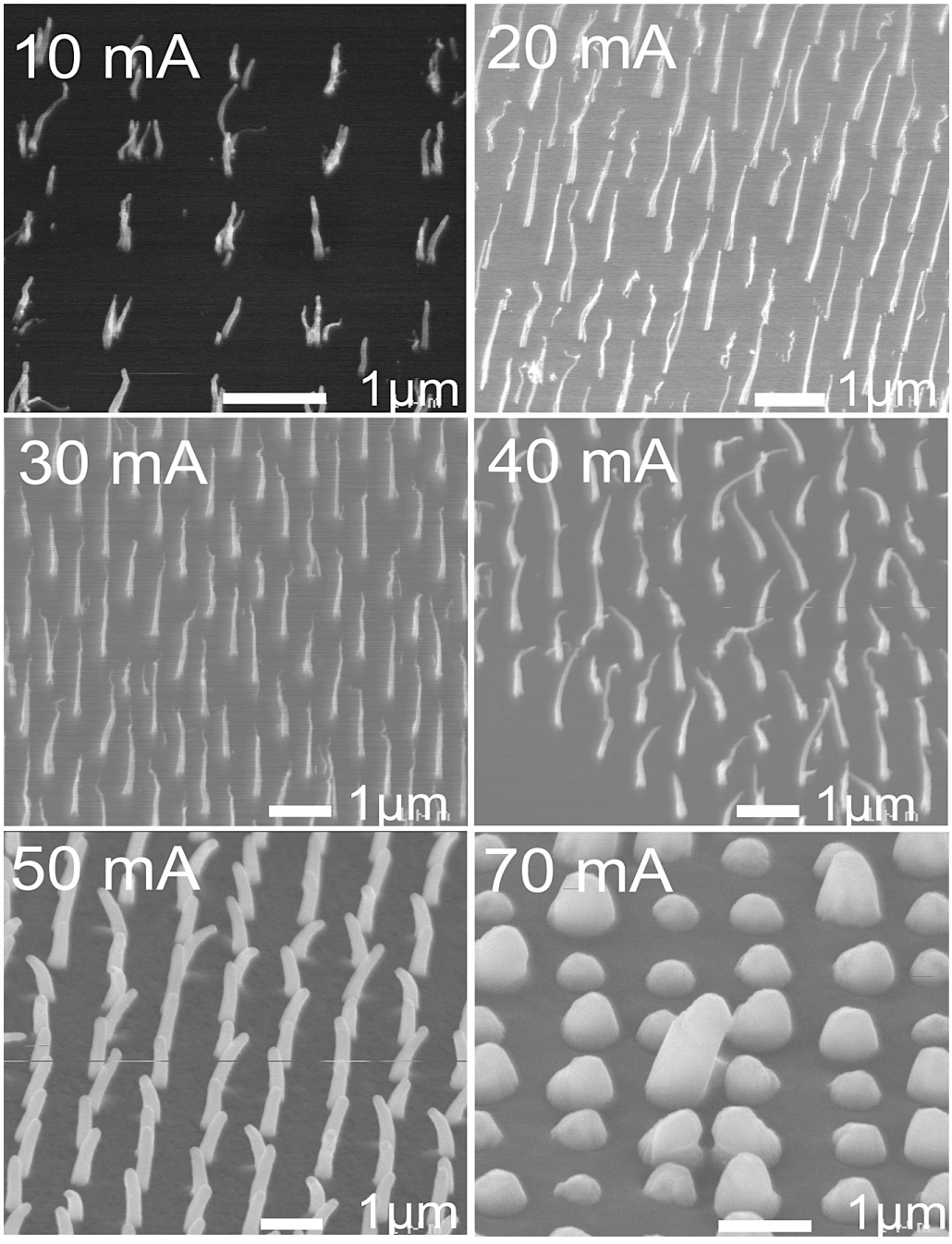

Figure 6.2: SEM micrographs of VACNF grown for 15 minutes at different plasma currents.

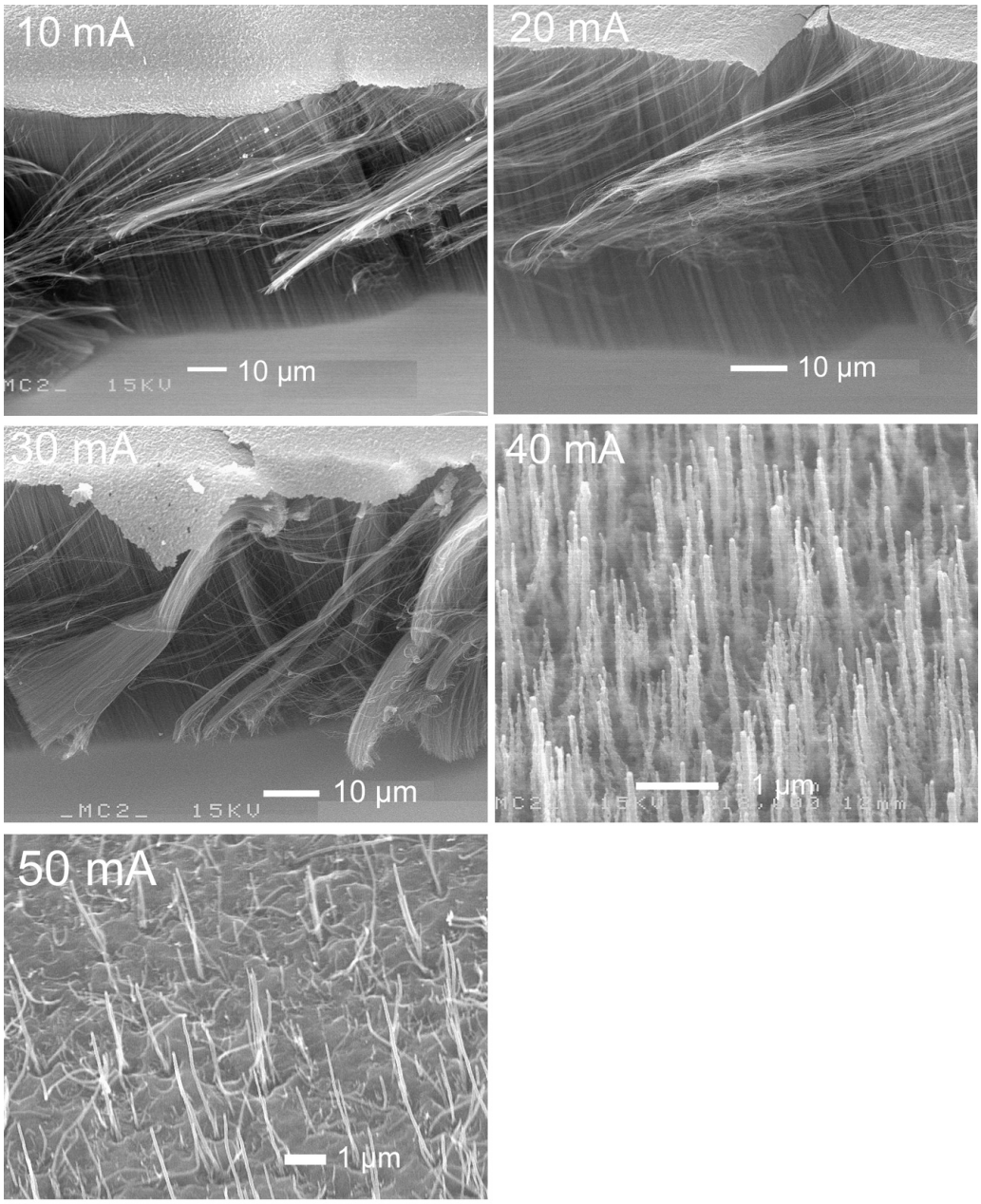

Figure 6.3: SEM micrographs of MWCNT films grown for 15 minutes at different plasma currents.

the effect was even more dramatic. For $10 - 30\,\mathrm{mA}$ no discernable difference between the films could be seen. With a plasma current of $40\,\mathrm{mA}$ the nanotube growth changed abruptly. Instead of a dense forest of thin MWCNTs there was growth of squiggly fibre-like structures. When the current was increased further the forest became sparser. Between the fibres the substrate is covered by a layer of amorphous carbon. If the current was increased further the complete surface was covered with amorphous carbon with no tubes nor fibres sticking up. In order to investigate the changing growth conditions the OES was set-up. A thorough discussion about these results are presented in Paper III.

The behaviour of a transition from MWCNT growth to VACNF growth has been seen earlier by Delzeit *et al.* [76]. In an inductively coupled plasma (ICP) they noticed that if the rf power on the substrate was increased beyond a transition point of ca $40\,\mathrm{W}$ the MWCNT growth instead turned into tip-grown VACNF. The increase of rf power in the substrate leads to a higher self-dc bias of the substrate. At $120\,\mathrm{W}$ rf power this correspond to a dc bias of ca -400 V. They attribute this, using OES to monitor the emission from H, to the increase in hydrogen atoms in the plasma. A similar but opposite trend is presented in the review article on PE-CVD growth of CNTs by Meyyappan *et al.* [102] where Ni catalysts grow forests of VACNFs at low bias dc PE-CVD and MWCNTs at higher biases. In our experiments we have not succeeded in growing forest of MWCNTs from Ni catalysts, but this is probably be due to not being able to reach high enough bias in our set-up. When growing VACNF forests from films of catalyst the fibres don't swell as much as in figure 6.2 from dots, but rather just grow short and stocky, with "hairy" protrusions as can be seen in figure 6.4A. However, very close to the edge of the sample, where the field is amplified by the edge, nanotubes are interlaced with the fibres as in figure 6.4B. There is also an indication of grass-like growth of tubes between the fibres in panel A. If we could reach higher current, maybe the growth would result in aligned forests of MWCNTs.

The first analysis of the OES spectra was to look at the Swan bands of C_2 to calculate the vibrational temperature of that species. The Swan bands are easily visible and typical spectra are shown in figure 6.5. The spectra were fitted using Gaussian peaks in a peak fit program. Summation over the different band strengths were performed according to eq. 4.10. In figure 6.6 the sum of the band strengths is plotted against the term value. A linear fit through the data points gives the vibrational temperature of the C_2 for this particular current. Similar plots were prepared for currents in the interval $7 - 70\,\mathrm{mA}$. The error bars on the points in figure 6.6 come from an estimated error in peak area ranging from 10% for clearly resolved peaks to 50% for very small peaks hardly distinguishable from the noise level. The total error for each band was calculated using the Gaussian

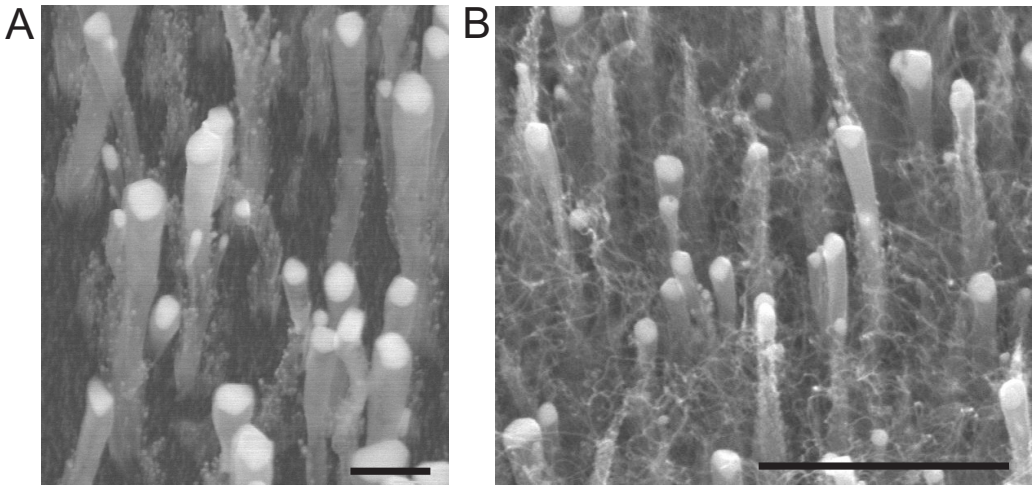

Figure 6.4: SEM images of VACNFs grown at high plasma current, $70\,\mathrm{mA}$. The image in A is from the middle of the wafer. The scale bar is $100\,\mathrm{nm}$. The image is B is taken very close to the edge of the sample where the field is enhanced by the edge. The scale bar is $1\,\mu\mathrm{m}$.

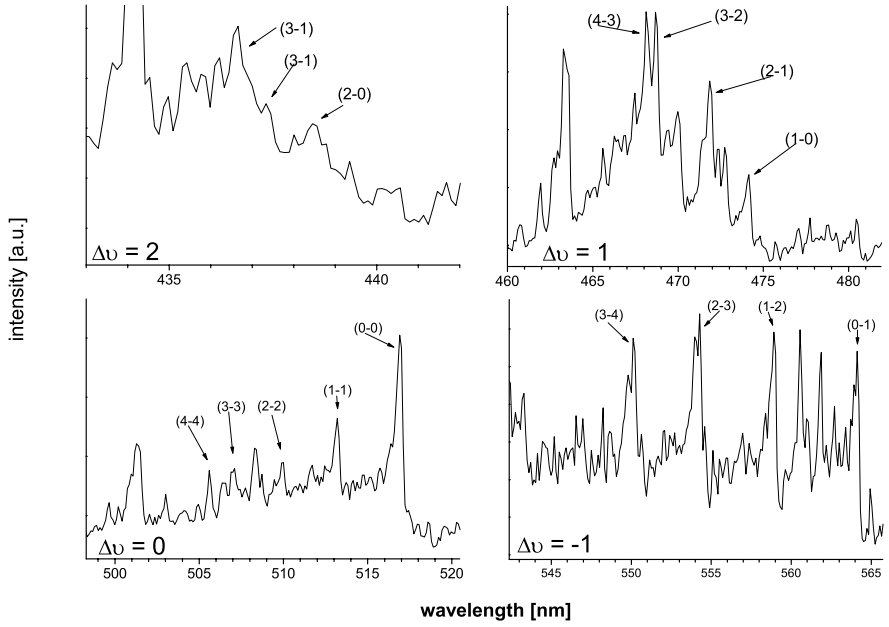

Figure 6.5: Typical spectra showing the Swan bands with $\Delta\upsilon =, -1 - 0, 1, -2$

.

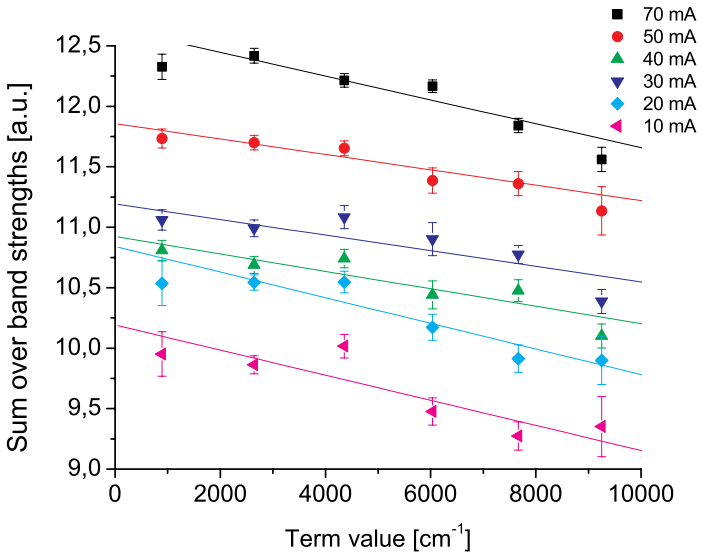

Figure 6.6: The logarithm of the sum of band strengths for the Swan band in a C_2H_2:NH_3 plasma. The x-values are calculated according to eq. 4.12. The lines are linear fits to the data points.

error propagation formula. The temperature is calculated by making a linear fit to the sums of band strengths. The slope of the line gives the vibrational temperature according to eq. 4.13.

The temperature for the two plasmas at different plasma currents can be seen in figure 6.7. What one immediately notices is the very high temperature compared to the "normal" translational temperature of the gas. This should be somewhere between the room-temperature of the chamber walls and the 700°C of the heater. Instead the vibrational temperature is in excess of 10000 K. There are also no large variations over the range of plasma currents. The large uncertainty makes it difficult to say whether there really is a peak around 40 mA for the C_2H_2:NH_3 plasma or if the temperature keeps constant. The temperature of the different plasmas is also almost identical. Since the coupling between the vibrational and translational degrees of freedom in a molecule is quite weak the vibrational temperature can be completely independent from the gas temperature [103]. In the plasma the hot electrons dissipate energy through collisions with the gas molecules, mainly exciting the vibrational and rotational degrees of freedom. Since the electrons in the cathode sheet of a DC glow discharge can have energies of tens of eV [104, 105] it is not surprising that we find such high temperatures in our measurements. The very weak dependence of the temperature on the plasma current is also not sur-

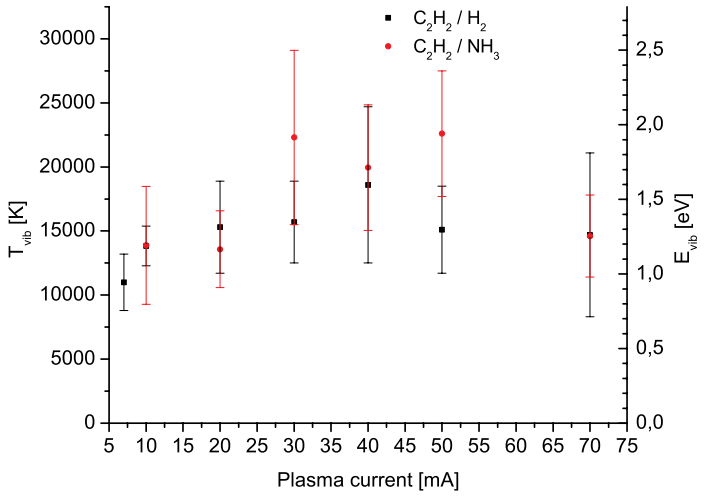

Figure 6.7: The vibrational temperature of the C_2 molecule as a function of the plasma current for both C_2H_2:H_2 and C_2H_2:NH_3 plasmas. On the right-hand y-axis the temperature is translated to energy in eV.

prising. Calculations by Hash *et al.* [104] show that the variation of the electron energy with the bias voltage is very small. This is confirmed by recent measurements by Lin *et al.* [106]. Measuring the electron temperature using the hydrogen emission according to eq. 4.14 showed that the hydrogen atoms are not in thermal equilibrium. The levels 4 and 5 are over-populated, and the effect is more pronounced for the NH_3 plasma than for the H_2 plasma. The reason for this is not clear at the moment.

The spectra were also analysed for the emission intensities of the species C_2, CH, CN and H_2. The emission intensity can be seen as an indication of changing composition of the plasma. The lines chosen for this purpose were the dominant lines in the central region of the spectra, the hydrogen line at $485\,\mathrm{nm}$, the C_2 Swan $\Delta\upsilon = 0$ band head at $516\,\mathrm{nm}$, the CH Q-head at $431\,\mathrm{nm}$ and the CN violet band head at $388\,\mathrm{nm}$. In figure 6.8 the emission ratios for the C_2H_2:H_2 plasma are shown. At $30\,\mathrm{mA}$ plasma current the CH peak saturated the camera. Thus the emission intensity is displayed as much lower than in reality. Compared to the H line both CH and C_2 are decreasing as the current goes up. The same trend can be seen in the C_2H_2:NH_3 plasma, shown in figure 6.8. Both CH and C_2 decrease, whereas the emission from CN is increasing dramatically with higher current. This is a clear indication of increased decomposition of acetylene in the gas phase since the cyanide radical cannot be produced directly by partial decomposition of any of the provided gases. A possibility is that it is produced

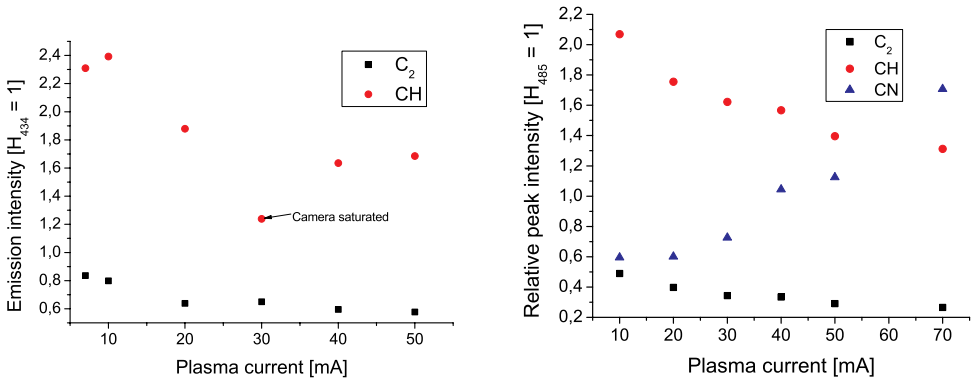

Figure 6.8: The relative emission intensity for the C_2H_2:H_2 plasma (left) and the C_2H_2:NH_3 plasma (right) for different currents. The intensity of the H_γ line is set as unity.

in the reaction between the plasma and the fibres instead of in the gas phase. The emission from atomic hydrogen also increases with increasing plasma current. Hydrogen has been shown to change the angle between the graphitic basal planes and the nanotube axis [107, 108]. One mechanism that could be responsible for this is the hydrogen atoms can stabilise the dangling carbon bonds at the edges of the graphite planes that make up the fibre.

The decrease of C_2 with increasing current is in opposition to the findings of Lin *et al.* [106] in an ICP. In their experiment the emission from both CH and C_2 increase as the ICP power is turned up. However, our results are in concordance with recent experiments by Lim *et al.* [77], also using a DC glow discharge plasma.

Plasma-enhanced CVD growth of carbon nanotubes is a delicate balance between catalytic growth of tubes, non-catalytic deposition of amorphous carbon and etching of the tubes/film by reactive species in the plasma. Looking at the evolution of VACNF growth with increasing current one can see an increasing growth rate up to about 25 mA after which the fibres become shorter and more conical. This is due to increased etching by the high ion flux [109]. In the case of Fe growth MWCNT films the growth rate is constant up to 30 mA. That the growth changes so abruptly at 40 mA shows that the balance is more delicate in the case of MWCNTs than for VACNFs. Looking at the I-V curve for the C_2H_2:H_2 plasma (see figure 6.9) one sees that the voltage drop over the plasma increases slowly at low currents, but shows a higher increase between 30 and 40 mA. This is probably because we are leaving the normal glow discharge region and entering the abnormal glow with an increased current density. The increased amount of reactive species in the plasma can lead to an increase in non-catalytic deposition of carbon on the sub-

strate which may lead to poisoning of the catalyst particle. The poisoning has been shown to lower the growth rate, or even terminate the growth completely [110]. Also, molecular dynamics calculations have shows that an excessive carbon flux to the catalyst particle will lead to the particle becoming covered by a graphitic layer. The particle then loses its catalytic activity [67]. An interesting side-note is

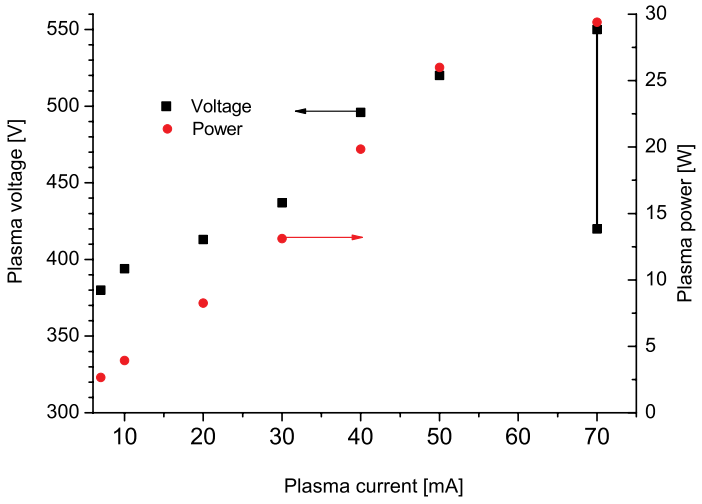

Figure 6.9: The voltage drop over the plasma as a function of the plasma current. On the right hand axis the plasma power is plotted. The two data points at 70 mA shows that the plasma was unstable and shifted between two different configuration.

that close to the clamp used to hold the substrate to the heater the tubes are growing normally. This is because the metallic clamp shields the electric field which is markedly lower near the clamp.

The OES measurements showed that although the plasma conditions do not change dramatically the effect on the growth is still significant. In agreement with Delzeit et al. [76] and calculations by Meyyappan et al. [102] increasing the current is accompanied by an increase in the amount of, or at least emission from, hydrogen atoms. It was also shown that changing the plasma current does not lead to a significant change of the vibrational temperature of the C_2 molecule.

One other plausible explanation to the change in growth behaviour with changing plasma current is that the increased ion flux to the cathode leads to a local temperature increase at the substrate surface. This effect is examined in an article by Teo *et al.* [111], where the heating by the plasma alone is enough to heat the substrate to 700°C and accommodate for good growth conditions. Compared

our conditions the plasma power used by Teo *et al.* are very high, an according to their figures the power used in our set-up should only amount to very limited heating of the substrate. Interestingly, despite a very high plasma current (up 294 mA with a cathode surface comparable to our) the manage to grow quite nice nanofibres, albeit with a much lower rate than at "normal" conditions using an external heater and lower plasma power. They attribute this decrease in growth rate with the increased gas phase decomposition of acetylene and increase in methane abundance. Calculations and experiments by the same group [112] also show a significant increase in the acetylene decomposition already at low plasma powers.

The plasma power is not large enough to lead to significant heating of the whole substrate in our case, but if the thermal contact between the substrate and the heater is bad, so that only the substrate is heated and not the bulk of the heater, the substrate can be heated by the ion impact on the surface. However, the high thermal conductivity of silicon does quickly equalises any temperature difference over the substrate. Calculations with reasonable assumptions on heat-losses, but neglecting convection, shows that if the thermal contact between the heater and the substrate is very poor, the ion flux might heat the substrate up to 50°C. This should not be enough to account for the dramatic change in growth conditions. Attempts to test the plasma heating of the substrate has been made by trying to grow nanotubes at a high current, but with a lower heater temperature. These experiments have failed to achieve good nanotube/fibre growth.

6.2 *In situ* growth rate measurements

Using the laser reflection measurements described in section 5.2.1 the growth of carbon nanotubes was monitored in situ. Unfortunately, the placement of the view-ports and the substrate heater in our set-up did not allow for simultaneous LAR and OES measurements. Measurements were performed at standard growth conditions with an Fe catalyst and mostly using a plasma current of 15 mA, which is the one most commonly used during growth of MWCNT films.

The reflected intensity is measured before the gases are let into the system, and drops rapidly when the growth starts. During growth one can clearly observe oscillations from Fabry-Perot interference as is seen in figure 6.10. As can be seen the oscillations are not exactly simultaneous which shows some variation in the growth speed for different samples. By stopping the growth after various times during this initial Fabry-Perot stage and measuring the length of the grown tubes using SEM the oscillation period can be related to an increment in the film

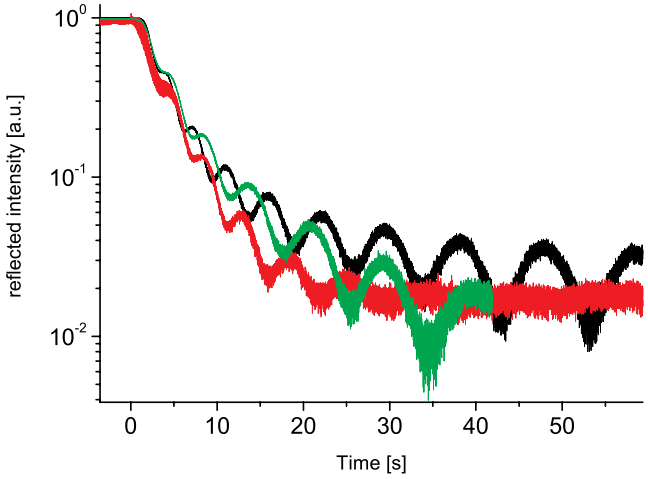

Figure 6.10: Typical LAR measurements for three different samples under similar conditions.

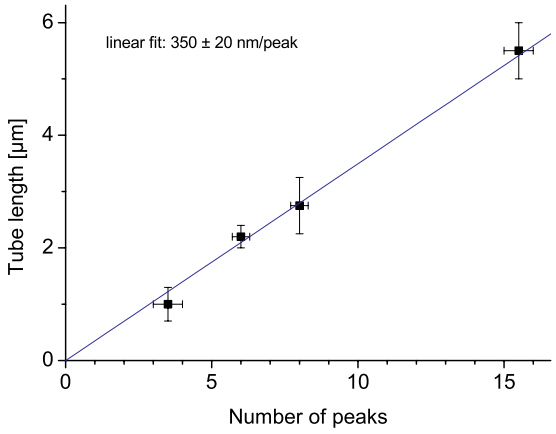

Figure 6.11: The Fabry-Perot peaks plotted against the length of the grown tubes as measured by SEM.

thickness. In figure 6.11 the thickness of the vertically aligned MWCNT film is plotted against the number of Fabry-Perot peaks that have passed since growth started. The SEM images used for the length measurements are seen in figure 6.12. The measured tube-lengths and the peaknumber was fitted with a line which gives an increment in tube-length of $350 \pm 20\,\mathrm{nm}$ per peak. Using eq. 5.2, with $d = 350\,\mathrm{nm}$, the effective refractive index of the MWCNT film is calculated to

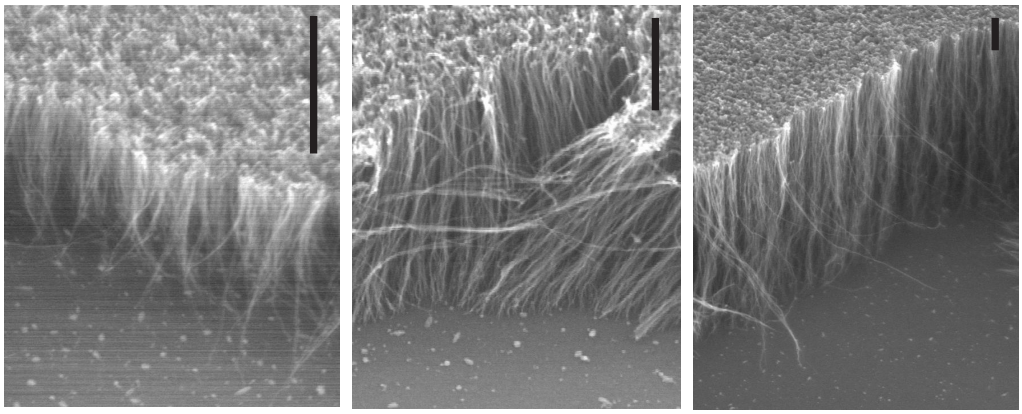

Figure 6.12: SEM images of three vertically aligned MWCNT films. The images were taken where the films were scraped with tweezers to show a side-view of the forests. The images are taken at 45° angle, and the scale bar on each image is $1\,\mu\mathrm{m}$ in the vertical direction.

$n_{\mathrm{eff}} = 1.12 \pm 0.06$, in good agreement with Geohegan *et al.* [100]. By plotting the time of the appearance of the peaks against the tube length one can get information about the growth rate of the tubes. In figure 6.13A the times for the peak

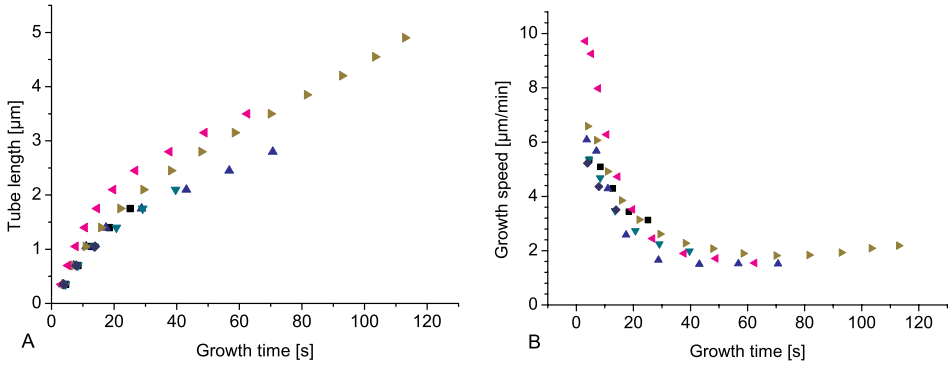

Figure 6.13: In A) the length of the grown tubes as a function of time. The dots are the times of maxima in the LAR intensity, and the different series are different samples grown under nominally the same conditions. In B) is the derivative of A), which gives the instantaneous growth rate.

values have been plotted against the length of the tubes at those times, given as $350\,\mathrm{nm}\times$ number of the peak. In figure 6.13B the derivative of the curves in A are plotted. One can see that the growth rate initially is quite high, $\sim 6\,\mu\mathrm{m/min}$, but quickly slows down to reach a stable value around $2\,\mu\mathrm{m/min}$. The initial growth value is comparable to the one published by Kim *et al.* [113], however,

they never follow up their growth until the the growth rate levels out, but rather just see a steady decrease up until periods of Fabry-Perot peaks. The similar measurements performed by Geohegan *et al.* [100] show a comparable overall growth rate, though they do not show any time development of the rate. As can be seen most of the samples grow at a very similar rate, but one sample starts off much faster than the others. The reason for this is not known, since all the samples were grown under nominally the same conditions. Usually, the growth conditions in the plasma are very reproducible when the tubes are growing, but from many samples there is simply no growth at all, even though they were prepared from the same wafer and grown under the same conditions. In figure 6.14 LAR measurements and SEM image of a sample with only very few non-aligned tubes in a layer of amorphous carbon are shown. As was mentioned in section 3.2 about thermal

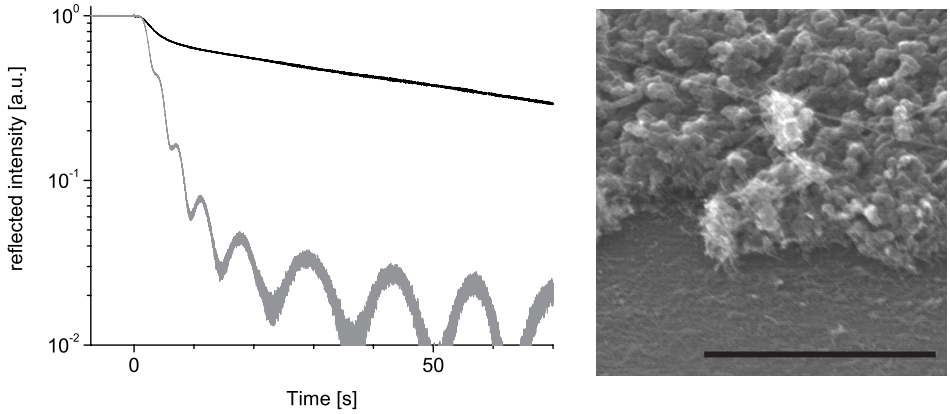

Figure 6.14: The LAR from a sample with no growth. The grey curve is the same as in figure 6.10 included for comparison. The right panel shows an SEM image of the film after growth. The scale bar in 1 μm.

CVD the reason for this behaviour is not known, but there must exist some critical component in the growth process that either turns growth off, or lets it proceed normally. Identifying this step must be given high priority.

When growing forests of nanotubes in the PE-CVD we have observed the emergence of a carbonaceous layer on top of the forests. This layer is very hard to remove and causes some problems during certain experiments. The layer is present on longer tubes, and is probably caused either by etching of the grown tubes by the ion bombardment in the plasma, or by non-catalytic deposition of carbon on top of the grown tubes. Although not mentioned in any papers, it can be seen in many published SEM images of PE-CVD grown nanotubes, e.g. figure 5 in ref. [102] if one knows what to look for. The development of this layer can be

seen in the LAR measurement as an increase in the reflectivity after some time of growth. A typical example is shown in figure 6.15. First the intensity drops as the

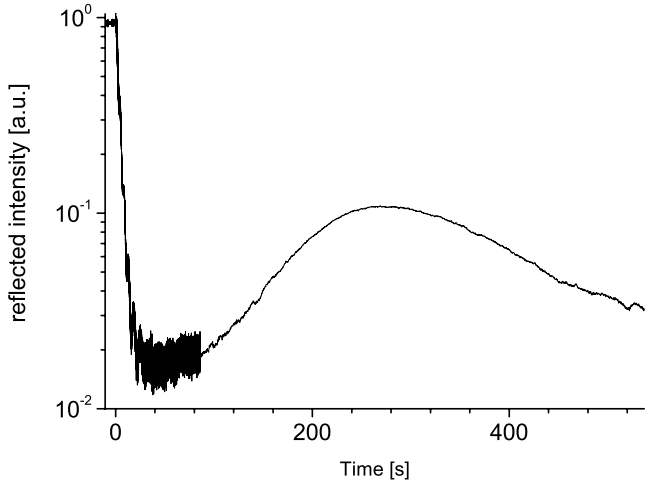

Figure 6.15: LAR measurements of a sample of nanotube growth. Note the increase in reflectivity after about 100 s.

nanotubes absorb the laser radiation. After a while the carbonaceous layer stars developing, and the scattered light from the cover layer increases the signal in the photo-diode again. This increase continues as the layer grows denser. When the amorphous carbon on top of the tubes starts resembling a homogenous layer, on the scale of the wavelength of the laser, the scattering turns into a more specular reflection. However, since the surface is not flat, only a small portion of the light is reflected towards the detector, and hence the intensity starts dropping again. To investigate the development of the cover layer the growth was stopped at different stages. In figure 6.16 one sees the clean nanotubes in the left panel, where the growth was stopped before the reflectivity started increasing. In the middle panel the growth was stopped when the reflectivity reached it local maximum after about five minutes growth. In the right hand panel one sees the fully developed cover, as a homogenous layer.

Raman spectra from MWCNTs are usually not as nice as from SWCNTs. Often, the D/G ratio is much larger than in the typical spectrum in figure 3.5 [109]. In figure 6.17 Raman spectra are shown for three different samples. The bottom sample is the sample from fig. 6.14 with only few tubes. One can clearly see that the D-line is much larger than the G-line. Also the G' line is visible at 2690 cm^{-1} as well as the C-H stretching line at 2950 cm^{-1} [114]. The latter is frequently

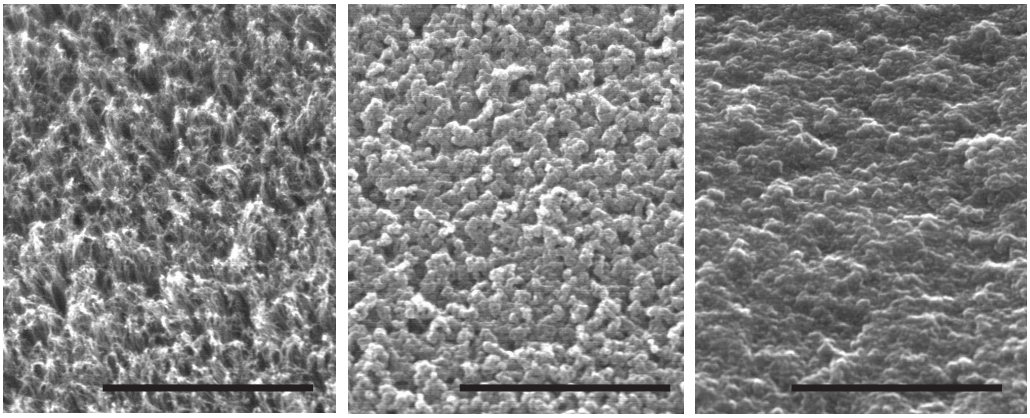

Figure 6.16: SEM images of the cover of the MWCNT forests grown with PE-CVD. The growth was stopped at different times. Left the growth was stopped when the reflection was at a minima, middle shows the film when the reflection has reached its local maximum, and the right panel shows the fully developed cover. The scale bars are 1 μm.

present in amorphous carbon films prepared by PE-CVD from hydrocarbon feedstocks [115]. At 521 cm^{-1} a small peak from the Si substrate is visible. The middle line comes from a sample with a developed cover on the top of the tubes. The D/G-ratio is lower than for the previous curve, but the disordered vibrations still dominate. The top curve shows the spectrum from a sample where the growth was stopped before the top-layer had time to form. The D/G-ratio is still not good, but there is a clear difference to the other films. The reason for the still bad D/G-ratio might be that amorphous carbon is already deposited on the tubes, but not abundantly enough to start growing together, or that the substrate is covered by carbonaceous material between the tubes. The film of tubes is very thin, so the laser penetrates through the film, as can be seen by the large Si peaks.

The LAR measurements give insight into the growth of the nanotubes in the PE-CVD system, and gives the possibility of monitoring the growth in situ. It gives valuable information about the formation of the cover layer on the films and a tool to optimise the growth to avoid it.

6.3 Blackbody radiation from MWCNTs during electron field emission

Carbon nanotubes look ideal as electron field emitters. They can conduct high currents, withstand high temperature, and their high aspect ratio amplifies the field

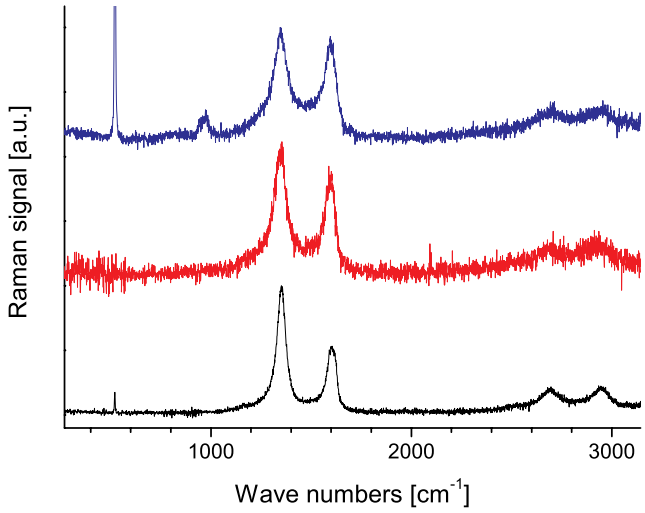

Figure 6.17: Raman spectra from three samples grown in the PE-CVD. The bottom curve shows the spectrum from the film in figure 6.14. The second curve is from a film with a fully developed covering layer, and the top curve is from a film where growth was stopped before the cover was formed. The excitation wavelength was $514\,\mathrm{nm}$.

strongly around the tip. During early field emission experiments it was noted that light emits from the space of the sample under the anode. Light like this had been noted previously, and the spectra measured consisted of a broad emission peak [116, 117]. This was interpreted as luminescence from discreet energy levels in the emitter tip. A OES set-up was constructed to investigate the the phenomena more closely. The result of this investigation is presented in Paper I. The field emission from films of MWCNTs is highly reproducible at low emission currents $\lesssim 1\,\mathrm{mA/cm^2}$. If the emission current is increased above this level the emission characteristic is no longer reproducible and a higher field is required to reach the same current again. In a Fowler-Nordheim plot, where $\ln\left(I/V_{\mathrm{appl}}^2\right)$ is plotted against $1/V_{\mathrm{appl}}^2$, I being the emission current and V_{appl}^2 the applied voltage, a metallic emitter is expected to give a linear relation. That this is also the case can be seen in figure 6.18. However at about $1\,\mathrm{mA/cm^2}$ the slope in the Fowler-Nordheim plot changes abruptly, something that has been observed both in films [118] and from individual tubes [119].

The behaviour is still linear, but with a lower slope. This is probably due to degradation of the emitters and/or the onset of "non-metallic" emission. The changes are more marked during the first scan than for subsequent ones. As can be seen in figure 6.18 the knee in the Fowler-Nordheim plot also mark the onset of light

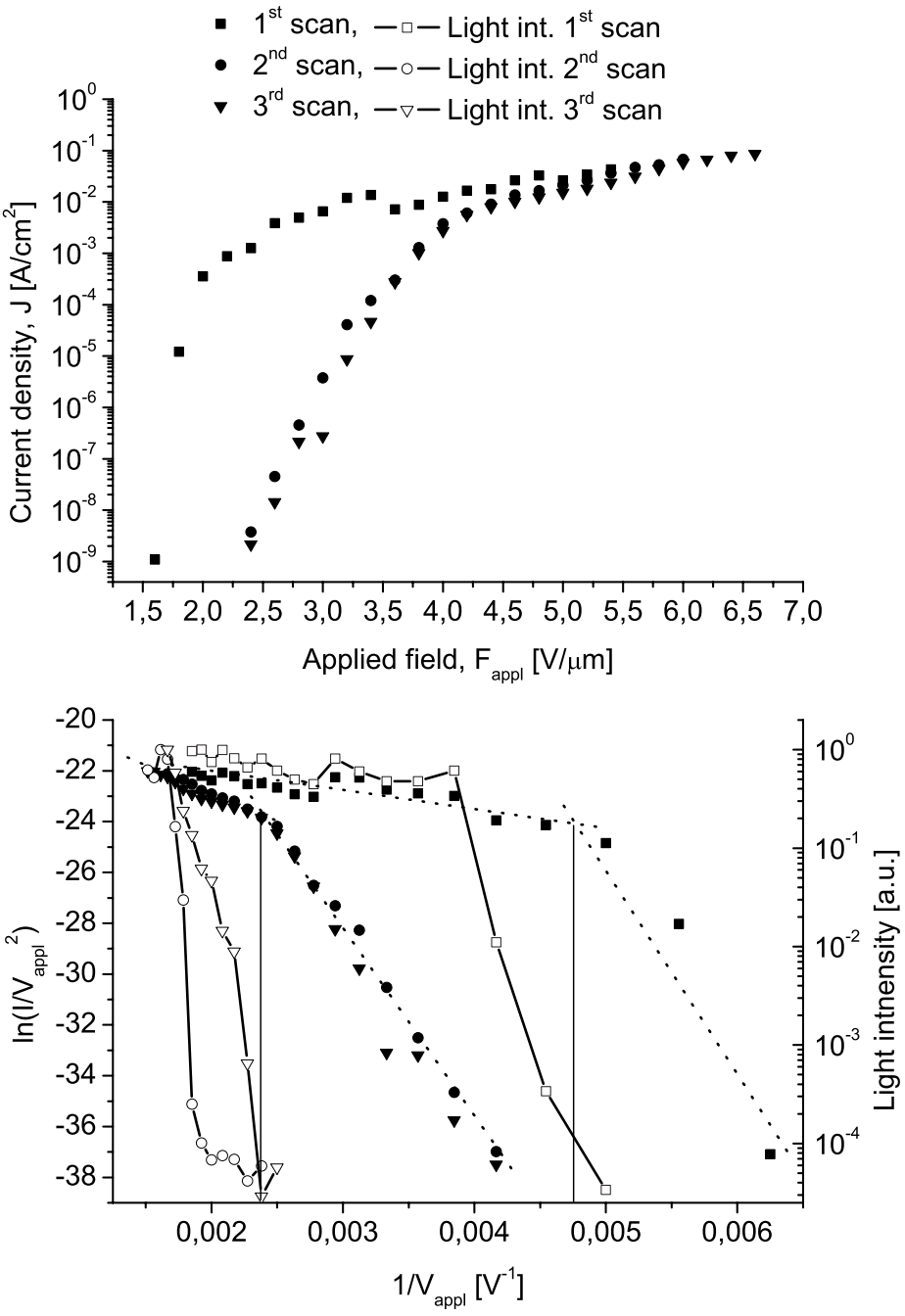

Figure 6.18: (upper panel) The field emission current density plotted against the applied field. (lower panel) Fowler-Nordheim plot of the data above. The right hand axis shows the total light intensity on a logarithmic scale. The onset of light emission is indicated by the vertical lines and corresponds to a change in the Fowler-Nordheim slope.

emission. This strengthens the case that the knee marks a real change in the film properties. Spectral measurement of the emitted light from a film of aligned MWCNTs is presented in figure 6.19 for a field emission current of $35\,\mathrm{mA/cm^2}$. The data is fitted using Planck's blackbody equation. This provides very strong

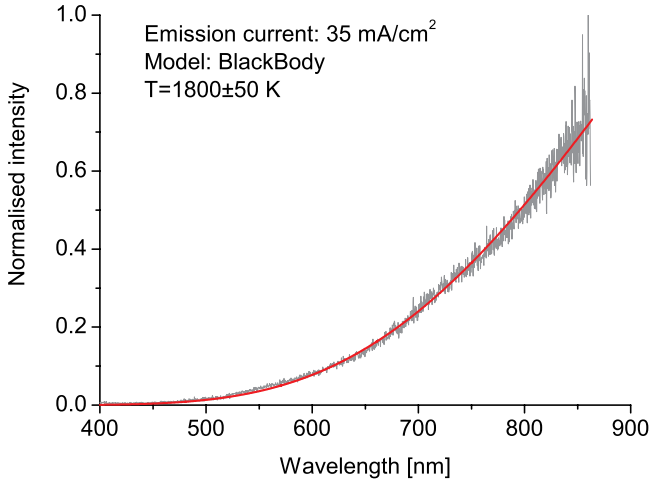

Figure 6.19: Spectroscopic measurement of the light emitted form a film of MWCNTs at a field emission current of $35\,\mathrm{mA/cm^2}$. The dark curve is a blackbody fit with $T = 1800\,\mathrm{K}$.

evidence that the light is thermal emission from the hot nanotubes. No evidence of the luminescence peaks reported previously [116, 117] were found. Temperatures from $1450\,\mathrm{K}$ for low current densities up to about $2200\,\mathrm{K}$ for the highest current densities were measured. The measured temperatures are in good agreement with field emission measurements by Purcell et al. [120] on individual MWCNTs where the emitted electron temperature was found to be $1500\,\mathrm{K}$ at the onset of light emission and increasing to $\sim 2000\,\mathrm{K}$ as the current was turned up. Further evidence for the light emission emanating from joule heating of the tubes can be found if one compares the relative light intensity with the emission current. The light intensity scales with temperature as T^4 according to Stefan-Boltzmann's law. However, that is only valid if one integrates over the whole wavelength spectrum. In the range relevant for our case ($400 - 900\,\mathrm{nm}$) the relation is rather $I_{\mathrm{Light}} \propto T^8$. Ohmic heating scales as J^2, where J is the current density. Thus if the light emission is due to ohmic heating of the CNTs $I_{\mathrm{Light}}^{1/8}$ plotted against J^2 should render a straight line. In figure 6.20 one clearly sees the linear behaviour for the second and third scans. The first scan does not follow the same line. The reason is that the light emission, which is very unstable, probably comes from the thermal an-

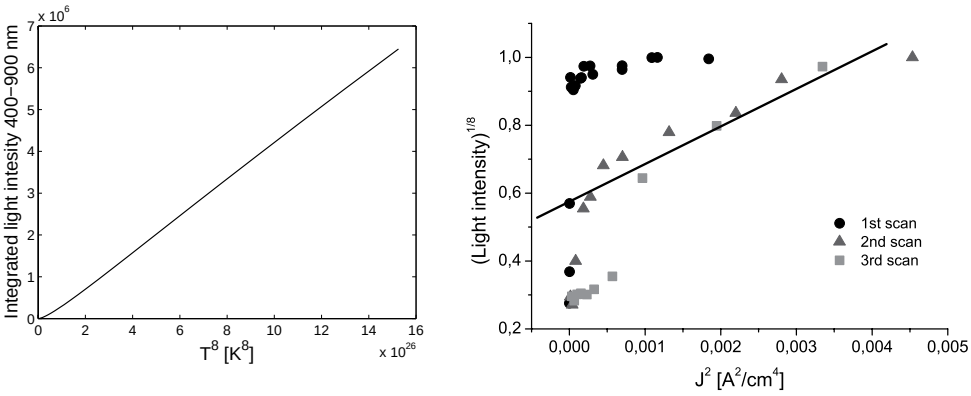

Figure 6.20: (left panel) The integrated intensity from a blackbody emitter in the wavelength interval $400 - 900\,\mathrm{nm}$ plotted against T^8 for $T = 1000 - 2500\,\mathrm{K}$. (right panel) The measured light emission intensity to the power $1/8$ against J^2 for the data in figure 6.18. The black line is a guide for the eye.

nealing/destruction of defect-rich tubes. The temperature from the blackbody fit during the first measurement cycle shows a fairly stable value around $2000\,\mathrm{K}$ for a wide range of current densities above the Fowler-Nordheim knee at $1\,\mathrm{mA/cm^2}$. However, the measured intensity fluctuates dramatically at high current densities probably indicative of catastrophic thermal failures of lower quality tubes.

The measurement have shown clear evidence for ohmic heating of CNTs during field emission. The temperature of the tubes are in the range of $1500 - 2200\,\mathrm{K}$, with current densities of $1 - 100\,\mathrm{mA/cm^2}$.

7

Nanotubes for applications

7.1 Using MWCNTs as microcoolers

One of the major challenges for the semiconductor industry is the ever increasing heat dissipation from the devices. The miniaturisation leads to larger leakage currents, which in turn means that the transistors use energy also when they are in the off-state. All in all there is ultimately a cooling problem. How to remove all this dissipated energy? Modern processors already run at powers well over $100\,\mathrm{W}$ from an area of just a few cm^2. Soon, heat-sinks and fans will not be able to cope with the increasing cooling demands because of the thermal resistance of transferring the heat from the chip to the heat-sink. One solution can be on-chip cooling in the form of micro-fluidic channels. Already in 1981 Tuckerman and Pease showed that by etching Si channels on the backside of the chip containing the circuits and flowing water through them, one can limit the thermal resistance to about $0.1\,\mathrm{K/W}$ down from ca $50\,\mathrm{K/W}$ for a standard IC package [121]. In this manner they managed to achieve a cooling of $790\,\mathrm{W/cm}^2$ for a substrate-to-coolant temperature difference of 71°C.

Due to their excellent thermal properties and the way that they can easily be grown from pre-patterned catalysts, carbon nanotubes are good candidates for this sort of application. For making the cooling fins a $1\,\mathrm{nm}$ Fe catalyst film was deposited in strips with different width and pitches. MWCNTs were grown on the substrates

using thermal CVD. An example of a tube array for microcoolers can be seen in figure 7.1. The microfluidic cell is constructed by attaching a lid from Si on

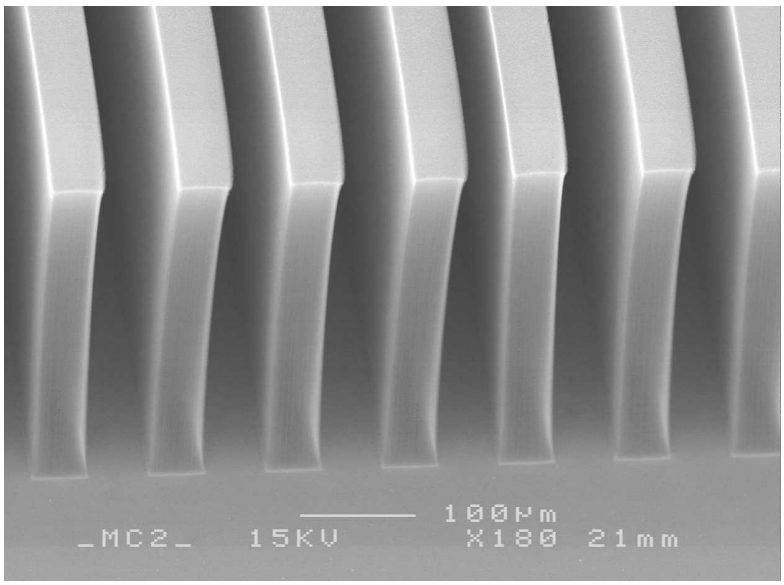

Figure 7.1: An array of MWCNTs that can be used as fins in a microfluidic cooler. The height of the fins are $355\,\mu\mathrm{m}$ then the width and pitch $50\,\mu\mathrm{m}$. The length of the fins is $10\,\mathrm{mm}$.

the wafer with the tubes as shown in figure 1 in Paper II. A micropump capable of sustaining a flow of $500\,\mathrm{ml/min}$ was attached to the cell with flexible tubes. The difference in flowrates in table 7.1 is due to the fact that the pump works at a constant pressure, so the different flowrates indicates different flow resistances for the samples. The flow cell was mounted on a power resistor and the temperature of the resistor was monitored using a thermocouple. In similar experiments by Mo et al. it was shown that the CNT fins provide more cooling than a cell without any fins [122]. It was the purpose of this experiment to compare the cooler with CNT fins with an identical cooler, but with fins made from Si. The Si fins were prepared by deep ion reactive etching. Also a sample with the same dimensions as the Si and CNT coolers but without fins was also used. When the resistor was run without any cooling but the convective air-flow its temperature reached 56°C at a working power of $1.85\,\mathrm{W}$.

In table 7.1 the results of the measurements are presented. It shows clearly that the CNT fins are more efficient than the Si fins. Unfortunately the present design does not allow the calculation of the thermal power transfer from the resistor to the cooler due to additional cooling by natural convection and large uncertainty in the thermal resistance between the resistor and the cooler. The quality of the ther-

Table 7.1: Comparison of the performance of microcoolers of different configurations.

Description	CNT cooler	Si cooler with fins	Si cooler, no fins
Power of resistor (W)	2.13	1.95	1.95
Flow rate (ml/min)	35.7	38.5	34.5
Temp of resistor (°C)	42	42	50

mal interface between the heat source and the sink is one of the largest unknown parameters in this experiment. Thermal interface materials is also an intensive research area, and one where CNTs might play a role in the future [123].

There is also room for improvement of the CNT cooler design. Similar to the experiments by Mo et al. the tubes used in our experiments were not tall enough to reach all the way to the lid leaving considerable space for the water to flow over the fins. This leads to a very low flow in the lowest part of the trenches between the fins. That is, where the cooling would be most efficient the flow is suppressed. Further experiments will address that concern. A new design is also in preparation, where a Cu stripresistor will be prepared on the flip-side of the cooler chip. Further improvement could hopefully be made by experimenting with different patterns to increase the surface area of the cooler. This however would put increased demands on the adhesion of the tubes to the Si surface.

7.2 Anisotropic conduction in nanofibre composites

Much work has been done to incorporate carbon nanotubes into different composites to increase the mechanical strength of the material [124]. Because of their fine mechanical properties the carbon nanotubes can lend strength to the composite material. Similarly the thermal properties of nanotubes have lead to investigation into nanotube composites for thermal conductance enhancement [125]. Recently a MWCNT/PDMS (Polydimethylsiloxane) composite was manufactured, with 500 μm diameter islands of 100 μm MWCNTs in a PDMS membrane [126].

We want to make a nanotube composite material that has a anisotropic conductivity, being conductive in one direction and isolating in the other. Such a material would be interesting e.g. for flip chip applications [127]. To achieve this, VACNF were grown from prepatterned Ni dots, like shown in figure 6.2. The grown fibres were covered with polystyrene (PS, BASF 144C Q599) in a toluene solution by spin-coating. The polymer is interlaced between the standing fibres. The fibres

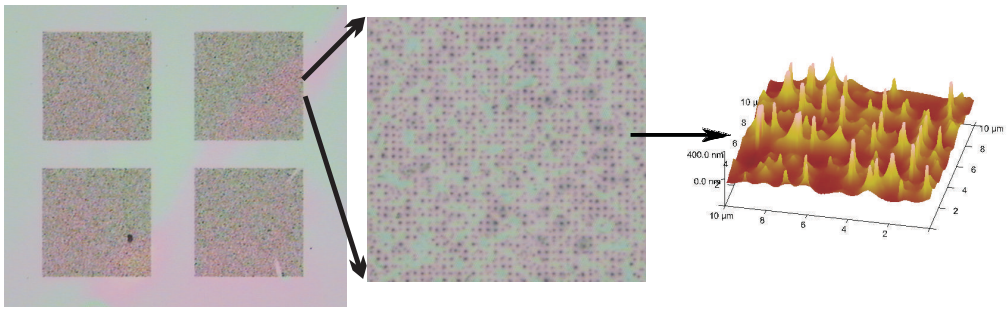

Figure 7.2: A VACNF/PS composite membrane seen in optical microscope. The left panel shows an AFM image of the top of the membrane with the fibres sticking up.

remain vertically aligned also after the spin-coating. The PS film is dried for 90 minutes in a N_2 atmosphere at 100°C. After drying it is treated in an O_2 plasma to remove any PS covering the fibres. By adjusting the rotation speed in the spin-coating and the time of plasma etching one can create a PS membrane where the fibres reach all the way through. The ready membrane is shown in figure 7.2. By leaving the membrane in a 30% solution of KOH it was possible to remove the membrane from the substrate. The membrane is stable enough to be handled with tweezers.

Electric characterisation of the membrane shows promising results. The measurements were performed by putting the membrane on a Si wafer covered with a $50\,\mathrm{nm}$ layer of Mo and evaporating gold electrodes through a mask. The electrodes were $500\,\mu\mathrm{m}$ in diameter and spaced two mm apart and placed both on top of the membrane as well as on the bare substrate. The I-V data from the measurements are shown in figure 7.3. The membrane measured on had a thickness of $2.7\,\mu\mathrm{m}$, penetrated by $2.8\,\mu\mathrm{m}$ long VACNFs. The curves for the membrane are not perfectly linear, and the resistivity of the composite shows large variations between different pairs of electrodes. Typically the resistivity of the membrane with fibres is around $120 - 150\,\Omega$. Between different samples the variation in conductivity can be very large. In some cases the resistance through the VACNF/PS membrane is several kiloohms. The variation depends on how many nanofibres are protruding from the polystyrene, and how many that manage to make good contact with the gold electrode. The resistivity of the membrane without fibres is more than $10\,\mathrm{k}\Omega$, measured from an electrode on the membrane to one on the Mo substrate. When the membrane was placed on an isolating substrate (Si wafer with $400\,\mathrm{nm}$ SiO_2) the resistance between two electrodes was in the gigaohm range.

The membranes thus show great promise as anisotropic conductors. However, more testing is needed, especially to resolve the problems of poor contact between the fibres and the electrodes. It is also necessary to test the membrane in the

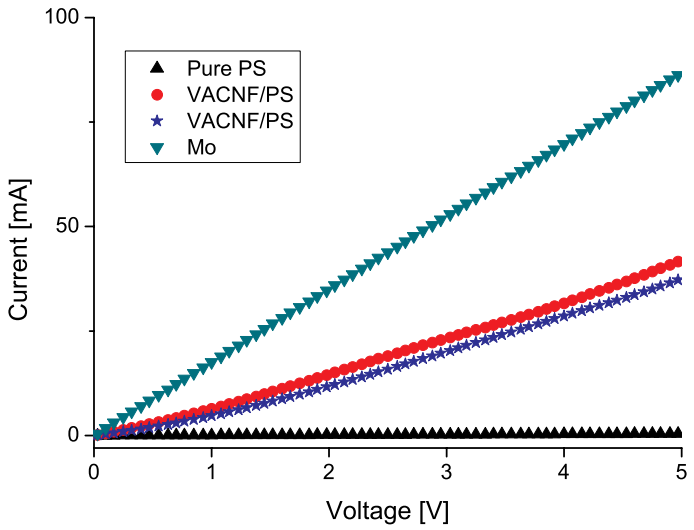

Figure 7.3: I-V data for the VACNF/PS membrane.

interface between two chips, and also to work on simplifying the production.

8

Conclusions and outlook

Most of the work presented in this thesis has been dedicated to the characterisation of the nanotube-growth using PE-CVD. It was shown that changing the growth conditions in the plasma leads to abrupt changes in the growth characteristics in the case of Fe-catalysed MWCNT growth, and a more gradual change in the case of Ni-catalyst. It was also shown that the change in growth is not accompanied by a similarly abrupt change in vibrational temperature of the C_2 molecule. Also, the plasma composition changes only slowly with changing conditions. From the in situ monitoring of the CNT growth it was shown that the layer of amorphous carbon on top of the forests of MWCNTs starts developing about 2 minutes after the plasma is started, and grows to a fully covering layer after about 5-7 minutes.

The optical emission spectroscopy gives information of plasma-composition during growth, and the laser reflection measurements tell us how the tubes are growing. The combination of these techniques could give valuable insight into the parameters that control the CNT growth. The knowledge can also be used for optimising the growth conditions for different applications, especially where the cover layer is unwanted. The possibility of doing these experiments simultaneously would be a great advantage, that would require the reconstruction of our setup. As was mentioned several times, finding out which parameters control the nanotube growth, and especially, why the growth sometimes fails completely should be prioritised. Questions to answer include which parameters determine the type of tubes grown; what influence does the catalyst have, and how does

the deposition method influence the growth; what determined tip vs. base growth; what species are responsible for CNT growth . . . and many more. As can be seen, many of these questions are quite fundamental and that they still remain unanswered tells something about the complex situation that nanotube growth is.

The development of nanotubes applications is another task that goes hand in hand with the previous. It is difficult to make stable applications if the growth cannot be controlled accurately, but without any possible applications there is no need for growing nanotubes. The microcooler project mentioned in chapter 7 is only one of several ongoing attempts to find practical applications for nanotubes. Another is in the development of flip chip interconnects, both in the form of CNT bumps [128] and as part of a CNT-polymer composite. More applications are in progress, and it is our hope that we can help make nanotubes live up to the hopes pinned on them.

Acknowledgements

There are many people who have contributed to the work in this thesis, both directly in experiments and discussions, but also by creating a nice work atmosphere. First of all I want to thank my supervisor Prof. Eleanor Campbell for her support and guidance through the years. Her knowledge is inspiring, as are the dreaded words “I think you need a deadline”. I wish her good luck when she’s returning to her alma mater in Edinburgh. Dr. Oleg Nerushev, our long time visitor from Novosibirsk, has always been interested in my work, always open for discussions, and always willing to lend a hand in the lab and share of his vast experience both in experiments and physics in general. I shared office for five years with Dr. Andrei Gromov, and he showed me around in the world of chemistry, not to mention showing me literally thousands of his photos. For your friendship, good mood and strange Russian jokes, спасибо! Also, many thanks to Dr. Raluca Morjan for helping me into the field of nanotubes and for her inimitable cheerful manner.

A special thanks to Mats for help with technical stuff, Heinrich for keeping us alive, and Wiman for turning my incomprehensible drawings into useful equipment.

Thanks also to the Martins, Emma, Johannes, Mikael, Staffan and all the other people in the Atomic physics group, both present and former. You’re a good crowd and I enjoyed the time with you, both in the lab and after work.

I am very grateful for the support of my friends and family, without whom this would not have been possible.

Cheers!

Bibliography

[1] M. Jönsson, *Structure and Oxygen Sensitivity of Endohedral Fullerenes*. Phil. lic. thesis, Göteborg University, 2005. Available at: http://www.box.net/public/54ty98pa4l.

[2] V. L. Colvin, "The potential envirionmental impact of engineered nanomaterials," *Nat. Biotechnol.* **21**, pp. 1166–1170, 2003.

[3] P. H. M. Hoet, I. Brüske-Hohlfeld, and O. V. Salata, "Nanoparticles – known and unknown health risks," *J. Nanobiotechnology* **2**, p. 12, 2004.

[4] L. Sweet and B. Strohm, "Nanotechnology—life-cycle risk management," *Hum. Ecol. Risk Assess.* **12**, pp. 528–551, 2006.

[5] A. D. Maynard, R. J. Aitken, T. Butz, V. Colvin, K. Donaldson, G. Oberdorster, M. A. Philbert, J. Ryan, A. Seaton, V. Stone, S. S. Tinkle, L. Tran, N. J. Walker, and D. B. Warheit, "Safe handling of nanotechnology," **444**, pp. 267–269, 2006.

[6] M. Crichton, *Prey*, HarperCollins, London, 2002.

[7] "Google, searchword: 'nanotechnology'." http://www.google.com/search?q=nanotechnology, Accessed 2007-02-15.

[8] "The Smalley Group picture gallery." http://smalley.rice.edu/, Accessed 2006-12-26.

[9] H. W. Kroto, J. R. Heath, S. C. O'Brien, R. F. Curl, and R. E. Smalley, "C_{60}: Buckminsterfullerene," *Nature* **318**, pp. 162–163, 1985.

[10] H. Shinohara, "Endohedral metallofullerenes," *Rep. Prog. Phys.* **63**, pp. 843–892, 2000.

[11] J. Giles, "Top five in physics," *Nature* **441**, p. 206, 2006.

[12] C. J. Brabec, N. S. Sariciftci, and J. C. Hummelen, "Plastic solar cells," *Adv. Funct. Mater.* **11**(1), pp. 15–26, 2001.

[13] M. Meyyappan, *Carbon nanotubes: science and applications*, CRC Press, Boca Raton, Fla., 2005.

[14] L. V. Radushkevich and V. M. Lukyanovich, "О СТРУКТУРЕ УГЛЕРОДА, ОБРАЗУЮЩЕГОСЯ ПРИ ТЕРМИЧЕСКОМ РАЗЛОЖЕНИЙ ОКИСИ УГЛЕРОДА НА ЖЕЛЕЗНОМ КОНТАКТЕ (Structure of the carbon produced in the thermal decomposition of carbon monoxide on an iron catalyst)," *Zhurnal Fizicheskoi Khimii* **26**, pp. 88–95, 1952.

[15] A. Oberlin, M. Endo, and T. Koyama, "Filamentous growth of carbon through benzene decomposition," *J. Cryst. Growth* **32**(3), pp. 335–349, 1976.

[16] H. G. Tennent, J. J. Barber, and R. Hoch, "Carbon fibrils, method for producing them, and compositions containing them." United States Patent 4663230, June 1987.

[17] W. Krätschmer, L. D. Lamb, K. Fostiropoulos, and D. R. Huffman, "Solid C_{60}: a new form of carbon," *Nature* **347**, p. 354, 1990.

[18] S. Iijima, "Helical microtubules of graphitic carbon," *Nature* **318**, pp. 56–58, 1991.

[19] S. Iijima and T. Ichihashi, "Single-shell carbon nanotubes of 1-nm diameter," *Nature* **363**(6430), pp. 603–605, 1993.

[20] D. S. Bethune, C. H. Kiang, M. S. de Vries, G. Gorman, R. Savoy, J. Vazquez, and R. Beyers, "Cobalt-catalyzed growth of carbon nanotubes with single-atomic-layer walls," *Nature* **363**(6430), pp. 605–607, 1993.

[21] M. Monthioux and V. L. Kuznetsov, "Who should be given the credit for the discovery of carbon nanotubes?," *Carbon* **44**, pp. 1621–1623, 2006.

[22] "Wikipedia, article 'orbital hybridisation'." http://en.wikipedia.org/wiki/Orbital_hybridisation, Accessed 2006-12-26.

[23] Y. Saito, T. Yoshikawa, S. Bandow, M. Tomita, and T. Hayashi, "Interlayer spacings in carbon nanotubes," *Phys. Rev. B* **48**(3), pp. 1907–1909, 1993.

[24] L.-C. Qin, X. Zhao, K. Hirahara, Y. Miyamoto, Y. Ando, and S. Iijima, "The smallest carbon nanotube," *Nature* **408**, p. 50, 2000.

[25] N. Wang, Z. K. Tang, G. D. Li, and J. S. Chen, "Single-walled 4 Å carbon nanotube arrays," *Nature* **408**, pp. 50–51, 2000.

[26] X. Zhao, Y. Liu, S. Inoue, R. O. Jones, and Y. Ando, "Smallest carbon nanotube is 3 Å in diameter," *Phys. Rev. Lett.* **92**, p. 125502, 2004.

[27] S. Huang, M. Woodson, R. Smalley, and J. Liu, "Growth mechanism of oriented long single walled carbon nanotubes using "fast-heating" chemical vapor deposition process," *Nano Lett.* **4**, pp. 1025–1028, 2004.

[28] C. Zhou, J. Kong, and H. Dai, "Intrinsic electrical properties of individual single-walled carbon nanotubes with small band gaps," *Phys. Rev. Lett.* **84**(24), pp. 5604–5607, 2000.

[29] R. Martel, V. Derycke, C. Lavoie, J. Appenzeller, K. K. Chan, J. Tersoff, and P. Avouris, "Ambipolar electrical transport in semiconducting single-wall carbon nanotubes," *Phys. Rev. Lett.* **87**(25), p. 256805, 2001.

[30] S. J. Tans, M. J. Devoret, H. Dai, A. Thess, R. E. Smalley, L. J. Geerligs, and C. Dekker, "Individual single wall carbon nanotubes as molecular wires," *Nature* **386**, pp. 474–477, 1997.

[31] W. Liang, M. Bockrath, D. Bozovic, J. H. Hafner, M. Tinkham, and H. Park, "Fabry-Perot interference in a nanotube electron waveguide," *Nature* **411**, pp. 665–669, 2001.

[32] A. Javey, J. Guo, M. Paulsson, Q. Wang, D. Mann, M. Lundstrom, and H. Dai, "High-field quasiballistic transport in short carbon nanotubes," *Phys. Rev. Lett.* **92**, p. 106804, 2004.

[33] R. Saito, G. Dresselhaus, and M. S. Dresselhaus, "Electronic structures of double-layer graphene tubules," *J. Appl. Phys.* **73**, pp. 494–500, 1993.

[34] C. Schönenberger, A. Bachtold, C. Strunk, J.-P. Salvetat, and L. Forró, "Interference and interaction in multi-wall carbon nanotubes," *Appl. Phys. A* **69**(3), pp. 283–295, 1999.

[35] P. J. de Pablo, E. Graugnard, B. Walsh, R. P. Andres, S. Datta, and R. Reifenberger, "A simple, reliable technique for making electrical contact to multiwalled carbon nanotubes," *Appl. Phys. Lett.* **74**, pp. 323–325, 1999.

[36] Y. Yi, *Ballistic Conduction in Multiwalled Carbon Nanotubes at Room Temperature*. Ph.d. thesis, Georgia Institute of Technology, 2004. Available at: http://etd.gatech.edu/theses/available/etd-05102004-103121/unrestricted/yi_yan_200407_phd.pdf.

[37] S. Frank, P. Poncharal, Z. L. Wang, and W. A. de Heer, "Carbon nanotube quantum resistors," *Science* **280**, pp. 1744–1746, 1998.

[38] J. P. Lu, "Elastic properties of carbon nanotubes and nanoropes," *Phys. Rev. Lett.* **79**, pp. 1297–1300, 1997.

[39] A. Krishnan, E. Dujardin, T. W. Ebbesen, P. N. Yianilos, and M. M. J. Treacy, "Young's modulus of single-walled nanotubes," *Phys. Rev. B* **58**(20), pp. 14013–14019, 1998.

[40] P. Poncharal, Z. L. Wang, D. Ugarte, and W. A. de Heer, "Electrostatic deflections and electromechanical resonances of carbon nanotubes," *Science* **283**, pp. 1513–1516, 1999.

[41] J. Han, "Structures and properties of carbon nanotubes," in *Carbon nanotubes: science and applications*, M. Meyyappan, ed., pp. 1–24, CRC Press, Boca Raton, Fla., 2005.

[42] M.-F. Yu, O. Lourie, M. J. Dyer, K. Moloni, T. F. Kelly, and R. S. Ruoff, "Strength and breaking mechanism of multiwalled carbon nanotubes under tensile load," *Science* **287**(5453), pp. 637–640, 2000.

[43] J. Kinaret, T. Nord, and S. Viefers, "A carbon-nanotube-based nanorelay," *Appl. Phys. Lett.* **82**, pp. 1287–1289, 2003.

[44] S. W. Lee, D. S. Lee, R. E. Morjan, S. H. Jhang, M. Sveningsson, O. A. Nerushev, Y. W. Park, and E. E. B. Campbell, "A three-terminal carbon nanorelay," *Nano Lett.* **4**(10), pp. 2027–2030, 2004.

[45] S. Berber, Y.-K. Kwon, and D. Tománek, "Unusually high thermal conductivity of carbon nanotubes," *Phys. Rev. Lett.* **84**, pp. 4613–4616, 2000.

[46] M. A. Osman and S. K. Srivastava, "Temperature dependence of the thermal conductivity of single-wall carbon nanotubes," *Nanotechnology* **12**, pp. 21–24, 2001.

[47] W. Yi, L. Lu, D.-l. Zhang, Z. W. Pan, and S. S. Xie, "Linear specific heat of carbon nanotubes," *Phys. Rev. B J1 - PRB* **59**, pp. R9015–R9018, 1999.

[48] P. Kim, L. Shi, A. Majumdar, and P. L. McEuen, "Thermal transport measurements of individual multiwalled nanotubes," *Phys. Rev. Lett.* **87**, p. 215502, 2001.

[49] Y. Murakami, Y. Miyauchi, S. Chiashi, and S. Maruyama, "Characterization of single-walled carbon nanotubes catalytically synthesized from alcohol," *Chem. Phys. Lett.* **374**, pp. 53–58, 2003.

[50] M. Sveningsson, M. Jönsson, O. A. Nerushev, F. Rohmund, and E. E. B. Campbell, "Blackbody radiation from resistively heated multi-walled carbon nanotubes during field emission," *Appl. Phys. Lett.* **81**(6), pp. 1095–1097, 2002.

[51] W. A. de Heer, A. Châtelain, and D. Ugarte, "A carbon nanotube field-emission electron source," *Science* **270**(5239), pp. 1179–1180, 1995.

[52] T. Guo, P. Nikolaev, A. Thess, D. T. Colbert, and R. E. Smalley, "Catalytic growth of single-walled nanotubes by laser vaporization," *Chem. Phys. Lett.* **243**, pp. 49–54, 1995.

[53] A. A. Puretzky, H. Schittenhelm, X. Fan, M. J. Lance, L. F. Allard, and D. B. Geohegan, "Investigations of single-wall carbon nanotube growth by time-restricted laser vaporization," *Phys. Rev. B* **65**(24), p. 245425, 2002.

[54] H. M. Cheng, F. Li, G. Su, H. Y. Pan, L. L. He, X. Sun, and M. S. Dresselhaus, "Large-scale and low-cost synthesis of single-walled carbon nanotubes by the catalytic pyrolysis of hydrocarbons," *Appl. Phys. Lett.* **72**, pp. 3282–3284, 1998.

[55] Y. Homma, K. Kobayashi, T. Ogino, and T. Yamashita, "Growth of suspended carbon nanotube networks on 100-nm-scale silicon pillars," *Appl. Phys. Lett.* **81**, pp. 2261–2263, 2002.

[56] D. S. Lee, J. Svensson, S. W. Lee, Y. W. Park, and E. E. B. Campbell, "Fabrication of crossed junctions of semiconducting and metallic carbon nanotubes: A CNT-gated CNT-FET," *J. Nanosci. and Nanotechn.* **6**, pp. 1325–1330, 2006.

[57] C. N. R. Rao, R. Sen, B. C. Satishkumar, and A. Govindaraj, "Large aligned-nanotube bundles from ferrocene pyrolysis," *Chem. Commun.* , pp. 1525–1526, 1998.

[58] J.-M. Bonard, P. Chauvin, and C. Klinke, "Monodisperse multiwall carbon nanotubes obtained with ferritin as catalyst," *Nano Lett.* **2**, pp. 665–667, 2002.

[59] P. Nikolaev, M. J. Bronikowski, R. K. Bradley, F. Rohmund, D. T. Colbert, K. A. Smith, and R. E. Smalley, "Gas-phase catalytic growth of single-walled carbon nanotubes from carbon monoxide," *Chem. Phys. Lett.* **313**, pp. 91–97, 1999.

[60] M. J. Bronikowski, P. A. Willis, D. T. Colbert, K. A. Smith, and R. E. Smalley, "Gas-phase production of carbon single-walled nanotubes from carbon monoxide via the HiPco process: A parametric study," *J. Vac. Sci. Technol. A* **19**, pp. 1800–1805, 2001.

[61] K. Hata, D. N. Futaba, K. Mizuno, T. Namai, M. Yumura, and S. Iijima, "Water-assisted highly efficient synthesis of impurity-free single-walled carbon nanotubes," *Science* **306**(5700), pp. 1362–1364, 2004.

[62] N. R. Franklin and H. Dai, "An enhanced CVD approach to extensive nanotube networks with directionality," *Adv. Mater.* **12**, pp. 890–894, 2002.

[63] Z. F. Ren, Z. P. Huang, J. W. Xu, J. H. Wang, P. Bush, M. P. Siegal, and P. N. Provencio, "Synthesis of large arrays of well-aligned carbon nanotubes on glass," *Science* **282**(5391), pp. 1105–1107, 1998.

[64] H. S. Kang, H. J. Yoon, C. O. Kim, J. P. Hong, I. T. Han, B. K. Song, J. E. Jung, N. S. Lee, and J. M. Kim, "Low temperature growth of multi-wall carbon nanotubes assisted by mesh potential using a modified plasma enhanced chemical vapor deposition system," *Chem. Phys. Lett.* **349**, pp. 196–200, 2001.

[65] J. I. B. Wilson, N. Scheerbaum, S. Karim, N. Polwart, P. John, Y. Fan, and A. G. Fitzgerald, "Low temperature plasma chemical vapour deposition of carbon nanotubes," *Diamond Relat. Mater.* **11**, pp. 918–921, 2002.

[66] S. Hofmann, C. Ducati, J. Robertson, and B. Kleinsorge, "Low-temperature growth of carbon nanotubes by plasma-enhanced chemical vapor deposition," *Appl. Phys. Lett.* **83**(1), pp. 135–137, 2003.

[67] F. Ding, K. Bolton, and A. Rosén, "Nucleation and growth of single-walled carbon nanotubes: A molecular dynamics study," *J. Phys. Chem. B* **108**, pp. 17369–17377, 2004.

[68] V. Vinciguerra, F. Buonocore, and G. Panzera, "Growth mechanisms in chemical vapour deposited carbon nanotubes," *Nanotechnology* **14**, pp. 655–660, 2003.

[69] O. A. Nerushev, S. Dittmar, R.-E. Morjan, F. Rohmund, and E. E. B. Campbell, "Particle size dependence and model for iron-catalyzed growth of carbon nanotubes by thermal chemical vapor deposition," *J. Appl. Phys.* **93**(7), pp. 4185–4190, 2003.

[70] V. L. Kuznetsov, A. N. Usoltseva, A. L. Chuvilin, E. D. Obraztsova, and J.-M. Bonard, "Thermodynamic analysis of nucleation of carbon deposits on metal particles and its implications for the growth of carbon nanotubes," *Phys. Rev. B J1 - PRB* **64**(23), p. 235401, 2001.

[71] P. J. F. Harris, "Solid state growth mechanisms for carbon nanotubes," *Carbon* **45**, pp. 229–239, 2007.

[72] A. V. Melechko, V. I. Merkulov, T. E. McKnight, M. A. Guillorn, K. L. Klein, D. H. Lowndes, and M. L. Simpson, "Vertically aligned carbon nanofibers and related structures: Controlled synthesis and directed assembly," *J. Appl. Phys.* **97**, p. 041301, 2005.

[73] A. Windle, "Introduction to poster session A: Synthesis," 2006. Slide for talk available at: http://nanotube.msu.edu/nt06/presentations/NT06S-Windle.pdf.

[74] T. Kato, G.-H. Jeong, T. Hirata, and R. Hatakeyama, "Structure control of carbon nanotubes using radio-frequency plasma enhanced chemical vapor deposition," *Thin Solid Films* **457**, pp. 2–6, 2004.

[75] Y. S. Woo, D. Y. Jeon, N. S. Lee, J. E. Jung, and J. M. Kim, "In situ diagnostics of chemical species for the growth of carbon nanotubes in microwave plasma-enhanced chemical vapor deposition," *Diamond Relat. Mater.* **11**, pp. 59–66, 2002.

[76] L. Delzeit, I. McAninch, B. A. Cruden, D. Hash, B. Chen, J. Han, and M. Meyyappan, "Growth of multiwall carbon nanotubes in an inductively coupled plasma reactor," *J. Appl. Phys.* **91**(9), pp. 6027–6033, 2002.

[77] S. H. Lim, H. S. Yoon, J. H. Moon, K. C. Park, and J. Jang, "Optical emission study for optimization of carbon nanotubes growth by a triode plasma chemical vapor deposition," *Appl. Phys. Lett.* **88**, p. 033114, 2006.

[78] Y. Chen, Z. L. Wang, J. S. Yin, D. J. Johnson, and R. H. Prince, "Well-aligned graphitic nanofibers synthesized by plasma assisted chemical vapor deposition," *Chem. Phys. Lett.* **272**, pp. 178–182, 1997.

[79] Y. P. Raizer, *Gas discharge physics*, Springer, Berlin, 1991.

[80] Y. Yao, L. K. L. Falk, R. E. Morjan, O. A. Nerushev, and E. E. B. Campbell, "Synthesis of carbon nanotube films by thermal CVD in the presence of supported catasyst particles. Part I: The silicon substrate/nanotube film interface," *J. Mater. Sci.: Mater. Electron.* **15**, pp. 533–543, 2004.

[81] O. A. Nerushev, R.-E. Morjan, D. I. Ostrovskii, M. Sveningsson, M. Jönsson, F. Rohmund, and E. E. B. Campbell, "The temperature dependence of Fe-catalysed growth of carbon nanotubes on silicon substrates," *Physica B* **323**(1-4), pp. 51–59, 2002.

[82] S. Dittmer, O. A. Nerushev, and E. E. B. Campbell, "Low ambient temperature CVD growth of carbon nanotubes," *Appl. Phys. A* **84**(3), pp. 243–246, 2006.

[83] S. Dittmer, *Low temperature growth of carbon nanotubes*. Ph. lic. thesis, Chalmers tekniska högskola, 2006.

[84] O. A. Nerushev, M. Sveningsson, L. K. L. Falk, and F. Rohmund, "Carbon nanotube films obtained by thermal chemical vapour deposition," *J. Mater. Chem.* **11**, pp. 1122–1132, 2001.

[85] M. Sveningsson, R.-E. Morjan, O. A. Nerushev, Y. Sato, J. Backstrom, E. E. B. Campbell, and F. Rohmund, "Raman spectroscopy and field-emission properties of CVD-grown carbon-nanotube films," *Appl. Phys. A* **A73**(4), pp. 409–418, 2001.

[86] R. E. Morjan, O. A. Nerushev, M. Sveningsson, F. Rohmund, L. K. L. Falk, and E. E. B. Campbell, "Growth of carbon nanotubes from C_{60}," *Appl. Phys. A* **78**, pp. 253–261, 2004.

[87] M. S. Kabir, R. E. Morjan, O. A. Nerushev, P. Lundgren, S. Bengtsson, P. Enokson, and E. E. B. Campbell, "Plasma-enhanced chemical vapor deposition growth of carbon nanotubes on different metal underlayers," *Nanotechnology* **16**(4), pp. 458–466, 2005.

[88] A. Jorio, R. Saito, J. H. Hafner, C. M. Lieber, M. Hunter, T. McClure, G. Dresselhaus, and M. S. Dresselhaus, "Structural (n, m) determination of isolated single-wall carbon nanotubes by resonant Raman scattering," *Phys. Rev. Lett.* **89**, pp. 1118–1121, 2001.

[89] G. Herzberg, *Molecular spectra and molecular structure: Volume I - Spectra of Diatomic Molecules*, Van Nostrand, New York, 2. ed., 1950.

[90] "Wikipedia, article 'Franck-Condon principle'." http://en.wikipedia.org/wiki/Franck-Condon, Accessed 2007-01-29.

[91] J. J. Sakurai and S. F. Tuan, *Modern quantum mechanics*, Addison-Wesley, Reading, Mass., rev. ed., 1994.

[92] S. S. Harilal, R. C. Issac, C. V. Bindhu, V. P. N. Nampoori, and C. P. G. Vallabhan, "Optical emission studies of C_2 species in laser-produced plasma from carbon," *J. Phys. D* **30**, pp. 1703–1709, 1997.

[93] S. Menmuir, *Visible spectroscopy as a sensitive diagnostic tool for fusion plasmas*. Ph. lic. thesis, Royal Institute for Technology, Stockholm, 2005.

[94] J. Ott, A. Weiss, C. Henkel, and F. Walter, "The temperature distribution of dense molecular gas in the center of NGC 253," *Astroph. J.* **629**(2), pp. 767–780, 2005.

[95] J. Luque, W. Juchmann, E. A. Brinkman, and J. B. Jeffries, "Excited state density distributions of H, C, C_2, and CH by spatially resolved optical emission in a diamond depositing dc-arcjet reactor," *J. Vac. Sci. Technol. A* **19**, pp. 397–408, 1998.

[96] J. Felts and E. Lopata, "Measurements of electron temperature in a capacitively coupled plasma using emission spectroscopy," *J. Vac. Sci. Technol. A* **6**, pp. 2051–2053, 1988.

[97] R. E. Morjan, *Towards controlled growth and applications of carbon nanotubes*. Ph. d. thesis, Chalmers tekniska högskola, 2005.

[98] M. Sveningsson, R. E. Morjan, O. A. Nerushev, E. E. B. Campbell, D. Malsch, and J. A. Schaefer, "Highly efficient electron field emission from decorated multiwalled carbon nanotube films," *Appl. Phys. Lett.* **85**(19), pp. 4487–4489, 2004.

[99] V. I. Merkulov, A. V. Melechko, M. A. Guillorn, D. H. Lowndes, and M. L. Simpson, "Alignment mechanism of carbon nanofibers produced by plasma-enhanced chemical-vapor deposition," *Appl. Phys. Lett.* **79**, pp. 2970–2972, 2001.

[100] D. B. Geohegan, A. A. Puretzky, I. N. Ivanov, S. Jesse, G. Eres, and J. Y. Howe, "*In situ* growth rate measurements and length control during chemical vapor deposition of vertically aligned multiwall carbon nanotubes," *Appl. Phys. Lett.* **83**(9), pp. 1851–1853, 2003.

[101] M. Sveningsson, *Field emission from multi-walled carbon nanotubes and its application in nanoelectromechanical systems*. Phd-thesis, Chalmers tekniska högskola, 2006.

[102] M. Meyyappan, L. Delzeit, A. Cassell, and D. Hash, "Carbon nanotube growth by pecvd: a review," *Plasma Sources Sci. Technol.* **12**, pp. 205–216, 2003.

[103] S. Ono and S. Teii, "Vibrational temperature in a weakly ionised steady-state nitrogen discharge plasma," *J. Phys. D* **16**, pp. 136–170, 1983.

[104] D. Hash, D. Bose, T. R. Govindan, and M. Meyyappan, "Simulation of the dc plasma in carbon nanotube growth," *J. Appl. Phys.* **93**(10), pp. 6284–6290, 2003.

[105] W. H. Tao, M. A. Prelas, and H. K. Yasuda, "Spatial distributions of electron density and electron temperature in direct current glow discharge," *J. Vac. Sci. Technol. A* **14**, pp. 2113–2121, 1996.

[106] Y. Y. Lin, H. W. Wei, K. C. Leou, H. Lin, C. H. Tung, M. T. Wei, C. Lin, and C. H. Tsai, "Experimental chacterization of an inductively coupled acetylene/hydrogen plasma for carbon nanofiber synthesis," *J. Vac. Sci. Technol. B* **24**, pp. 97–103, 2006.

[107] P. E. Nolan, M. J. Schabel, D. C. Lynch, and A. H. Cutler, "Hydrogen control of carbon deposit morphology," *Carbon* **33**, pp. 79–85, 1995.

[108] P. E. Nolan, D. C. Lynch, and A. H. Cutler, "Carbon deposition and hydrocarbon formation on group VIII metal catalysts," *J. Chem. Phys. B* **102**, pp. 4165–4175, 1998.

[109] M. Chhowalla, K. B. K. Teo, C. Ducati, N. L. Rupesinghe, G. A. J. Amaratunga, A. C. Ferrari, D. Roy, J. Robertson, and W. I. Milne, "Growth process conditions of vertically aligned carbon nanotubes using plasma enhanced chemical vapor deposition," *J. Appl. Phys.* **90**, pp. 5308–5317, 2001.

[110] A. A. Puretzky, D. B. Geohegan, S. Jesse, I. N. Ivanov, and G. Eres, "In situ measurements and modeling of carbon nanotube array growth kinetics

during chemical vapor deposition," *Appl. Phys. A* **A81**(2), pp. 223–240, 2005.

[111] K. B. K. Teo, D. B. Hash, R. G. Lacerda, N. L. Rupesigne, M. S. Bell, S. H. Dalal, D. Bose, T. R. Govindan, B. A. Cruden, M. Chhowalla, G. A. J. Amaratunga, M. Meyyappan, and W. I. Milne, "The significance of plasma heating in carbon nanotube and nanofiber growth," *Nano Lett.* **4**(5), pp. 921–926, 2004.

[112] D. B. Hash, M. S. Bell, K. B. K. Teo, B. A. Cruden, W. I. Milne, and M. Meyyappan, "An investigation of plasma chemistry for dc plasma enhanced chemical vapour deposition of carbon nanotubes and nanofibres," *Nanotechnology* **16**, pp. 925–930, 2005.

[113] D.-H. Kim, H.-S. Jang, C.-D. Kim, D.-S. Cho, H.-D. Kang, J.-G. Jee, and H.-R. Lee, "In situ monitoring of carbon nanotube growth," *Carbon* **41**(3), pp. 583–585, 2003.

[114] J. W. Robinson, *Handbook of spectroscopy. Vol. 2*, CRC Press, Cleveland, Ohio, 1974.

[115] F. Thièry, C. Valée, Y. Arnal, and J. Pelletier, "PECVD and PIID processing of diamondlike carbon," *Surf. Coat. Tech.* **186**, pp. 146–152, 2004.

[116] J.-M. Bonard, T. Stöckli, F. Maier, W. A. de Heer, A. Châtelain, J. P. Salvetat, and L. Forró, "Field-emission-induced luminescence from carbon nanotubes," *Phys. Rev. Lett.* **81**, pp. 1441–1444, 1998.

[117] A. G. Umnov and V. Z. Mordkovich, "Field-induced evaporation of carbon nanotubes," *Appl. Phys. A* **73**, pp. 301–304, 2001.

[118] J.-M. Bonard, F. Maier, T. Stöckli, A. Châtelain, W. A. de Heer, J. P. Salvetat, and L. Forró, "Field emission properties of multiwalled carbon nanotubes," *Ultramicroscopy* **73**, pp. 7–15, 1998.

[119] J.-M. Bonard, J.-P. Salvetat, T. Stöckli, L. Forró, and A. Châtelain, "Field emission from carbon nanotubes: perspectives for applications and clues to the emission mechanism," *Appl. Phys. A* **69**, pp. 245–254, 1999.

[120] S. T. Purcell, P. Vincent, C. Journet, and V. T. Binh, "Hot nanotubes: Stable heating of individual multiwall carbon nanotubes to 2000 k induced by the field-emission current," *Phys. Rev. Lett.* **88**(10), p. 105502, 2002.

[121] D. B. Tuckerman and R. F. W. Pease, "High-performance heat sinking for VLSI," *IEEE Electr. Device L.* **2**(5), pp. 126–129, 1981.

[122] Z. Mo, R. Morjan, J. Anderson, E. E. B. Campbell, and J. Liu, "Integrated nanotube microcooler for microelectronics applications," in *Proceedings of the 55th Electronic Components & Technology Conference*, **1**, pp. 51–54, 2005.

[123] F. Sarvar, D. C. Whalley, and P. P. Conway, "Thermal interface materials—A review of the state of the art," in *1st Electronics Systemintegration Technology Conference*, **2**, pp. 1292–1302, (Dresden, Germany), 2006.

[124] E. T. Thostenson, Z. Ren, and T.-W. Chou, "Advances in the science and technology of carbon nanotubes and their composites: a reveiw," *Compos. Sci. Technol.* **61**, pp. 1899–1912, 2001.

[125] H. Huang, C. Liu, Y. Wu, and S. Fan, "Aligned carbon nanotube composite films for thermal management," *Adv. Mater.* **13**, pp. 1652–1656, 2005.

[126] Y. J. Jung, S. Kar, S. Talapatra, C. Soldano, G. Viswanathan, X. Li, Z. Yao, F. S. Ou, A. Avandhanula, R. Vajtai, S. Curran, O. Nalamasu, and P. M. Ajayan, "Aligned carbon nanotube-polymer hybrid architectures for diverse flexible electronic applications," *Nano Lett.* **6**, pp. 413–418, 2006.

[127] I. Watanabe, T. Fujinawa, M. Fujii, and G. Yasushi, "Recent advances of interconnection technologies using anisotropic conductive films in flat panel display applications," in *9th International Symposium on Advanced Packaging Materials: Processes, Properties and Interfaces.*, pp. 11–16, 2004.

[128] T. Wang, M. Jönsson, E. E. B. Campbell, and J. Liu, "Development of carbon nanotube bumps for ultra fine pitch flip chip interconnection," in *Proceedings of the 1st IEEE CPMT Electronics Systemintegration Technology Conference (ESTC2006)*, **2**, pp. 892–895, (Dresden, Germany), 2006.

Paper I

DC plasma-enhanced chemical vapour deposition
growth of carbon nanotubes and nanofibres:
in situ spectroscopy and plasma current density dependence
Submitted to Appl. Phys. A.

Submitted to Applied Physics A

DC plasma-enhanced chemical vapour deposition growth of carbon nanotubes and nanofibres: in situ spectroscopy and plasma current dependence.

M. Jönsson, O.A. Nerushev[†], E.E.B. Campbell*

Department of Physics, Göteborg University, SE-41296 Göteborg, Sweden

†: Permanent address: Institute of Thermophysics, RAS SB, 1 Acad. Lavrentyev Ave., 63090 Novosibirsk, Russia

*. Corresponding author: Email: Eleanor.campbell@physics.gu.se, tel. +46 31 772 3272, Fax: +46 31 772 3496

Abstract:

Dc plasma-enhanced CVD growth of nanotubes and nanofibres is studied as a function of plasma power (3-40 W). The dependence of the nanotube/nanofibre morphology for growth on thin iron films and lithographically prepared individual nickel dots is investigated. In both cases, large differences in the morphology of the carbon nanostructures are observed as the plasma power is changed. In situ optical emission spectroscopy is used to obtain insight into the important parameters affecting the growth. The best growth results are found for intermediate plasma powers (15 W).

PACS: 81.07.-b; 52.70.Kz

1. Introduction

Carbon nanotubes have considerable potential for applications in many areas due to their attractive mechanical, thermal and electrical properties. Plasma-enhanced chemical vapour deposition (PECVD) provides a means of growing vertically aligned multiwalled carbon nanotubes or carbon nanofibres on a variety of substrates that can be of interest for e.g. interconnects, field emission devices, sensors, nanoelectromechanical devices etc. [1]. Although the presence of a plasma is not essential for inducing aligned growth of nanotubes [2], PECVD is still the only practical method of large scale aligned growth on a patterned substrate. An additional potential advantage of PECVD is the hope for developing practical methods for low substrate temperature growth by avoiding the necessity of heating the substrate to the elevated temperatures typically needed for thermal CVD growth. However, many of the PECVD studies use high power plasmas where the substrate surface temperature is not well defined and is increased by the interaction with the plasma [3]. Many studies have emerged in recent years that explore the PECVD mechanisms and obtain insight into the important growth parameters and plasma chemistry by carrying out in situ mass spectrometry and optical emission spectroscopy studies of the plasma [3-14]. In spite of this activity our knowledge of the PECVD process is still very limited and many important issues remain to be clarified [15]. In this paper we study the plasma power dependence of aligned carbon nanotube growth, using Fe catalyst films and individual aligned carbon nanofibre growth using lithographically prepared Ni catalyst dots. We compare the morphology of the grown structures as a function of plasma current using scanning electron microscopy (SEM) and relate the results to the information obtained from in situ optical emission spectroscopy.

In both cases, there is a very strong dependence of the growth rate, quality and morphology of the grown carbon nanostructures as a function of the plasma current. For Fe catlalysed growth there is a sharp transition from aligned multiwalled nanotube growth to individual tip-grown nanofibres as the plasma current is increased. This can be related to the relative intensity of hydrogen atoms in the plasma and supports the interpretation of earlier results for growth in an inductively coupled rf plasma reactor [4]. The situation for Ni catalysed growth appears more complicated but can be rationalized in terms of the relative intensities of active plasma species and the interplay between surface and gas phase reactions. An interesting observation is that under nominally identical growth conditions quite different results are obtained from growth from 100 nm diameter Ni dots and a thin Ni film of the same thickness (10 nm) showing the importance of understanding the role of catalyst preparation and the initial stages of growth.

Note that throughout the paper we distinguish between base-grown multiwalled nanotubes and tip-grown carbon nanofibres [5]. For multiwalled nanotube growth the catalyst remains at the interface with the surface and the nanotube walls are well graphitized concentric cylinders. The tip-grown structures typically have a stacked-cone arrangement where the angle between the graphite basal planes and the tube axis is non-zero but small so that the nanofibres structures are typically also hollow.

2. Experimental

Films of vertically aligned carbon nanotubes and arrays of vertically aligned carbon nanofibres were grown on silicon wafers using DC plasma-enhanced chemical vapour

deposition (CVD). The set-up has been described earlier for both nanotube [16] and nanofibre [17,18] growth. Note that here, in contrast to [17,18] we do not grow the Ni-catalysed structures on a metal layer but grow directly on a doped silicon wafer with a native oxide layer. Samples were prepared for growing vertically aligned carbon nanotubes by evaporating a 1 nm thick catalyst film of Fe onto a silicon wafer with native oxide. The samples for vertical nanofibre growth were prepared by depositing 10 nm thick, 100 nm diameter Ni dots (prepared by electron beam lithography) onto native oxide coated silicon(100) wafers. The substrates were attached to a grounded cathode and inserted in to the growth chamber. The chamber was pumped down to 5×10^{-6} Torr. After reaching this pressure, the substrate was heated to a temperature of 700 ^{o}C before the growth gas was introduced to the chamber. A voltage on the order of 400-500 V, adjusted to produce the desired plasma current (pressure dependent), is applied between the cathode and an anode (an M6 stainless steel screw) situated at a distance of 10-15 mm from the substrate surface. The nanotube growth was performed under continuous flow conditions. For the Fe-catalyst substrates, a C_2H_2:H_2 gas mixture in proportion 1:9 at flow rates of 225 sccm (H_2), 25 sccm (C_2H_2) and a total chamber pressure of 8 Torr was used. For the Ni case, a C_2H_2:NH_3 (1:5) mixture was used (100 sccm NH_3, 20 sccm C_2H_2) at a pressure of 4 Torr. The total plasma current was varied between 7 and 70 mA, corresponding to a current density at the cathode surface of 0.7 – 7 mA/cm^2. This was done by adjusting the bias voltage, Fig. 1. The plasma power was thus varied between 3.5 W and 40 W and is significantly lower than most other PECVD studies [3]. Any effect of plasma heating of the substrate is therefore minimized in our setup. For all the results reported here, the growth time was 15 minutes. After this time, the plasma power supply

was switched off, the substrate heater was turned off, the chamber was evacuated and the sample was allowed to cool down to room temperature under vacuum conditions before being removed from the chamber.

The substrates were examined after growth using a JEOL JSM-6301F scanning electron microscope.

The light emitted by the plasma during growth was collected using a telescope with a lens of 150 mm focal length, placed inside the growth chamber, and a cylindrical lens, outside the chamber, to focus the emitted light onto the entry slit of a SpectralPro 150 spectrometer. The spectrum was collected using a CCD camera. The focal point of the collecting telescope was set to be the centre of the sample holder, ca. 1 mm above the cathode surface.and the optics were aligned parallel to the cathode surface. The collected spectra were calibrated against the spectrum from a calibrated light source.

2.1. Spectral Analysis

The plasma emission spectra were analysed as a function of the plasma growth conditions (specifically the plasma current density) and the relative intensities of the most important plasma species were determined. In addition, the strong intensity of electronically excited C_2 molecules allowed the determination of the vibrational temperature of that species for different growth conditions. The emission spectra are very rich with dominant peaks that can be attributed to CH, C_2, atomic H and CN (from the NH_3:C_2H_2 gas mixture) emission. Typical spectra for the two different gas mixtures are shown in Fig. 2. The Swan bands from C_2 ($d\ ^3\Pi_g - a\ ^3\Pi_u$) are clearly visible with sequences Δv = -1, 0, 1 and 2 being clearly identifiable, as shown in Fig. 3, whereas the sequence Δv = -2 is only weakly

visible [19,20]. The C_2 Swan band intensities are used to determine the vibrational temperature of the molecule. According to the vibrational sum rule,

$$\sum_{v''}\left(I^{em}_{v''v'}\lambda^4\right) \propto N_{v'}, \tag{1}$$

where $I^{em}_{v''v'}$ is the band emission intensity, λ the emission wavelength and $N_{v'}$ is proportional to the population of the v' vibrational level. . For a plasma in local thermal equilibrium, the number density of molecules in an excited state is described by the Boltzmann distribution. Thus [20]

$$\ln\sum_{v''}\left(I^{em}_{v''v'}\lambda^4\right) = C_1 - \frac{G(v')hc}{k_B T_{vib}}, \tag{2}$$

where c is the speed of light, h Planck's constant, k_B Boltzmann's constant, $G(v')$ is the term value of the vibrational state v' and T_{vib} is the effective vibrational temperature of the molecule. C_1 is a constant. The term values were calculated using the anharmonic oscillator description of a vibrating rotator

$$G(v) = \omega_e\left(v+\frac{1}{2}\right) - \omega_e x_e\left(v+\frac{1}{2}\right)^2 + \omega_e y_e\left(v+\frac{1}{2}\right)^3 + \ldots \tag{3}$$

The constants for C_2 were taken from [19].

The vibrational temperature is therefore determined from the gradient of a plot of the logarithm of the sum of band strengths in the various v'' progressions against the term values, $G(v')$.

.

3. Results and Discussion

3.1. SEM Studies

SEM images of the structures produced for different plasma current densities are shown in Figs 4 and 5 for Fe catalysed growth and Ni catalysed growth, respectively. The quality of the grown structures depends critically on the plasma current. For Fe growth there is a well-defined transition from dense aligned multiwalled nanotube growth (predominantly base growth) for low plasma currents to individual tip-grown nanotubes at high plasma currents. This occurs for a plasma current of between 30 and 40 mA. Similar behaviour was observed previously by Delzeit et al. [4] using an inductively coupled rf plasma with the crossover occurring for plasma power in the range 30-40 W. The observation was discussed in terms of the relative concentration of H atoms. As the power is increased, the H intensity also increases. The H atoms can saturate the dangling bonds at the edges of the graphite basal planes that form the nanofibre structures. Delzeit et al. [4] also observed a decrease in the nanofibre density as the plasma power was further increased, as also observed in our results. For the highest plasma current investigated (Fig. 4) there is clearly enhanced deposition of amorphous carbon. Nolan et al. [8,21] showed a similar change in growth structures but in their case the change was initiated by introducing hydrogen. Multiwalled nanotubes were formed from CO on a supported Ni catalyst but when hydrogen was introduced the growth changed to that of nanofibres. The higher the concentration of hydrogen present, the larger was the angle of the graphite basal planes with respect to the nanofibre axis [8,21].

For Ni catalysed structures, the best growth conditions are also at approximately 30 mA. These conditions produce the best defined and straightest structures. The dependence on

plasma current is quite different for Ni compared to Fe. For low currents one does observe a tendency for the catalyst particle to break-up leading to the growth of multiple structures from one catalyst dot, however these are still tip-grown structures and do not resemble the dense multiwalled nanotubes found in the Fe case for low plasma currents. The small diameter nanofibre structures grown for low plasma currents typically show graphitic planes that are quasi-parallel to the axis, and are closer to multiwalled nanotubes than nanofibres [22]. It is possible that the higher relative concentration of carbon species for the low current conditions leads to enhanced metal dusting of the Ni catalyst [22] which, combined with the reduced requirement for hydrogen to saturate the edge atoms of the graphitic planes, leads to the observed change in growth. The much higher propensity for tip-grown nanofibres to be formed with Ni catalysts may be related to the much higher hydrogen solubility in Ni [8]. As the current is increased beyond 30 mA the structures become shorter and thicker and for the maximum current studied one can no longer regard the formed structures as nanofibres or nanotubes, instead domes of amorphous material are formed. The change in growth behaviour with increasing plasma current can be related to an increased influence of non-catalytic amorphous carbon deposition combined with enhanced etching. This behaviour is different from the trend observed by Meyyappan et al. for PECVD growth from a Ni catalyst film using a dc plasma and C_2H_2/NH_3 gas mixture [5]. In their study a transition from nanofibres to nanotubes was observed for high bias / high power growth (-600 V, 470 W). Note that the power used in that study was much higher than our maximum power (30 W) and the bias voltage was also larger corresponding to the abnormal regime of glow discharge. In the abnormal regime, the electric field inside the cathode sheath is significantly larger than in

a normal discharge (used here) which increases the mean energy of ions impinging onto surface [23] Higher ion energy results in increased penetration (implantation) depth of carbon atoms and the probability of unstable carbide phase formation is increased. When growth occurs from a thin (10nm) catalyst film, rather than lithographically patterned dots, under our maximum power conditions (30 W) then it is possible to observe some small nanofibres interspersed with nanotubes, Fig. 6. At the substrate edges the nanotube content is enhanced indicating an effect of the local electric field conditions. This growth more closely resembles the results discussed by Meyyappan et al. [5]. The catalyst preparation and initial geometry are thus also important factors in the growth process.

3.2. Optical Emission Measurements

The relative intensity of the main emission lines is plotted in Fig. 7 as a function of the plasma current for the C_2H_2/H_2 gas mixture (Fe catalysed growth). It is clear from Figs. 7(a) and 7(b) that in agreement with previous work [4], the relative intensity of H increases with increasing plasma current. This supports the discussion in the previous section related to the cross over from nanotube to nanofibre growth for Fe as the plasma current increases. The ratio of the CH and C_2 intensities remains constant with increasing plasma current, indicating that the CH is predominantly a product of C_2H_2 dissociation and is not a product of the reaction of hydrogen atoms with deposited carbon as observed by Caughman et al. [7]. Similar plots are shown in Fig. 8 for the C_2H_2/NH_3 gas mixture (Ni catalysed growth), in this case also including the relative intensity of the CN radical. The effect of plasma current is stronger in this case. Again one sees a clear increase in the relative intensity of H with respect to C_2 and CH. As for Fe (Fig. 7), the relative

intensities of C_2 and CH do not change significantly with increasing plasma current. There is, however, a very strong increase in the relative intensity of the CN radical for currents beyond 30 mA (the optimum current for nanofibre growth). The ammonia acts both as a supply of hydrogen atoms and serves to convert acetylene to HCN [13]. At high plasma currents the dissociation/reaction of acetylene in the gas phase is enhanced leading to a decrease in the nanofibre growth rate. This is in qualitative agreement with the study of Bell et al. [13] that showed that the nanofibre growth is a delicate balance between the concentration of carbon-removing species and the decomposition rate of C_2H_2, shown to be the main precursor to high quality nanofibre growth.

The temperature of the C_2 molecules in the plasma was determined using the method described in section 2. The analysis was not possible for the other molecular species due to poor signal to noise ratios and overlapping of the molecular emission lines with other plasma species. The logarithm of the sum of the band strengths is plotted in Fig. 9 as a function of the term value for different plasma currents using the NH_3 gas mixture (Ni catalysed growth). The measured gradients give the vibrational temperature of the C_2 molecules according to eq.(2). The extracted temperatures are shown in Fig. 10 for both Fe and Ni catalysed growth as a function of plasma current. There is very little dependence of the vibrational temperature on plasma current for the hydrogen plasma experiments (Fe catalysed growth). A weighted linear fit of the data gives a gradient of 91 ± 77 K/mA. The ammonia plasma data shows a more significant increase with plasma current with a weighted linear fit providing a gradient of 260 ± 140 K/mA.

In order to determine whether the plasma is in electronic thermal equilibrium we consider the intensities of the hydrogen Balmer lines. If the hydrogen atoms are in local thermal

equilibrium the Boltzmann plot method will allow the temperature, T_e, to be determined. The emission intensities, $I_{f\leftarrow i}$, are related to the temperature by

$$\ln\left(\frac{I_{f\leftarrow i}\lambda_{f\leftarrow i}}{g_i A_{f\leftarrow i}}\right) = \text{constant} - \frac{E_i}{k_B T_e} \tag{4}$$

where $A_{f\leftarrow i}$ and $\lambda_{f\leftarrow i}$ denote the spontaneous emission coefficient and the wavelength of the transition while g_i and E_i are the statistical weight and excitation energy of the upper state and k_B is the Boltzmann constant. Since we do not resolve the fine structure of the H_α, H_β and H_γ lines we sum over the individual fine structure contributions using the values of g and A listed in the NIST data base [24]. A plot of the logarithmic term versus the excitation energy of the upper state should therefore yield a straight line with negative gradient determined by the electronic temperature. Our data are shown in Fig. 11 and it is clear that the hydrogen atoms are not in thermal equilibrium. The content of more highly excited atoms is greater for the NH_3 plasma than for the H_2 plasma but there is a clearly an over-population of n = 4 and n = 5 in both cases. The relative populations do not change significantly with a change in the plasma current.

4. Conclusion

We have studied the plasma current dependence for dc PECVD growth of carbon nanotubes and carbon nanofibres under low plasma power conditions (3-30 W). The growth recipes were based on standard values for Fe [16] and Ni [18] catalysed growth. The morphology of the grown carbon nanostructures is seen to dependent strongly on the plasma power. For Fe catalysed growth there is a crossover from aligned multiwalled

nanotube growth at low plasma power (< 20 W) to individual carbon nanofibres at higher power. For Ni catalysed growth using lithographically defined catalyst dots we observe break up of the catalyst for the lowest power investigated and the formation of multiple small diameter tip-grown nanofibres. As the plasma power increases the nanofibre diameter is defined by the catalyst diameter [18] and the alignment improves as the local electric field at the substrate increases. The best structures are formed at an intermediate value of the plasma power (15 W). Beyond this value the nanofibres become shorter and thicker due to the non-catalytic deposition of amorphous carbon and the decrease in the availability of C_2H_2 as carbon precursor at the catalyst surface due to gas phase reactions involving nitrogen atoms.

Optical emission spectroscopy showed that the main parameter affecting the growth results in the case of the Fe catalyst was the relative intensity of hydrogen atoms with respect to molecular carbon species. For low H densities, base-grown multiwalled nanotubes are favoured but as the relative H density increases there is a sharp transition to tip-grown carbon nanofibres. The H atoms stabilize the nanofibres by saturating the dangling bonds at the edges of the graphitic planes. No significant variation in the vibrational temperature of the C_2 molecules in the plasma was found as a function of plasma power. For Ni growth, it is the interplay of the contributions from etching reactions and gas phase dissociation of the acetylene molecules that mainly determine the outcome. It was also shown that the growth results can depend strongly on the catalyst preparation (lithographically prepared dots versus thin film). The vibrational temperature was higher in the C_2H_2/NH_3 plasma than in the C_2H_2/H_2 plasma. There is an over-population of excited hydrogen atoms ($n > 3$) in both plasmas with the effect being larger

for the NH_3 plasma. The relative populations of the excited H levels do not change significantly with increasing plasma current within the investigated range.

The PECVD growth of carbon nanotubes and nanofibres is a complex multidimensional problem. Some insights into the important parameters and growth mechanisms are beginning to emerge from in situ spectroscopy studies. This work is a first step towards uunderstanding and optimizing the growth conditions in low power dc plasmas. The understanding and optimization of such low power plasmas is essential for the development of low substrate temperature growth that will allow the integration of carbon nanotubes with e.g. silicon electronics. Further studies concerning systematic pressure and gas composition variation combined with systematic studies of the role of catalyst preparation and detailed modeling are needed to develop a full understanding and control of the PECVD method for high quality nanotube and nanofibre growth.

Acknowledgements

Financial support from Vetenskapsrådet, the EC (NanoRF) and the Knut and Alice Wallenberg Foundation is gratefully acknowledged. OAN acknowledges financial support from KVA.

References

[1] *Carbon Nanotubes Science and Applications* ed. M. Meyyappan (CRC Press, 2005)

[2] Y. Zhang, A. Chang, J. Cao, Q. Wang, W. Kim, Y. Li, N. Morris, E. Yenilmez, J. Kog, H. Dai, Appl. Phys. Lett. **79** (2001) 8155

[3] K.B.K. Tao, D.B. Hash, R.G. Lacerda, N.L. Rupesinghe, M.S. Bell, S.H. Dalal, D. Bose, T.R. Govindan, B.A. Cruden, M. Chhowalla, G.A.J Amartunga, M. Meyyappan, W.I. Milne, Nano Lett. **4** (2004) 921

[4] L. Delzeit, I. McAninch, B.A. Cruden, D. Hash, B. Chen, J. Han, M. Meyyappan, J. Appl. Phys, **91** (2002) 6027

[5] M. Meyyappan, L. Delzeit, A. Cassell, D. Hash, Plasma Sources Sci. Technol. **12** (2003) 205

[6] T.Y. Lee, J.-H. Han, S.H. Choi, J.-B. Yoo, C.-Y. Park, T. Jung, S.G. Yu, W.K. Yi, I.T. Han, J.M. Kim, Diamond & Related Materials **12** (2003) 851

[7] J.B.O. Caughman, L.R. Baylor, M.A. Guillorn, V.I. Merkulov, D.H. Lowndes, L.F. Allard, Appl. Phys. Lett. **83** (2003) 1207

[8] P.E. Nolan, D.C. Lynch, A.H. Cutler, J. Phys. Chem. B **102** (1998) 4165

[9] B.A. Cruden, A.M. Cassell, D.B. Hash, M. Meyyappan, J. Appl. Phys. **96** (2004) 5284

[10] B.A. Cruden, M. Meyyappan, J. Appl. Phys. **97** (2005) 084311

[11] Y.Y. Lin, H.W. Wei, K.C. Leou, H. Li, C.H. Tung, M.T. Wei, C. Lin, C.H. Tsai, J. Vac. Sci, Technol. B **24** (2006) 97

[12] D.B. Hash, M.S. Bell, K.B.K. Teo, B.A. Cruden, W.I. Milne, M. Meyyappan, Nanotechnology **16** (2005) 925

[13] M.S. Bell, K.B.K. Teo, R.G. Lacerda, W.I. Milne, D.B. Hash, M. Meyyappan, Pure Appl. Chem. **78** (2006) 1117

[14] S.H. Lim, H.S. Yoon, J.H. Moon, K.C. Park, J. Jang, Appl. Phys. Lett. **88** (2006) 033114

[15] M. Meyyappan, "Growth: CVD and PECVD", Chapter 4 in *Carbon Nanotubes Science and Applications* ed. M. Meyyappan (CRC Press, 2005)

[16] R.E. Morjan, V. Maltsev, O.A. Nerushev, Y. Yao, L.K.L. Falk, E.E.B. Campbell, Chem. Phys. Lett. **383** (2004) 385

[17] M.S. Kabir, R.E. Morjan, O.A. Nerushev, P. Lundgren, S. Bengtsson, P. Enoksson, E.E.B. Campbell, Nanotechnology **16** (2005) 458

[18] M.S. Kabir, R.E. Morjan, O.A. Nerushev, P. Lundgren, S. Bengtsson, P. Enoksson, E.E.B. Campbell, Nanotechnology **17** (2006) 1

[19] G. Herzberg, *Molecular Spectra and Molecular Structure Vol. 1 – Spectra of Diatomic Molecules* (van Nostrand, New York, 2nd ed. 1950)

[20] D. Ono, S. Teii, J. Phys. D **16** (1983) 136

[21] P.E. Nolan, M.J. Schabel, D.C. Lynch, Carbon **33** (1995) 79

[22] Y. Yao, L.K.L. Falk, R.E. Morjan, O.A. Nerushev, E.E.B. Campbell, J. Microscopy, **219** (2005) 69

[23] Y. P. Raizer, *Gas discharge physics* (Springer, Berlin, 1991)

[24] http://www.physics.nist.gov/PhysRefData/Handbook/index.html

Figure Captions

Figure 1. Applied bias voltage to obtain plasma currents in the range 7 – 70 mA and the corresponding plasma power (a) for the C_2H_2/H_2 mixture at 8 Torr used for the Fe catalysed growth (b) for the C_2H_2/NH_3 mixture at 4 Torr used for the Ni catalysed growth.

Fig. 2. Optical emission spectra (a) Fe catalysed growth with an C_2H_2/H_2 gas mixture, plasma current 20mA (b) Ni catalysed growth with an C_2H_2/NH_3 gas mixture, plasma current 10mA.

Fig. 3. C_2 Swan bands used to determine the vibrational temperature. Data obtained for a C_2H_2/H_2 gas mixture, plasma current 50mA.

Fig. 4. SEM pictures of material grown from a thin Fe film for different values of the plasma current

Fig. 5. SEM pictures of material grown from lithographically patterned Ni dots for different values of the plasma current.

Fig. 6. SEM pictures of material grown from a Ni thin film with a plasma current of 70 mA. A: taken from the centre of the substrate, scale bar 100 nm B: taken at the substrate edge where there is a higher local electric field during growth, scale bar 1 μm.

Fig. 7. Relative intensity of selected emission lines as a function of the plasma current for Fe catalysed growth (C_2H_2/H_2 gas mixture)

Fig. 8. Relative intensity of selected emission lines as a function of the plasma current for Ni catalysed growth (C_2H_2/NH_3 gas mixture)

Fig. 9. Logarithm of the sum of the band strengths for the Swan band in a C_2H_2/NH_3 plasma for different plasma currents. The vibrational temperature is obtained from a linear fit to the data points.

Fig. 10. Vibrational temperature of C_2 (a) Fe catalysed growth (C_2H_2/H_2 gas mixture) (b) Ni catalysed growth (C_2H_2/NH_3 gas mixture)

Fig. 11. Boltzmann plot for the hydrogen Balmer transitions. The data clearly show an over-population of the states for n>3.

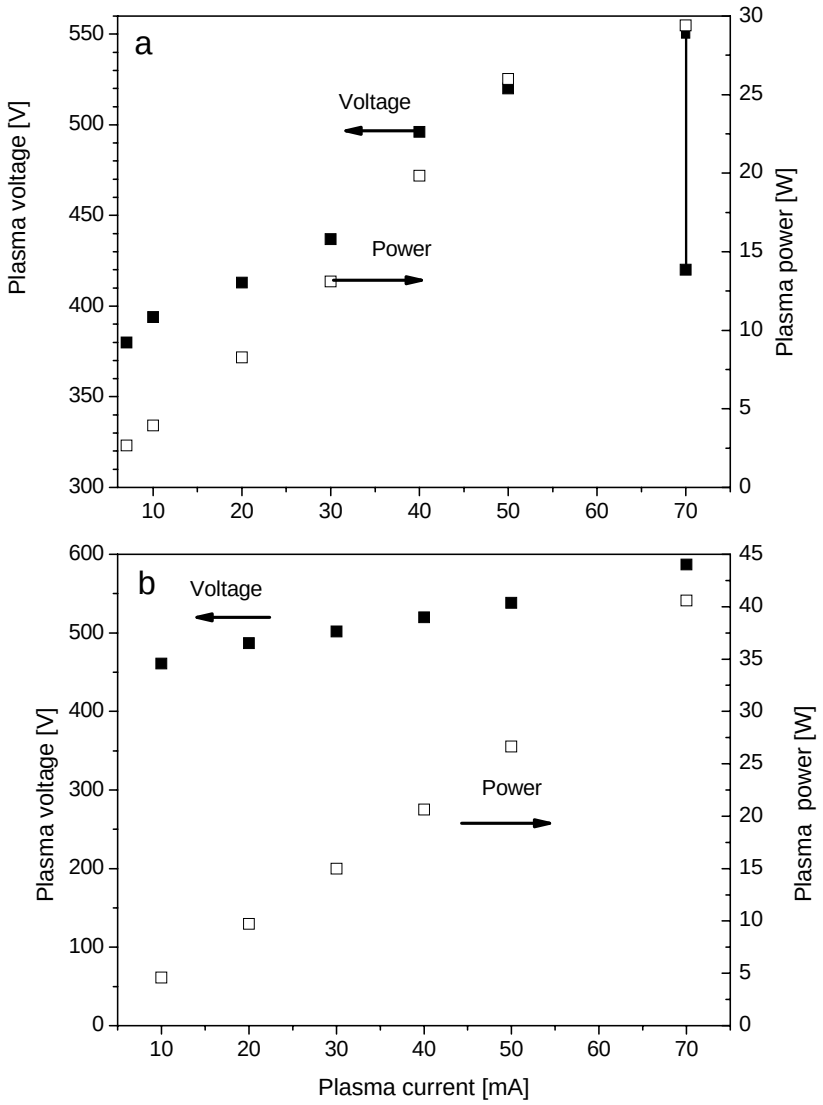

Fig. 1 Jönsson et al.

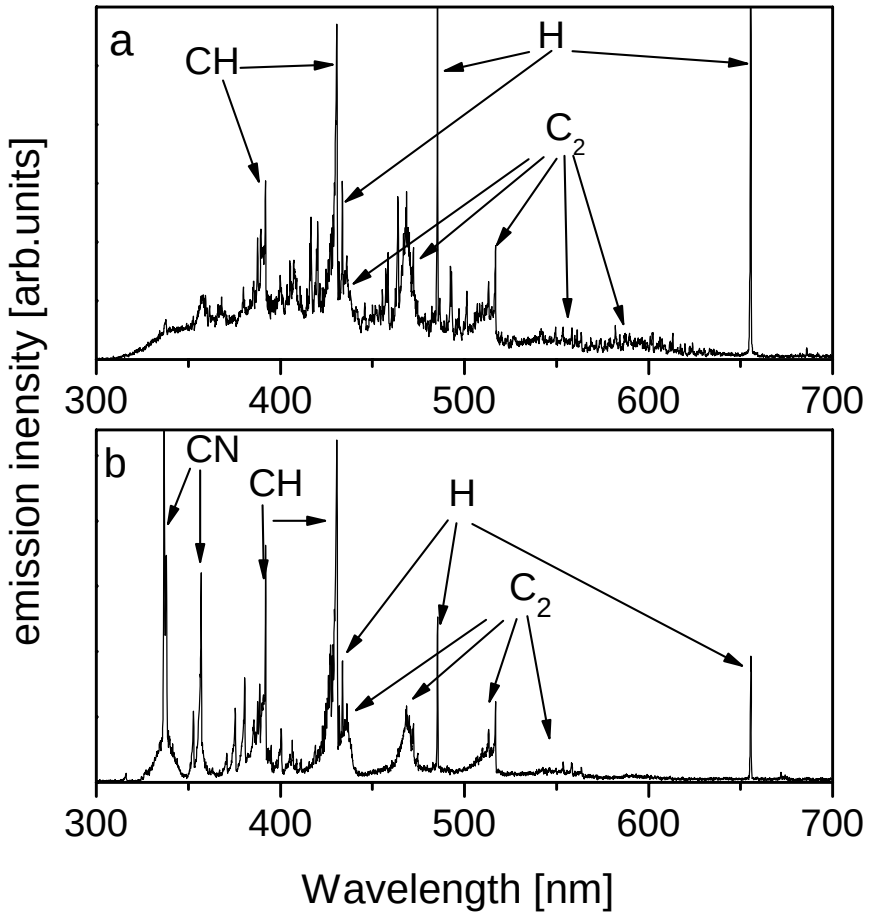

Fig. 2 Jönsson et al.

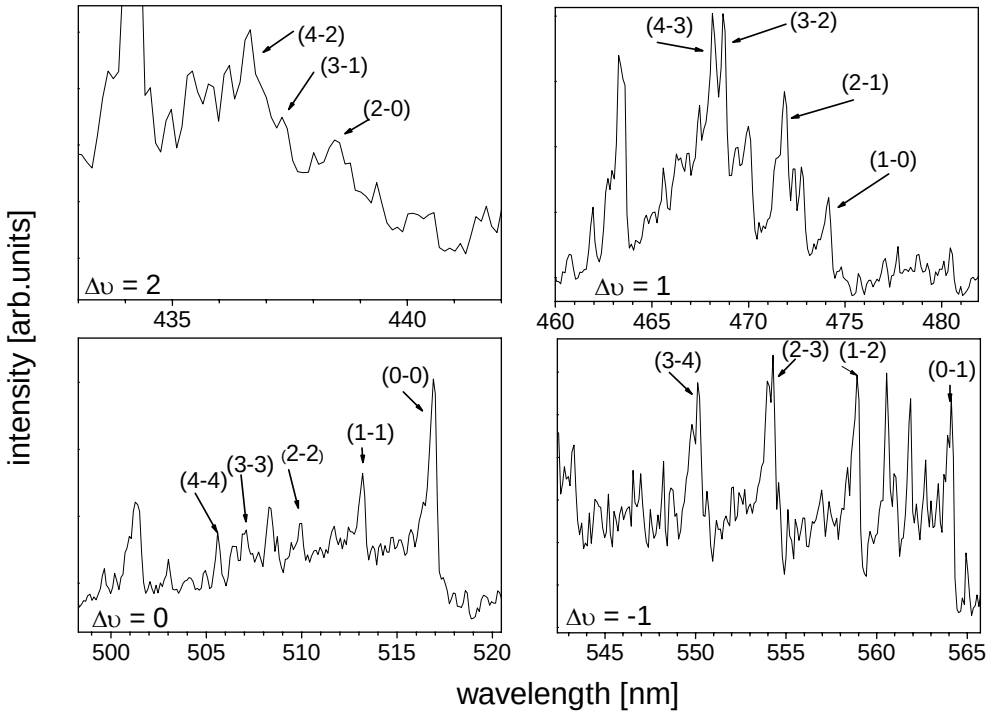

Fig. 3 Jönsson et al.

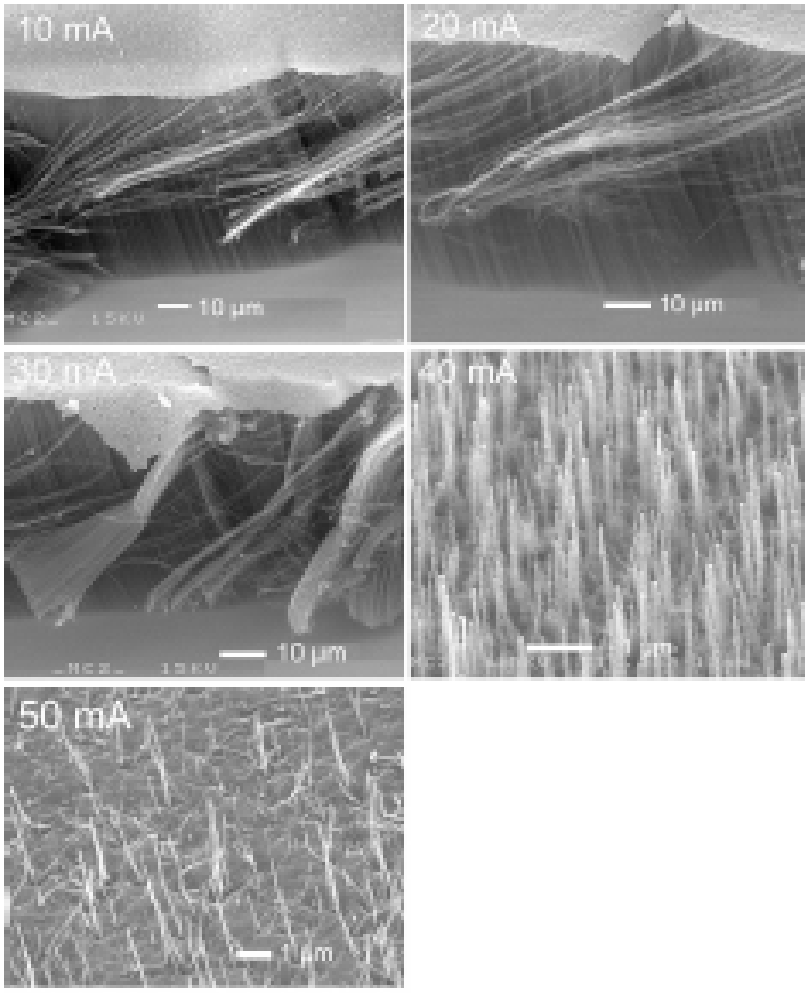

Fig. 4 Jönsson et al.

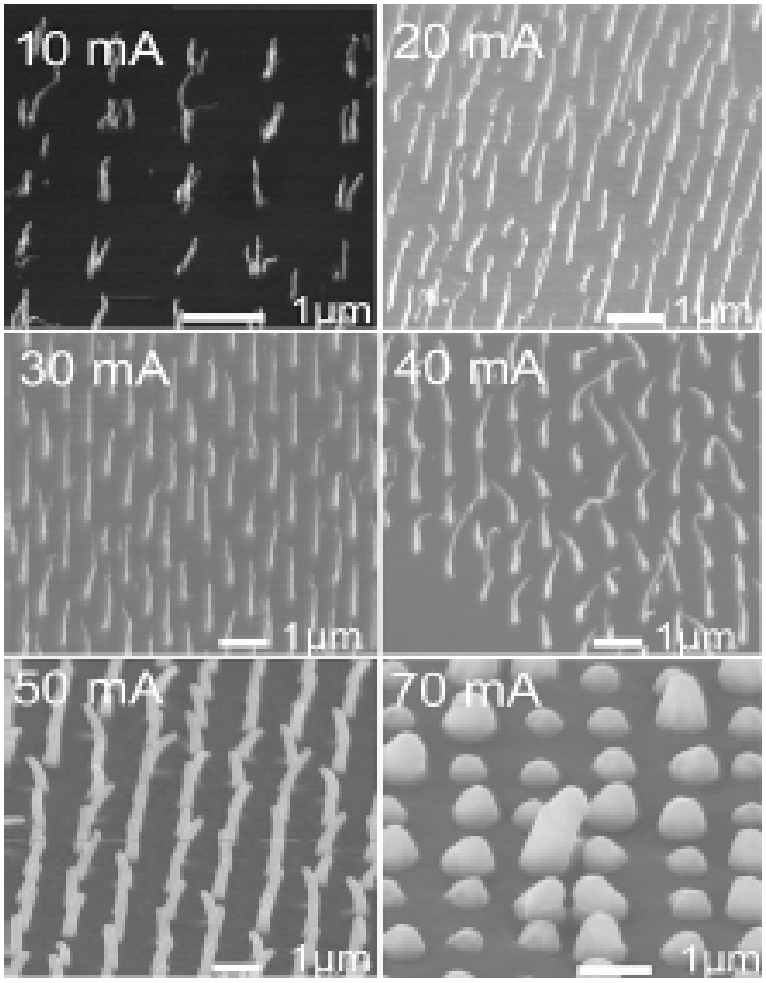

Fig. 5 Jönsson et al.

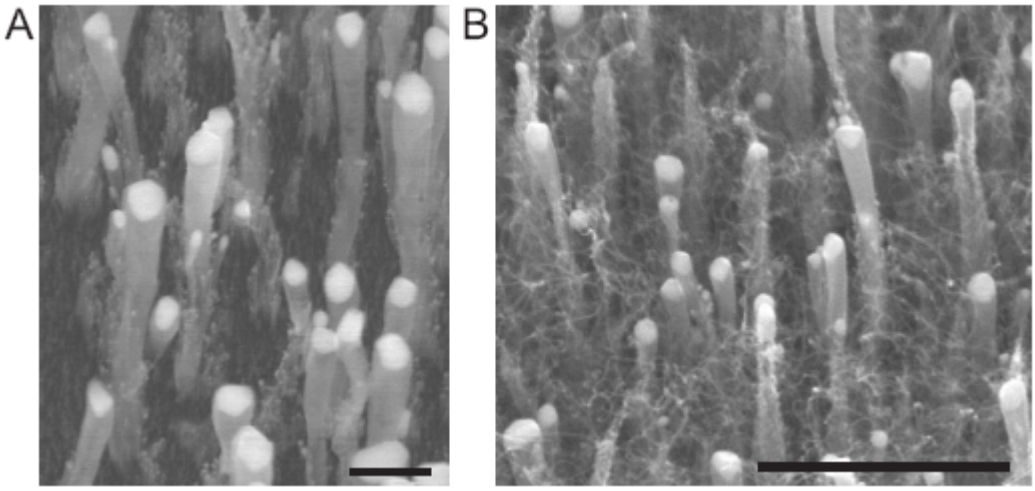

Fig. 6 Jönsson et al.

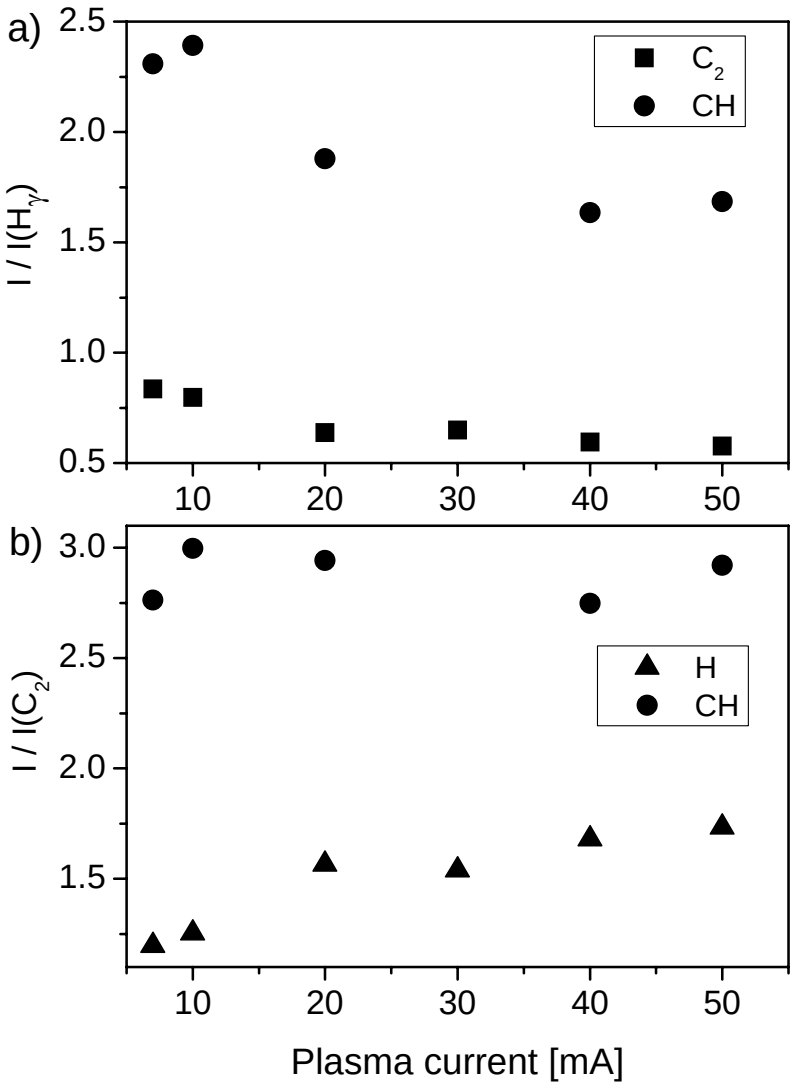

Fig. 7 Jönsson et al.

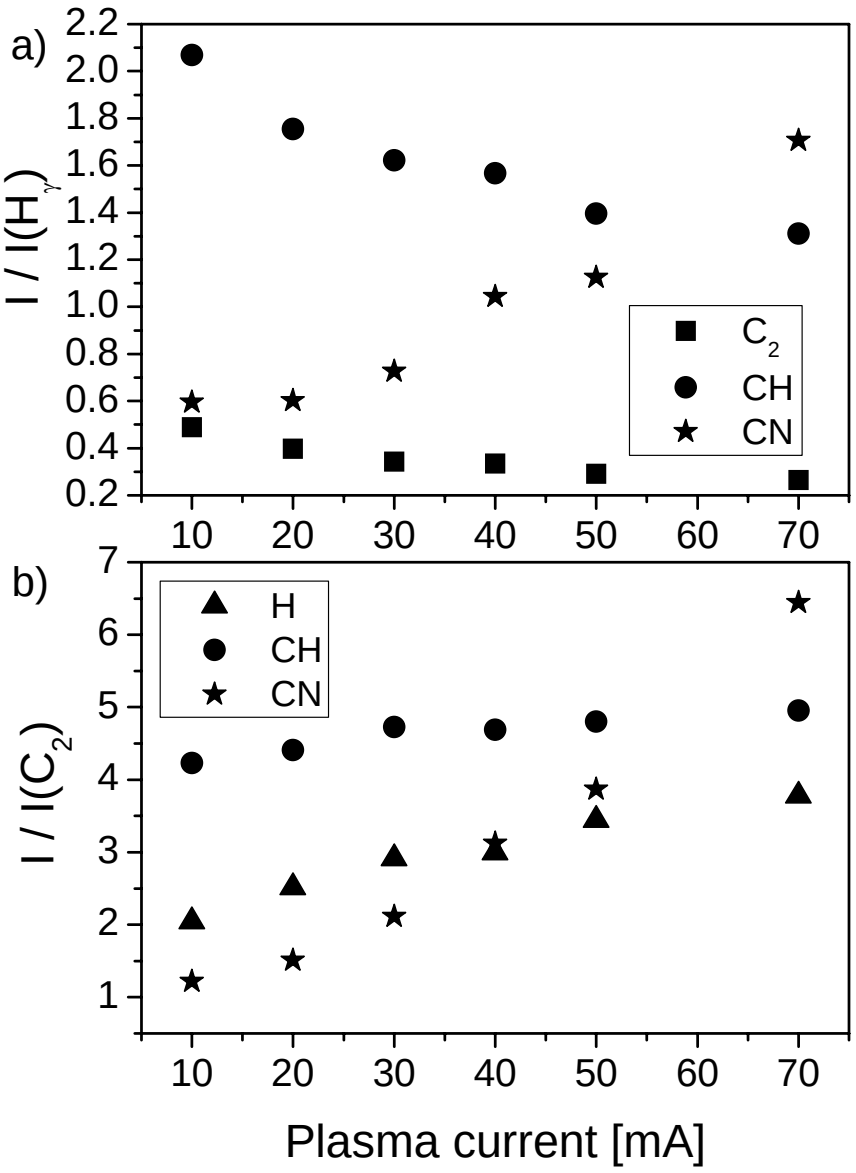

Fig. 8 Jönsson et al.

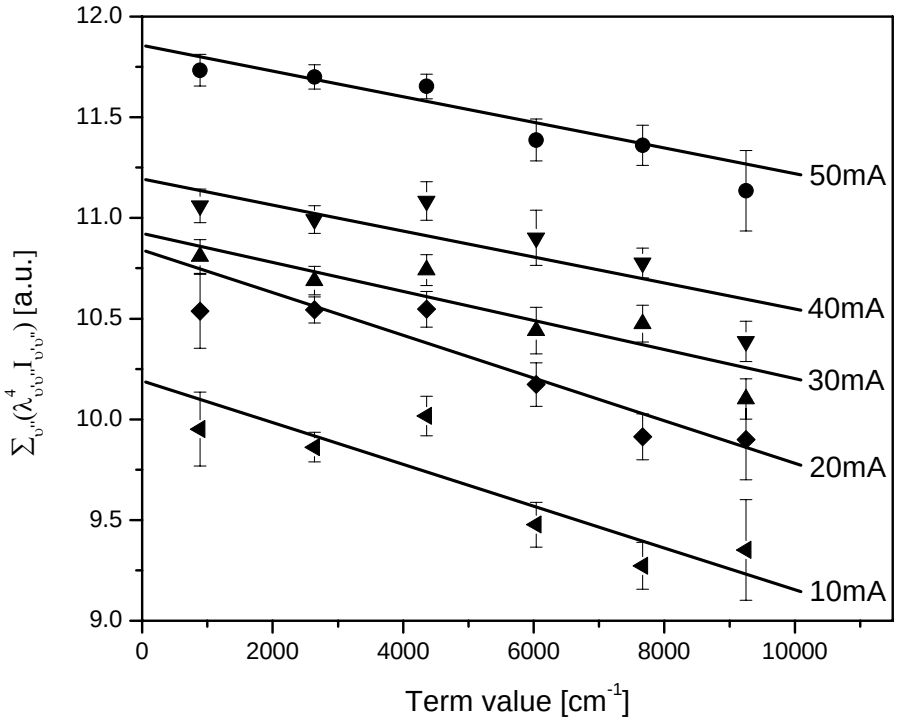

Fig. 9 Jönsson et al.

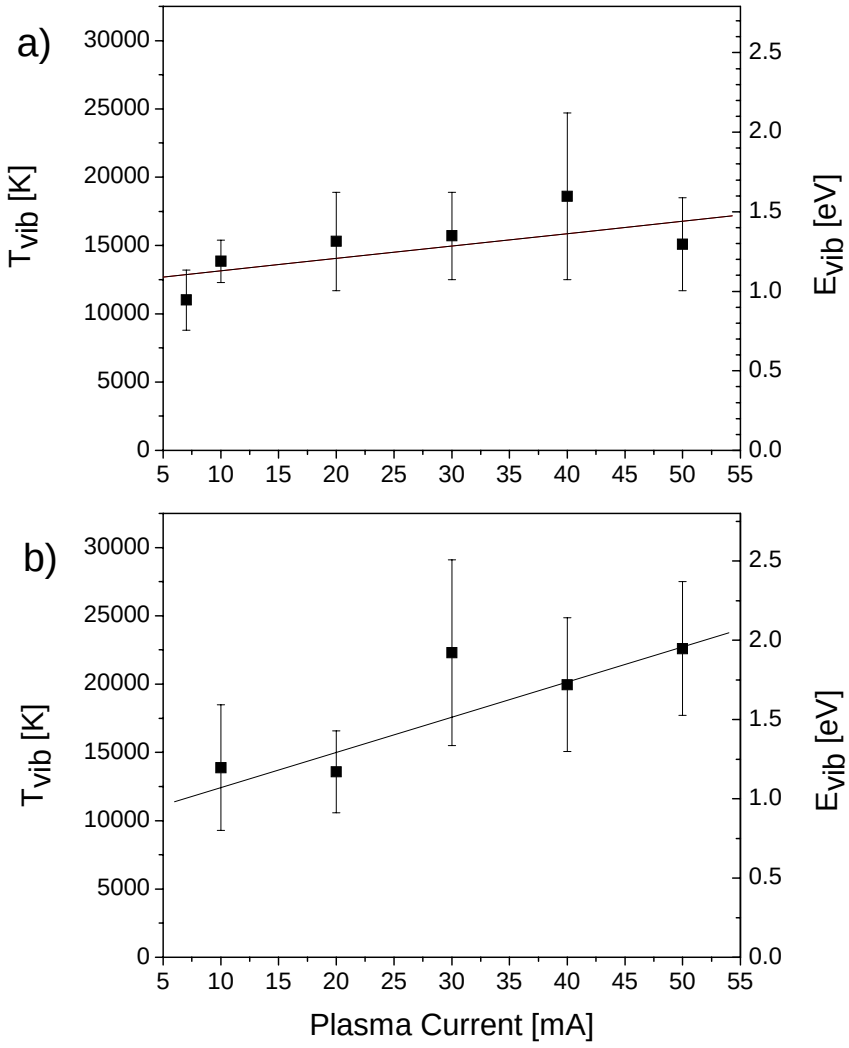

Fig. 10 Jönsson et al.

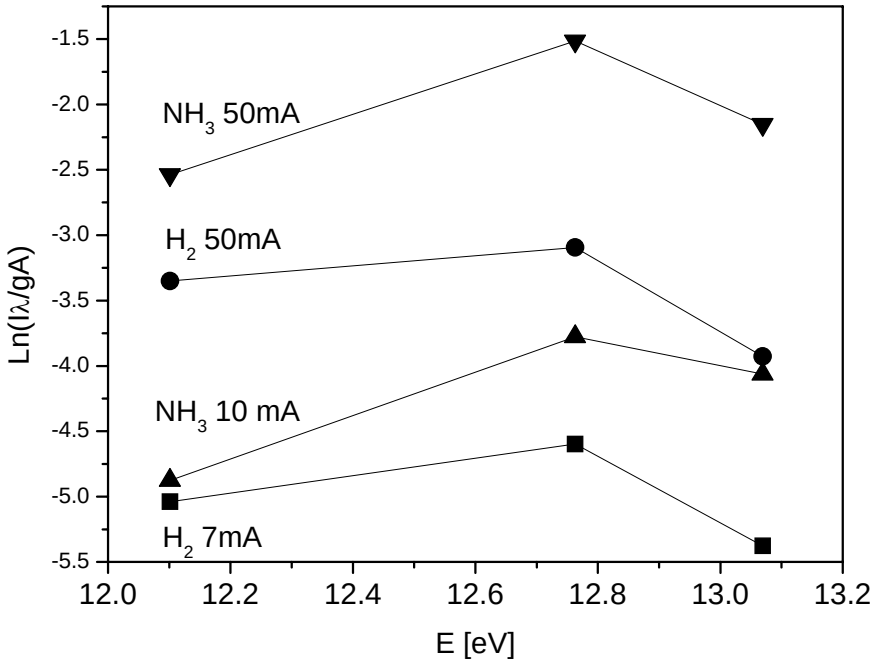

Fig. 11 Jönsson et al.

Paper II

In situ growth rate measurements during plasma enhanced chemical vapour deposition of vertically aligned multiwall carbon nanotube films
Submitted to Nanotechnology.

Submitted to Nanotechnology

In situ growth rate measurements during plasma enhanced chemical vapour deposition of vertically aligned multiwall carbon nanotube films

M. Jönsson, O.A. Nerushev[†], E.E.B. Campbell*

Department of Physics, Göteborg University, SE-41296 Göteborg, Sweden

†: Permanent address: Institute of Thermophysics, RAS SB, 1 Acad. Lavrentyev Ave., 63090 Novosibirsk, Russia

*. Corresponding author: Email: Eleanor.campbell@physics.gu.se, tel. +46 31 772 3272, Fax: +46 31 772 3496

Abstract

In situ laser reflectivity measurements are used to monitor the growth of multiwalled carbon nanotube films grown by dc PECVD from an iron catalyst film deposited on a silicon wafer. In contrast to thermal CVD growth, there is no initial increase in the growth rate, instead the initial growth rate is high (on the order of 8 μm per minute) and then drops off rapidly to reach a steady level (2 μm per minute) for times beyond 1 minute. We show that a limiting factor for growing thick films of MWNT using PECVD can be the formation of a thin amorphous carbon layer at the top of the growing nanotubes. *In situ* reflectivity measurements provide a convenient technique for detecting the onset of the growth of this layer.

1. Introduction

Plasma enhanced chemical vapour deposition (PECVD) is extensively used for growing aligned multiwalled carbon nanotubes and nanofibres [1]. For the growth of multiwalled nanotubes (MWNT) its main advantage at present is the improved alignment of the nanotubes that is frequently reported, but it may also provide a means of growing vertically aligned nanotubes at relatively low substrate temperatures that can be advantageous for a number of potential applications [2]. Although many studies concerning PECVD growth have been carried out in recent years we still know very little about the detailed mechanisms of growth and the main parameters affecting the growth process. This leads to many problems associated with reproducibility of growth results between different groups and even within the same group. It is therefore essential to develop and apply *in situ* measurement techniques to directly provide information on growth rate, plasma conditions etc. and correlate these studies with the quality and properties of the grown structures. Laser reflectivity measurements provide direct information on the thickness of the growing nanotube films and have provided important insight into the growth behaviour of aligned multiwalled nanotube films grown using thermal CVD [3,4]. This technique has not been applied so extensively to PECVD MWNT films [5,6] and to our knowledge has not yet been applied to the study of iron catalysed MWNT films that could be directly compared with the thermal CVD results.

In this paper we apply the laser reflectivity technique, based on optical interference, to determine the thickness of MWNT films during Fe-catalysed PECVD growth. We show that there is no initial incubation stage where the growth rate initially increases with time, as observed in thermal CVD. The growth begins at a high rate (equivalent to that

observed in thermal CVD) and then rapidly decreases to reach a steady state after about 1 minute. We also show that the presence of dissociation products from the plasma reactions of the precursor gases contribute to the non-catalytic deposition of carbon which leads to the formation of a thin amorphous carbon layer at the top of the growing nanotube film. The onset of the film deposition and its development with time can be monitored by detecting the reflected laser intensity.

2. Experimental Setup

Films of vertically aligned multiwalled carbon nanotubes (MWNT) were grown on silicon wafers using DC plasma-enhanced chemical vapour deposition (PECVD). The set-up has been described earlier [7,8]. Samples were prepared by evaporating a 1 nm thick catalyst film of Fe onto a doped silicon wafer with native oxide. The substrates were attached to a grounded cathode and inserted into the growth chamber. The chamber was pumped down to 5 x 10^{-6} Torr. After reaching this pressure, the substrate was heated to a temperature of 700 ^{o}C before the growth gas was introduced to the chamber. A voltage of 400 V was applied between the cathode and an anode (an M6 steel screw) situated at a distance of 10-15 mm from the substrate surface. This produced a plasma current on the order of 15 mA corresponding to a current density of 1.5 mA/cm^2. The nanotube growth was performed under continuous flow conditions. An C_2H_2:H_2 gas mixture in proportion 1:9 at flow rates of 225 sccm (H_2), 25 sccm (C_2H_2) and a total chamber pressure of 8 Torr was used.

For *in situ* monitoring of the carbon nanotube growth rate, a small 3 mW diode laser (λ = 670 nm) was mounted on the growth chamber. The laser was focused on the substrate

surface through a viewport at the top of the chamber and the reflected light was detected by a photodiode mounted outside a side viewport, Fig. 1. A band-pass filter was placed in front of the photodiode to limit the background emission from the plasma [8]. The incident angle of the light on the substrate was 35^{o}. The photocurrent was detected using an Agilent 3410A multimeter and readout via GPIB using Labview.

3. Results and Discussion

The reflected laser intensity is measured before the precursor gases are let into the vacuum chamber and drops rapidly when the growth starts. A typical run is shown in Fig. 2 and one can clearly see the expected interference oscillations, resulting from interference between the light reflected from the top of the MWNT film and light reflected from the nanotube-silicon interface. If the effective refractive index of the nanotube film was known then one could directly extract the film thickness from the peak positions. In order to calibrate the measurements, we stop growth after a defined number of interference fringes and determine the film height using SEM. The films were scraped with tweezers to expose a side-view. Some examples of the films are shown in Fig. 3. The images are taken at an angle of 45^{o}. The vertical scale bar (indicating a length of 1 μm) takes the viewing angle into account. The results are summarised in Fig. 4 where the measured film thickness is plotted against the number of interference maxima. A least squares fit of the data yields a spacing of 350 ± 20 nm/peak. The incremental height for successive maxima corresponds to a phase shift $\delta = 2\pi$ between the interfering light beams. One can therefore extract the effective refractive index of the MWNT film from the expression

$$\partial = \frac{4\pi d}{\lambda_0}\left(n_{eff}^2 - n_{vac}^2 \sin^2 \vartheta_i\right)^{1/2} \quad (1)$$

where d is the film thickness, λ_0 the laser wavelength (670 nm) and ϑ_i the angle of incidence of the laser beam on the nanotube film. We assume that the refractive index of the low density plasma $n_{vac} = 1$ and n_{eff} is the effective refractive index of the porous MWNT film. We obtain a value of $n_{eff} = 1.12 \pm 0.06$ nm for the growth temperature of 700 ^{o}C. This is in reasonably good agreement with the effective refractive index of 1.075 measured for thermal CVD grown MWNT films at 570 ^{o}C [4]. Following Puretsky et al. [4] we can estimate the porosity of our nanotube films using the Looyenga formula

$$\varepsilon_{eff}^{1/3} = (1-p)\varepsilon^{1/3} + p\varepsilon_m^{1/3} \quad (2)$$

where p is the film porosity (the ratio of the empty pore volume to the total volume), ε the dielectric constant of the embedded solid phase i.e. the nanotubes which we take to be the same as for amorphous carbon particles, $\varepsilon = 4$ [9], $\varepsilon_m = 1$ the dielectric constant of the host medium and $\varepsilon_{eff} = n_{eff}^2 = 1.25$ the dielectric constant of the film. We obtain a porosity of 0.87 ± 0.04 which can be compared with the porosity obtained for the thermal CVD grown films of 0.92 [4].

After the calibration, the thickness of the growing MWNT film could be monitored directly *in situ* from the time dependence of the reflected intensity. The results of *in situ* monitoring of the film thickness as a function of growth time are shown in Fig. 5(a) for four different growth runs. There is a certain amount of fluctuation from run to run but the trends are very similar. The corresponding growth rates are plotted in Fig. 5(b) for the same data. Most of the samples grow at a very similar rate but one of the samples starts

growing much faster than the others. The reason for this is not known but it clearly illustrates the necessity of having an in situ diagnostic method for accurate length growth. Unlike the thermal CVD measurements [4] we do not observe an initial increase in the growth rate. In the thermal CVD studies the growth rate was seen to increase for times in excess of 50 seconds. An initial increase in growth rate with increasing nanotube length was noted by Kim et al. [5] in PECVD growth of nanotube films from pretreated Ni film. However, the scatter in their data is very large and their films also appear to be a mixture of nanofibres (although unusually with the catalyst particle at bottom) and nanotubes [5], similar to the films discussed by Meyyappan et al. [10]. They interpret their results in terms of a surface diffusion mechanism [11] where one could expect the growth rate to increase as long as the carbon nanotubes are shorter than the diffusion length. We do not observe such an effect in our measurements. The initial high growth rate that we observe is very similar to the growth rate reported previously for PECVD growth of MWNT films from Fe thin films under somewhat different growth conditions where the growth rate was determined by measuring the film thickness in SEM as a function of growth time [7]. In those earlier experiments the high growth rate continued up to approximately 200 s, much longer than in the present experiments. We have recently been unable to repeat these high growth rate experiments in spite of (or because of) improving the gas handling system, one of the motivations for introducing *in situ* measurement techniques. In the present experiments, the growth rate rapidly decreases after the initial spurt until reaching a steady state rate of 0.03 μm/s at around 60 s. A decrease in growth rate has been related to the onset of catalyst poisoning either by over-coating or deactivating active sites on the catalyst surface [4]. This may be enhanced under the PECVD conditions due to the

presence of highly reactive gas phase species produced by the plasma which can lead to non-catalytic carbon deposition. Evidence for such non-catalytic deposition can be clearly seen in the present study. Fig. 6 shows an example of measurements of the reflected laser intensity over a much longer time (500 s). After 100 s the reflectivity increases. This is due to the deposition of an amorphous carbon layer at the top of the growing nanotube film. This film deposition is not normally discussed in the literature but evidence can be seen for it in a number of published SEM images of PECVD grown nanotubes, e.g. Figure 5 in [10]. As the carbonaceous layer starts to develop, the scattered light from the cover layer increases the signal measured by the photodiode. This increase in scattered light continues as the layer grows denser. When the amorphous carbon on top of the nanotubes starts to resemble a homogeneous layer, on the scale of the laser wavelength, the scattering becomes more specular in nature. However, since the surface is not completely flat, only a small portion of the light is reflected towards the detector and hence the detected intensity starts to decrease again. To investigate the development of the cover layer, growth was stopped at different stages. In Figure 7, SEM pictures of the top of the nanotube films are shown for different growth stages. Fig. 7(a) shows the nanotube film after 40 s growth, i.e. before the cover layer begins to form. Fig. 7(b) shows a nanotube film where growth was stopped after 150 s and Fig. 7(c) shows a film grown for 550 s where the cover layer has become flatter and more homogeneous. Note that the nanotubes continue to undergo base growth below the thin amorphous film (Fig. 3) until it forms an impervious layer.

4. Conclusions

We have investigated the PECVD growth of MWNT films using time-resolved reflectivity to obtain *in situ* information on the film thickness and growth rates. Unlike similar studies of thermal CVD grown carbon nanotubes [4], we do not observe an increase in the growth rate with growth time. Instead we have very efficient growth in the initial stages (equivalent to rates measured for thermal CVD growth) that rapidly falls off to a steady state for times beyond 60s. Although it is possible to grow long MWNT using PECVD [7], it is more frequently the case that the growth stops for film thicknesses much less than those reported for thermal CVD. Due to the presence of dissociation and reaction products of the precursor gases in the PECVD [8] there is a much greater propensity for non-catalytic deposition which can lead to enhanced catalytic poisoning. Here we show that this non-catalytic deposition can also lead to the formation of a thin amorphous carbon film at the top of the growing MWNT film. The *in situ* reflection method is very suitable for detecting the onset of such film formation. PECVD grown MWNT typically have a higher degree of alignment than thermal MWNT and are considered for a variety of possible applications such as field emission, composite materials etc. It is obviously essential to avoid the deposition of any amorphous coating if the properties of such films are to be maximized. *In situ* reflectivity measurements provide a way of ensuring that the nanotube films are clean.

There are still many open questions concerning the detailed growth mechanisms of carbon nanotubes and many problems associated with reproducibility of growth conditions. These problems can only be solved if we acquire a greater understanding of

the parameters that are affecting growth. *In situ* measurement techniques such as the reflectivity studies discussed here combined with other *in situ* methods such as optical spectroscopy and gas analysis will provide an important set of techniques for such essential systematic studies.

Acknowledgements

Financial support from Vetenskapsrådet, SSF and the Knut and Alice Wallenberg Foundation is gratefully acknowledged. OAN acknowledges financial support from KVA.

References

[1] Meyyappan M., 2005 *Carbon Nanotubes Science and Applications* (CRC Press)

[2] Boskovic B.O., Stolojan, V., Khan, R.U.A., Haq, S., Silva, R.P., 2002 *Nature Materials* **2** 165

[3] Geohegan, D.B., Puretzky, A.A., Ivanov, I.N., Jesse, S., Eres, G., Howe, J.Y., 2003 *Appl. Phys. Lett*. **83** 1851

[4] Puretzky, A.A., Geohegan, D.B. Jesse, S., Ivanov, I.N., Eres, G., 2005 *Appl. Phys. A* **81** 223

[5] Kim, D.-H., Jang, H.S., Kim, C.-D., Cho, D.S., Yang, H.-S., Kang, H.-D., Min, B.-K., Lee, H.-R., 2003 *Nano Lett.* **3** 863

[6] Kim, D.-H., Jang, H.S., Kim, C.-D., Cho, D.S., Jee, J.-G., Lee, H.-R., 2003 *Nanotechnol.* **14** 46

[7] Morjan, R.E., Maltsev,V., Nerushev, O.A., Yao, Y., Falk, L.K.L., Campbell, E.E.B., 2004 *Chem. Phys. Lett*. **383** 385

[8] Jönsson, M., Nerushev, O.A., Campbell, E.E.B., submitted to Appl. Phys. A

[9] Rohlfing, E.A., 2003 *J. Chem. Phys*. **118** 7622

[10] Meyyappan, M., Delzeit, L., Cassell, A.,Hash, D., 2003 *Plasma Sources Sci. Technol.* **12** 205

[11] Louchev, O.A., Sato, Y., Kanda, H., 2002 *Phys. Rev. E* **66** 011601

Figure Captions

Fig. 1. Schematic diagram of the measurement setup.

Fig. 2. Typical reflection measurement showing the interference fringes.

Fig. 3. SEM images of three vertically aligned MWNT films. The images were taken where the films were scraped with tweezers to expose a side-view. The images were taken at an angle of 45^{o} and the scale bar in each figure indicates 1 μm in the vertical direction. Growth stopped after (a) 15 s (b) 40 s (c) 120 s.

Fig. 4. Film length determined from SEM versus number of observed interference peak maxima.

Fig. 5. (a) Length of MWNT as a function of growth time (b) Growth rate as a function of growth time. The different symbols represent different measurement series.

Fig. 6. Reflectivity measurement extended to long growth times. Note the increase in reflectivity after about 100 s.

Fig. 7. SEM images of the top of MWNT films after different growth times showing the gradual formation of an amorphous coating (a) 40 s growth (b) 150 s growth (c) 550 s growth.

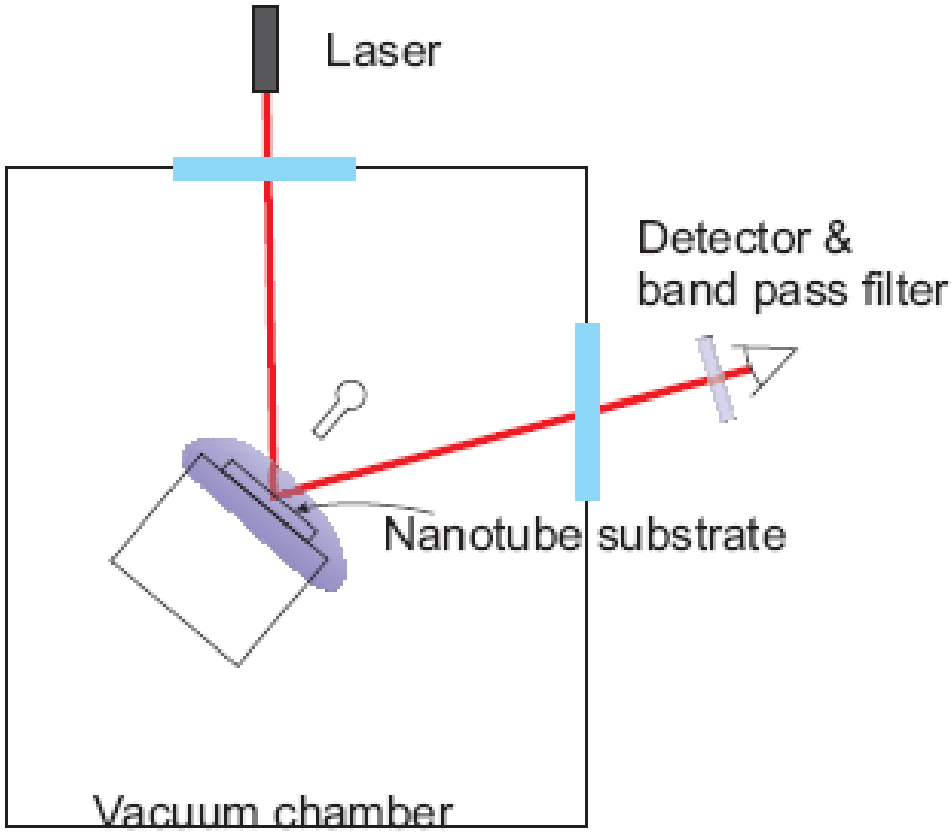

Fig. 1. Jönsson et al.

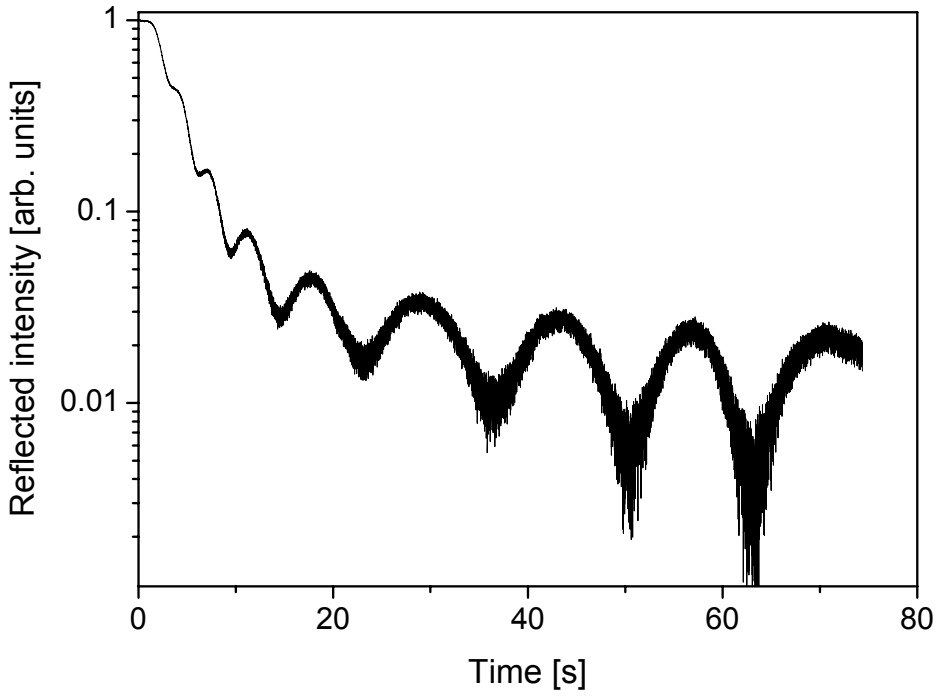

Fig. 2. Jönsson et al.

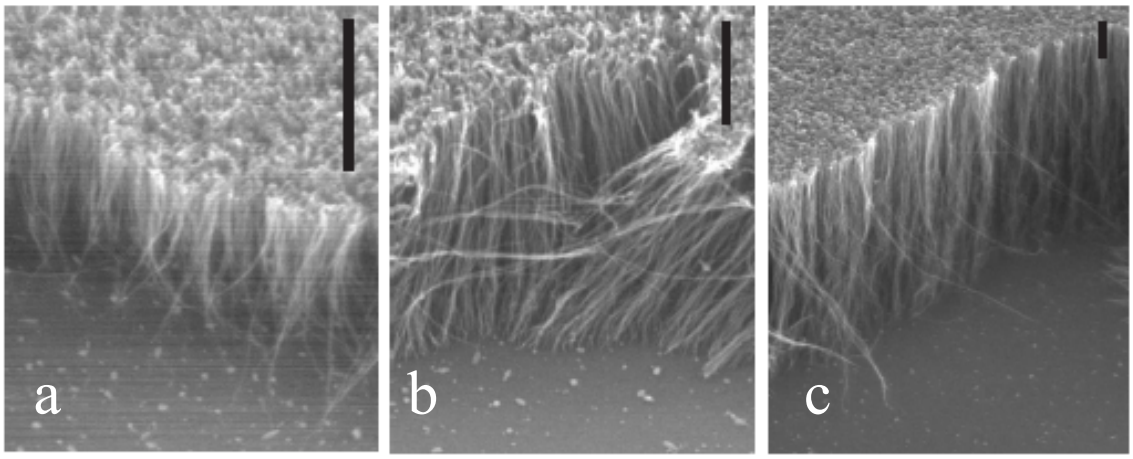

Fig. 3. Jönsson et al.

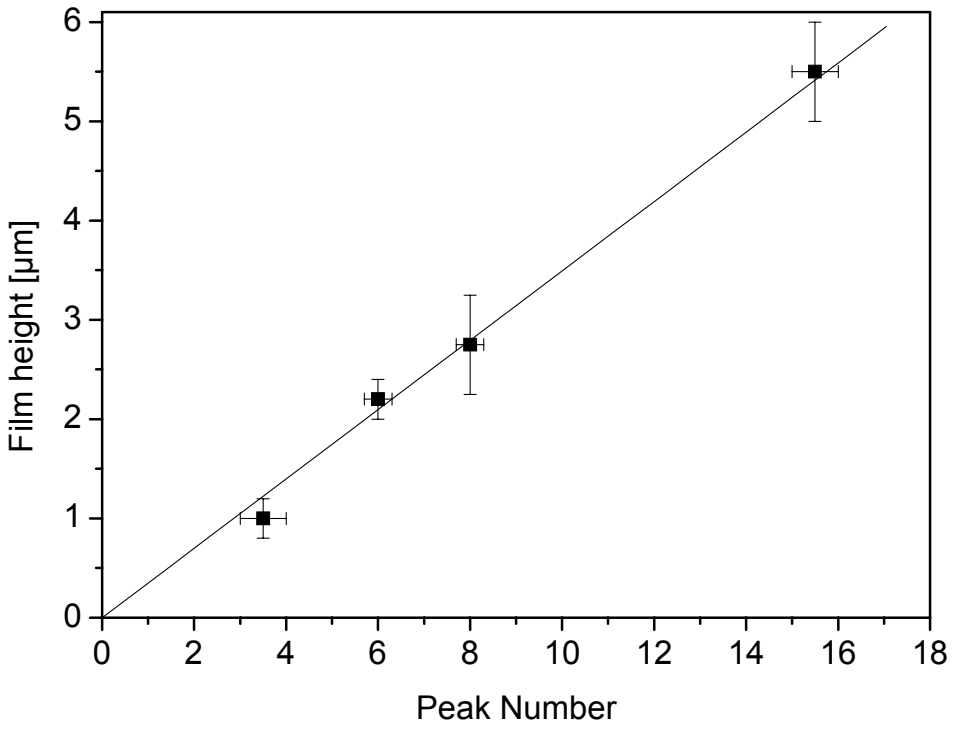

Fig. 4. Jönsson et al.

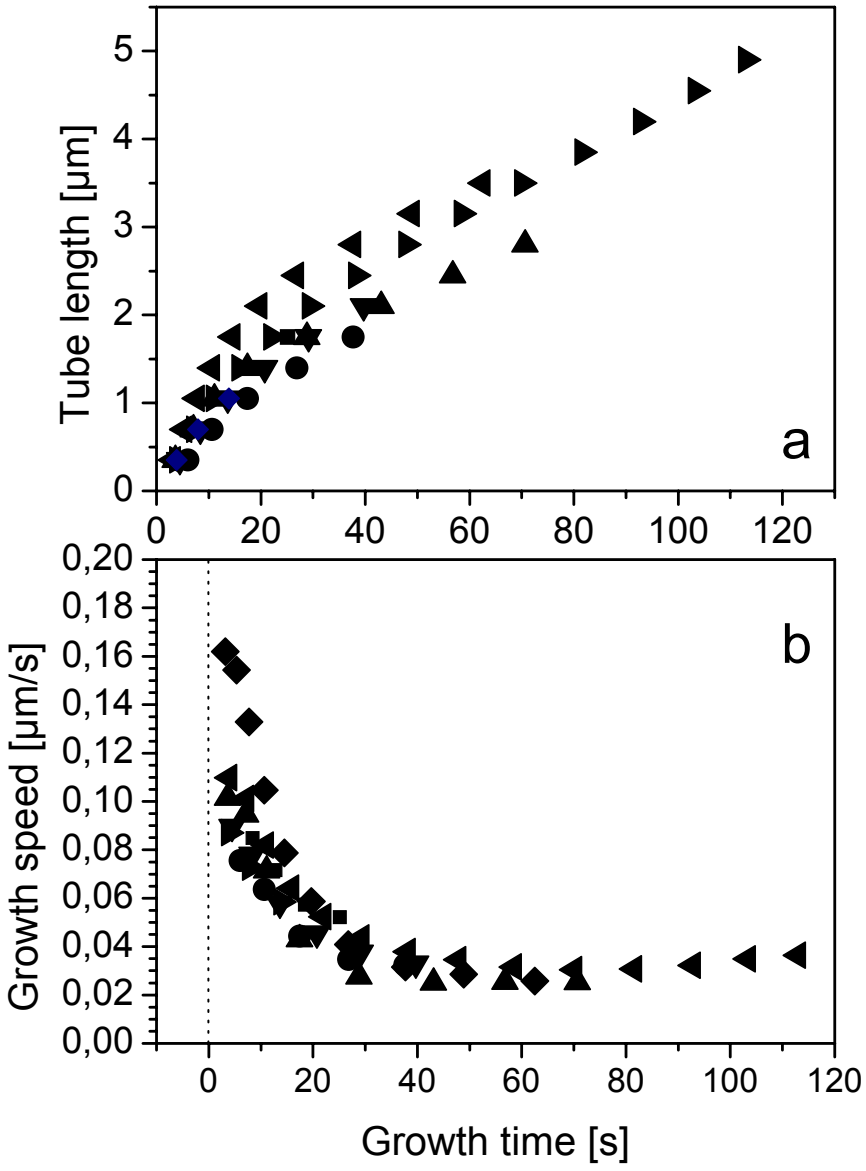

Fig. 5 Jönsson et al.

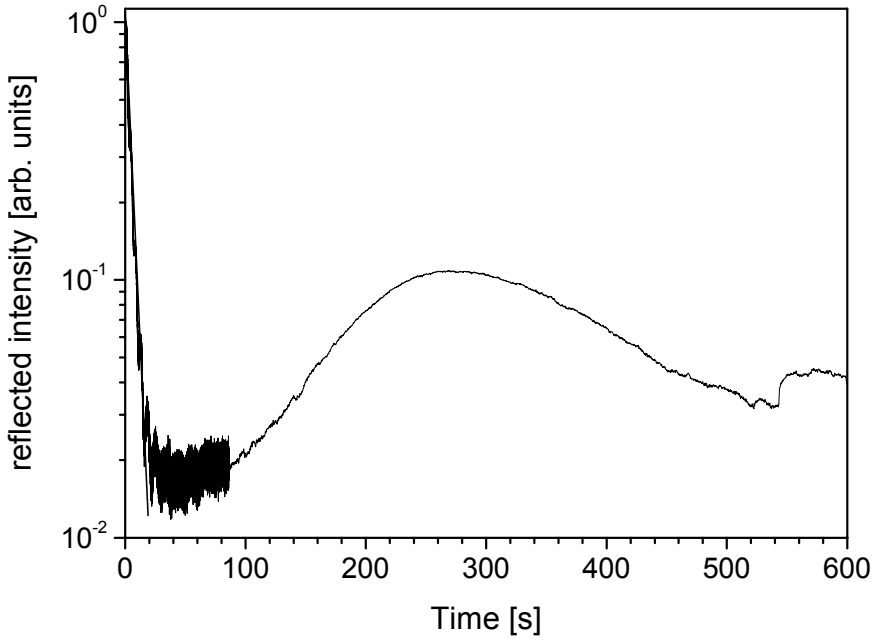

Fig. 6 Jönsson et al.

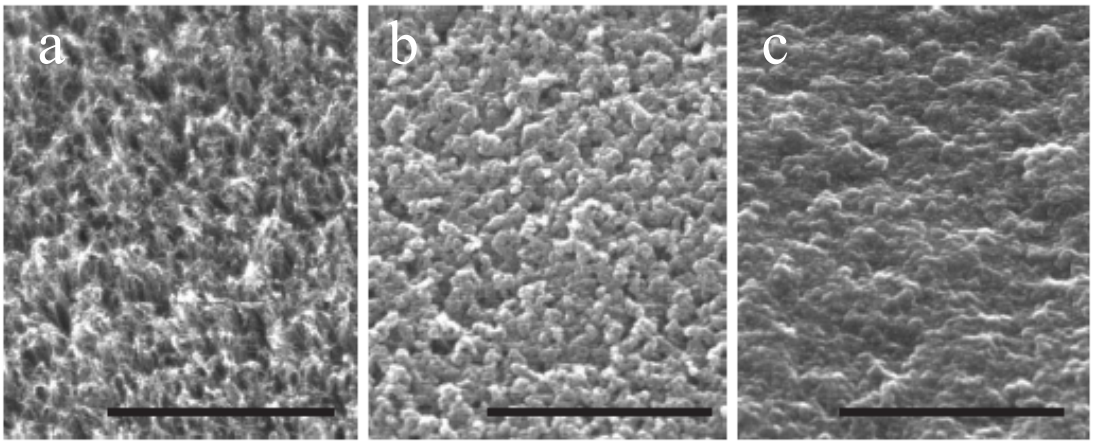

Fig. 7 Jönsson et al.

Paper III

Blackbody Radiation from Resistively Heated
Multi-Walled Carbon Nanotubes During Field Emission
Appl. Phys. Lett. **81**, 1095 (2002).

Blackbody radiation from resistively heated multiwalled carbon nanotubes during field emission

M. Sveningsson, M. Jönsson, O. A. Nerushev,[a] F. Rohmund,[b] and E. E. B. Campbell[c]
Department of Experimental Physics, School of Physics and Engineering Physics, Göteborg University and Chalmers, SE-41296 Göteborg, Sweden

(Received 11 March 2002; accepted for publication 6 June 2002)

We report the observation of blackbody radiation from aligned multiwalled carbon nanotubes undergoing field emission. The light intensity correlates with fluctuations in the emission current. The onset of light emission occurs at an emission current of 1 mA/cm^2 and corresponds to a temperature on the order of 1550 K. Beyond this critical current irreversible changes occur in the nanotube film. The correlation between light intensity and emission current provides convincing evidence for Joule heating and stable operation for nanotube temperatures up to at least 2000 K and emission current densities on the order of 10 mA/cm^2. © *2002 American Institute of Physics.* [DOI: 10.1063/1.1498493]

Carbon nanotubes have generated considerable interest recently as electron field emitters and have already been used to produce prototype flat panel displays.[1] In spite of the high technological relevance of the field emission application there is still relatively little known about the mechanism. A recent publication[2] has provided evidence from electron kinetic energy measurements for Joule heating of individual multiwalled nanotubes (MWNT) induced by the field emission current. At high temperatures (>1500 K) these authors also noted the onset of light emission. Light emission from nanotubes has been reported previously from either individual tubes[3,4] or from nanotube films.[5] The only previously reported spectral distributions of the emitted light[4,5] did not show any evidence for thermal radiation but reported broad luminescence peaks, interpreted as being due to discrete transitions between electronic states at the emitter tip. We have analyzed the spectral distribution of the radiation from films of aligned multiwalled nanotubes during field emission. In contrast to the earlier work, we detect blackbody radiation from the samples, which correlates strongly with the current density of the emitted electrons. The results are in good agreement with the conclusions of Purcell *et al.*[2] and provide conclusive proof of the Joule heating mechanism leading to light emission in our samples.

Films of aligned MWNT were prepared on a silicon wafer by thermal chemical vapor deposition (CVD) in a one-step process using $Fe(CO)_5$, as described in detail previously.[6,7] Initial field emission measurements along with Raman and transmission electron microscopy (TEM) characterization of the films were reported by Sveningsson *et al.*[7] The measurements were carried out under high vacuum conditions (10^{-7} mbar) by placing a hemispherical anode (radius$=2$ mm) at a distance of 100 μm from the surface of the carbon nanotube film and biasing the nanotube film with a negative voltage. The emission area was estimated to be 10^{-3} cm^2,[8] although there is a fairly large uncertainty in this value due to the difficulty of accurately determining the distance between film and anode. The emitted light was imaged onto a spectrograph slit and analyzed by an optical multichannel analyzer. Care was taken to ensure that the emitted light was coming directly from the nanotube films and not from the anode. The emission characteristics were independent of anode material. The wavelength-dependent sensitivity of the detection system was accounted for by recording the emission of a calibrated tungsten lamp. Wavelength-dependent correction factors were thus obtained with which the recorded light emission spectra were multiplied. The range of sensitivity of the system was 400–900 nm.

The field emisson characteristics of any given film are highly reproducible up to a critical value of the current density at around 1 mA/cm^2. Measurements on different films show that it is the emission current rather than the applied field that is critical—the field at which the critical current is reached varies somewhat from sample to sample. However, as soon as the applied field is increased to induce an emission current density $J>1$ mA/cm^2 the emission characteristics are no longer reversible and higher applied fields are required to produce the same emission current on subsequent cycles. This hysteresis has been noted previously.[7,9] The change in field emission behavior at 1 mA/cm^2 is accompanied by the onset of visible light emission from the nanotube film. Figure 1 shows a Fowler–Nordheim plot for three consecutive voltage scans on the same spot of a typical film of aligned multiwalled nanotubes. The logarithm of the integrated visible light emission intensity (400–900 nm) is shown for comparison. The light intensity closely follows fluctuations in the field emission current as is particularly clearly seen for the first voltage scan. The onset of light emission also occurs at approximately the same value of the applied field at which there is a noticeable change in the slope of the Fowler–Nordheim plot. A straight-line behavior on such a plot is indicative of a metallic emitter where the

[a]Also at: Institute of Thermophysics, 1 Acad. Lavrentyev Ave., Novosibirsk 630090, Russia.
[b]Now at: Carl Zeiss Semiconductor Manufacturing Technologies AG, HL-TB, Carl-Zeiss-Strasse 22, D-73447 Oberkochen, Germany.
[c]Author to whom correspondence should be addressed; electronic mail: eleanor.campbell@fy.chalmers.se

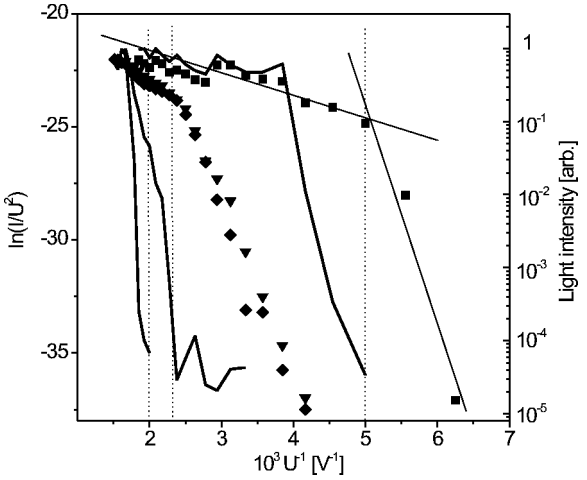

FIG. 1. Fowler–Nordheim plot (left-hand scale) from the same spot on an aligned multiwalled nanotube film for three different voltage scans. Squares: first scan; triangles: second scan; and diamonds: third scan. The integrated light intensity observed on each scan is also plotted (right-hand scale). I is the emission current (A) and U the applied voltage (V). Dashed lines indicate the onset of light emission for each scan.

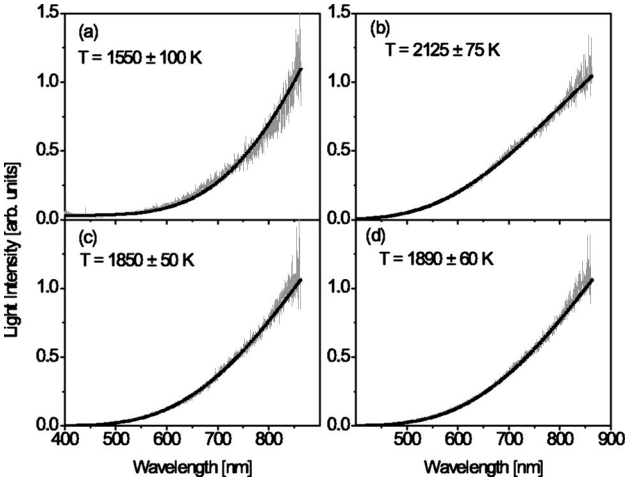

FIG. 2. Light emission spectra measured for four different emission current densities on the first voltage scan. The light intensity has been normalized to 1 at 850 nm. Thick lines are fits to the Planck blackbody formula. The fitted temperatures are given on the plots (a) $J=1$ mA/cm^2, (b) $J=10$ mA/cm^2, (c) 35 mA/cm^2, and (d) 120 mA/cm^2.

slope β is a measure of the field amplification factor at the emitter tip. The change in slope for high applied fields is very typical for carbon nanotube samples, both for films[7,10] and individual tubes,[11] and has been related to degradation of the field emitters and/or the onset of ''nonmetallic'' emission.

Light emission has been observed previously from individual nanotubes[2-4] and nanotube films.[5] The first report interpreted the light emission as due to incandescence but without any proof of heating.[3] More recently, electron energy distributions from individual multiwalled nanotubes have provided evidence for Joule heating,[2] with light being emitted under conditions for which the electron energy distributions imply temperatures of 1500 K and above, however, the spectral distribution of the emitted light was not studied. These conclusions are in contrast to the other studies.[4,5] where a spectral analysis of the emitted light showed broad luminescence peaks, interpreted as emission due to discrete electronic energy levels in the emitter tip. The emission spectra of light from our samples is shown in Fig. 2 for four different field-emission currents on the first voltage scan. The data provide very strong evidence for a thermal mechanism for light emission with no evidence of the luminescence peaks reported by others.[4,5] The spectra closely follow blackbody distributions and the temperatures obtained from the fit of the data to the Planck blackbody formula are given in Fig. 2. Figure 2(a) shows the spectrum obtained at the threshold for visible light emission (1 mA/cm^2), which corresponds to a temperature of 1550 ± 100 K. This is in excellent agreement with the observations of Purcell *et al.* concerning the electron temperature at which light is first observed from individual multiwalled nanotubes in their experiments (1500 K).[2] The temperature then increases as the field-emission current increases to a value of around 2000 K and stays close to this value for emission currents up to and beyond 100 mA/cm^2. The rather unstable field- and light-emission behavior on the first voltage scan is very likely due to desorption of adsorbates combined with thermal annealing and/or thermal destruction of very defect-rich emitters. At high emission currents on the first voltage scan (>100 mA/cm^2), although the fitted temperature remains fairly constant the overall intensity shows strong fluctuations indicating the catastrophic thermal destruction of tubes.[3] This is confirmed by electron microscopy studies and will be the subject of a more detailed publication, presently in preparation. The behavior on subsequent voltage scans is much more stable and reproducible, as long as the emission current is not allowed to increase much beyond 10–100 mA/cm^2. The heating during the first voltage scan not only removes impurities from the tubes but also serves to anneal the tubes and thus improve the stability. Another contribution could be thermally assisted field evaporation from the tube ends followed by nanotube cap reconstruction.[9]

Further evidence for the role of resistive heating can be obtained from considering the relationship between total emitted light intensity and field emission current density. The total integrated intensity of Planck blackbody radiation scales as T^4. In our experimental setup we are only able to detect light in the wavelength range 350–900 nm. For a temperature range of $\sim$1000–2800 K, relevant for the present

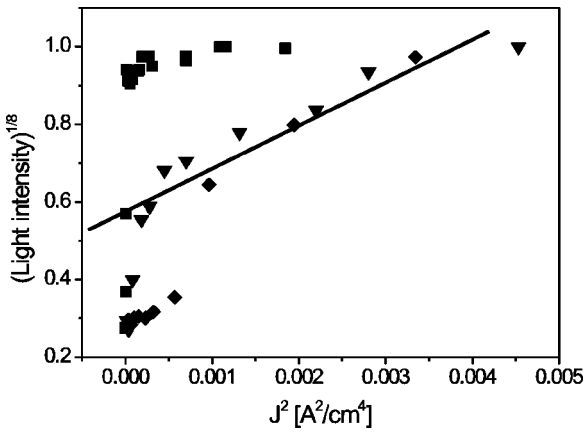

FIG. 3. Light intensity to the power 1/8 vs J^2 for the data of Fig. 1. A straight line plot indicates Joule heating of the nanotubes. Symbols as in Fig. 1.

studies, the detectable blackbody intensity in our experimentally accessible wavelength range actually scales to a good approximation as T^8. Thus, the temperature of our emitters should scale with $I_{\mathrm{Light}}^{1/8}$. On the other hand, the temperature due to Joule heating scales as J^2. If our observed light emission has its origins in Joule heating, then a plot of $I_{\mathrm{Light}}^{1/8}$ vs J^2 should show straight-line behavior. Such a plot is shown in Fig. 3. The first voltage scan does not show the expected correlation, for reasons discussed above. However, the subsequent scans do indeed show linear behavior providing conclusive evidence that the light emission is due to Joule heating and confirming the conclusions drawn by Purcell *et al.*[2] from their electron energy measurements on individual multiwalled nanotubes.

We have provided convincing evidence from blackbody radiation measurements for resistive heating of multiwalled nanotubes during field emission leading to temperatures on the order of 1500–2000 K. The field- and light-emission behavior is rather constant and reproducible over a long period at temperatures around 2000 K and field emission current densities on the order of $10-100\ \mathrm{mA/cm^2}$. Resistively heated nanotubes may, therefore, prove to be an interesting nanoscale light source for nanotechnological applications.

The authors thank R.-E. Morjan for help with sample preparation. Financial support from the Swedish Strategic Research Fund (CARAMEL consortium) and Vetenskapsrådet is gratefully acknowledged.

[1] W. B. Choi, D. S. Chung, J. H. Kang, H. Y. Kim, Y. W. Jin, I. T. Han, Y. H. Lee, J. E. Jung, N. S. Lee, G. S. Park, and J. M. Kim, Appl. Phys. Lett. **75**, 3129 (1999).
[2] S. T. Purcell, P. Vincent, C. Journet, and V. T. Binh, Phys. Rev. Lett. **88**, 105502 (2002).
[3] A. G. Rinzler, J. H. Hafner, P. Nikolaev, L. Lou, S. G. Kim, D. Tomanek, P. Nordlander, D. T. Colbert, and R. E. Smalley, Science **269**, 1550 (1995).
[4] J.-M. Bonard, T. Stöckli, F. Maier, W. A. d. Heer, A. Chatelain, J.-P. Salvetat, and L. Forro, Phys. Rev. Lett. **81**, 1441 (1998).
[5] A. G. Umnov and V. Z. Mordkovich, Appl. Phys. A: Mater. Sci. Process. **A73**, 301 (2001).
[6] O. A. Nerushev, M. Sveningsson, L. K. L. Falk, and F. Rohmund, J. Mater. Chem. **11**, 1122 (2001).
[7] M. Sveningsson, R.-E. Morjan, O. A. Nerushev, Y. Sato, J. Bäckström, E. E. B. Campbell, and F. Rohmund, Appl. Phys. A: Mater. Sci. Process. **A73**, 409 (2001).
[8] W. Zhu, C. Bower, O. Zhou, G. Kochanski, and S. Jin, Appl. Phys. Lett. **75**, 873 (1999).
[9] K. A. Dean, T. P. Burgin, and B. R. Chalamala, Appl. Phys. Lett. **79**, 1873 (2001).
[10] J.-M. Bonard, F. Maier, T. Stöckli, A. Chatelain, W. A. d. Heer, J.-P. Salvetat, and L. Forro, Ultramicroscopy **73**, 7 (1998).
[11] J.-M. Bonard, J.-P. Salvetat, T. Stöckli, L. Forro, and A. Chatelain, Appl. Phys. A: Mater. Sci. Process. **A69**, 245 (1999).

Paper IV

Development and Characterization of Microcoolers using Carbon Nanotubes
Proceedings of the 1st IEEE CPMT Electronics Systemintegration Technology Conference **1**, 881 (2006).

Development and Characterization of Microcoolers using Carbon Nanotubes

Teng Wang[1], Martin Jönsson[2], Elisabeth Nyström[1], Zhimin Mo[1], Eleanor E.B. Campbell[2] and Johan Liu[1,3]
[1]SMIT Center and Department of Microtechnology and Nanoscience, Chalmers University of Technology, SE 412 96 Göteborg, Sweden
[2]Department of Physics, Göteborg University, SE 412 96 Göteborg, Sweden
[3]Key State Lab for New Displays and System Applications and SMIT Center, Shanghai University, Box 282, Yanchang Road 149, Shanghai 200072, P.R. China

Abstract

The continuously increasing integration and packaging density of microelectronic systems requires high-performance cooling technologies, among which the microchannel cooler is considered as a good approach. This work aims to develop a microchannel cooler with vertically aligned carbon nanotubes as the fins. Carbon nanotubes have unusually high thermal conductivity along with the possibility of small-scale formatting and wafer-level integration with chips, thus they provide a promising solution to implement microchannel coolers. By using photolithography, chemical vapor deposition, and adhesive bonding techniques, microcoolers containing carbon nanotube fins of different sizes and spacings are fabricated and then tested. They are also compared to a cooler with common silicon fins, as well as one with no fins. The experimental results reveal good heat removal capability of microcoolers using carbon nanotubes. The measurement result of the CNT cooler is about 10-15% better than the silicon cooler.

Introduction

The challenge of developing high-performance and low-complexity cooling solutions for microelectronic systems is becoming a key factor as the overall power consumption of integrated circuits continuously rises, despite the drop of the supply voltage. There are no signs that this trend will change in the foreseeable future because the integration and packaging density is continuously increasing. Many new cooling techniques have emerged to meet the tougher requirements of microelectronics cooling, among which micro-channel cooler is a very important and promising approach. Many investigations about microchannels have been undertaken in past several decades, showing that extremely high rates of heat transfer can be obtained by applying microchannel structures [1]. One of the earliest implementation by Tuckerman and Pease [2] demonstrated a silicon microchannel cooler which can remove 790 W/cm^2 heat at a substrate-to-coolant temperature difference of 71 ^{o}C. Theoretical computation indicated that microscale narrow channels play a key role for efficient heat removal and gave an optimized width of 57 μm for 365 μm deep channels [2]. The most widely used method to make this microchannel structure is etching into the silicon substrate. This paper aims to develop a new method and material to manufacture microchannel coolers.

Carbon nanotubes (CNTs), a new form of carbon which can be described as rolled layers of graphite with 1-100nm diameter [3], are a very ideal choice to make this kind of microchannel cooler due to many reasons. Firstly, well-structured CNTs are believed to have very high thermal conductivity based on theoretical predictions, although the experimental results vary dramatically in different references [4-6] for both single-walled and multiwalled nanotubes (SWNTs and MWNTs). If the unusually high thermal conductivity of CNTs can be achieved by a suitable synthesis processes, the efficiency of the fins can be maximized, thus the total heat removal capability of the cooler can be promoted. Furthermore, CNTs can be grown directly on the surface of silicon and accurately according to pre-defined small-scale catalyst patterns normally transferred by standard photolithography processes. Therefore microscale channels can be fabricated, making the cooler very compact and efficient. CNTs also provide a possibility of low-cost bulk production with a potential compatibility with standard CMOS technology [7].

In this paper, previous research works on CNT microchannel coolers performed at SMIT Center have been generally reviewed firstly. The fabrication and measurements of some newly-designed CNT micro-channel coolers are introduced afterwards. The performance of these CNT coolers is examined in comparison to traditional silicon coolers of the same dimensions, as well as one with no fins. Some problems met in both manufacturing and characterization processes are discussed and possible improvements are proposed. The barriers of transforming this prototype to a real product are also considered.

1-4244-0553-1/06/$20.00 ©2006 IEEE

Previous Research

Mo et al. [8, 9] successfully fabricated and measured microcoolers made of CNT fins in the form of both one-dimensional and two-dimensional fin arrays (Figure 1), which revealed some promising prospects. The measurements showed that the microcooler with nanotube fins could keep the temperature of a power transistor 6°C lower than the reference cooler while the transistor was generating 23% higher power. It should be noticed that the reference cooler used in the measurement is without any fins. The finite element method (FEM) modeling of this CNT microchannel cooler is done by Ekstrand et al. [10], indicating that the flow velocity near the hot bottom of the cooler was very low due to the gap between the top of the CNT fins and the bottom of the lid in Mo's design (Figure 2). This reduced the heat transfer to the fluid so that the potential of CNTs had not been fully used. The present work brings one step in our research further by making silicon as a reference material.

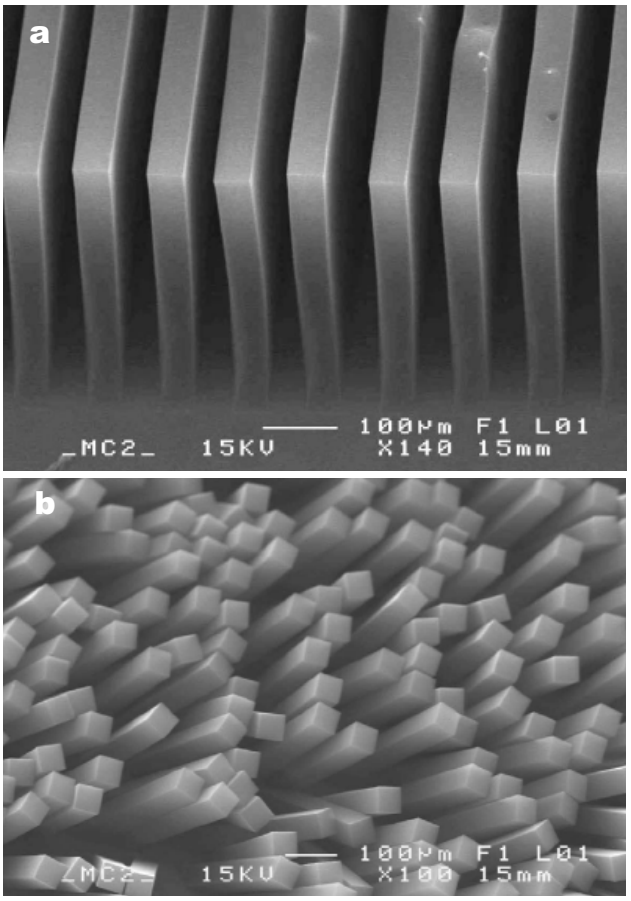

Figure 1: Channel formed (a) and array formed (b) nanotube fins.

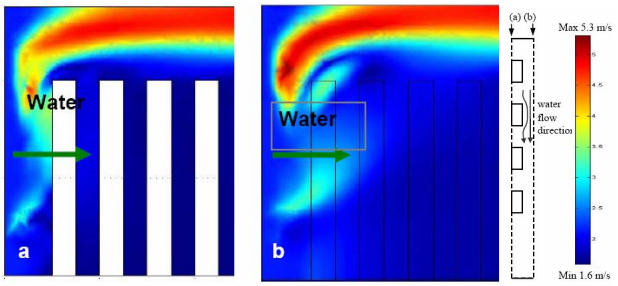

Figure 2: (a) Flow profile in the middle of the fin plane. (b) Flow profile between the fins. The present fin layout keeps the water flow from coming. The simulation is made for the array formed CNT fins.

Manufacturing

The flow chart of the overall manufacturing procedure of CNT microcoolers is illustrated in Figure 3. The catalyst pattern is firstly transferred to the silicon substrate by photolithography and evaporation. A 4-inch mask and 3-inch wafers are used in this project. The mask used in this project contains various patterns with different sizes and pitches. The catalyst used in this application is iron and its thickness is roughly 1 nm. The wafer is diced to small pieces before the growth of the nanotubes. By using thermal chemical vapor deposition (CVD), CNTs are then grown on the catalyst patterns, forming the fins of the microcooler. The sample is inserted into a sealed quartz tube in a high temperature oven. Under a flow of 300 standard cubic centimeters per minute (sccm) H_2 and 500 sccm Ar at atmospheric pressure the oven is heated to 750°C. When the oven has reached the set temperature an additional flow of 15 sccm of C_2H_2 is added as the carbon feedstock. After growth the sample is cooled down in a flow of Ar before being taken out. The silicon substrate carrying CNT fins is then bonded with a lid made of silicon to finish an entire cooler.

Figure 4 shows two SEM images of the CNT fins fabricated for a microchannel cooler. Both the fins and the channels are 25µm wide. All of the fins are approximately 100µm high. Figure 4 (a) provides an overall view of the fins, in which a few defects can be seen. Figure 4 (b) is a detailed picture of the CNT fins. It can be clearly seen that numerous parallel CNTs bunch together to form a fin.

In order to compare the performance of the CNT microcoolers to traditional microcoolers made of silicon, several silicon microcoolers are also fabricated, making the channels by etching into the silicon substrate. The same mask was used to transfer the patterns to wafers by photolithography. The deep ion reactive etching (DIRE) technique is chosen to achieve the high aspect-ratio channels.

Figure 5 shows a cooler with approximately 50µm wide and 300µm high silicon fins. The channels are also 50µm wide. The widths of the fins and channels are slightly uneven because this photo only shows the cross section at the edge of cooler, where the silicon fins are a little over-etched in the manufacturing process. The fins and channels are of the same width in the central part. Some pollution can be seen on the fins as this photo was taken after the measurements.

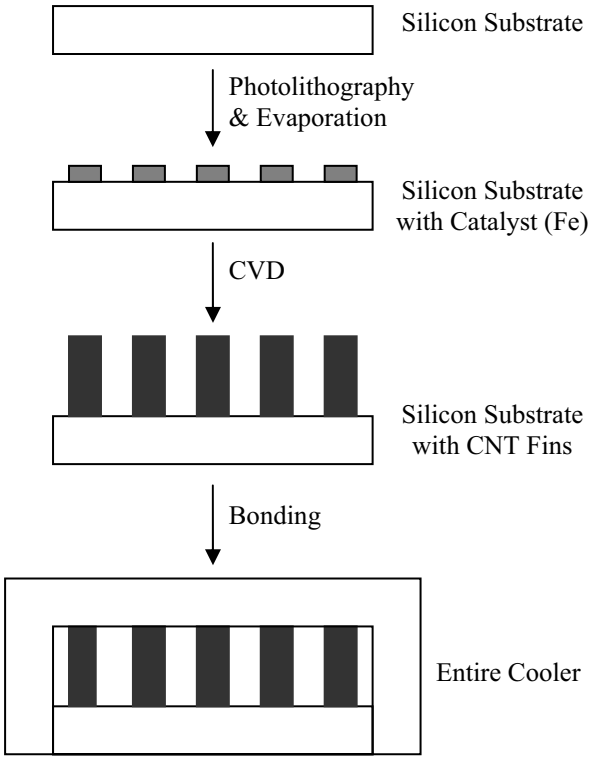

Figure 3: Overall manufacturing procedure of CNT microcooler.

Measurements

The measurement setup is illustrated in Figure 6. A power film resistor which can generate up to 30 watts power acts as the heat source in the experiments. The coolers are mounted on the exposed ceramic heat dissipating surface of the resistor. No heat transfer paste is applied. The coolers are connected to plastic tubes on both ports and water proof tape seals the connections to prevent leakage of water. A micropump which can deliver up to 500 ml/min flow rate provides a continuous, stable and controllable water flow through the channels of the coolers. The temperature of the resistor is obtained by a thermocouple glued on the heat dissipation surface of the transistor.

Based on the current experimental configuration, the power transferred from the heat source to the cooler cannot be measured or calculated precisely because an unknown portion of heat is dissipated by natural air convection. There is also some considerable thermal resistance existing between the resistor and the cooler, making accurate calculation more difficult. However, the experimental conditions for both CNT and silicon coolers are well controlled to be exactly identical. The comparison is thus meaningful and can reveal the advantages and drawbacks of CNT microcoolers.

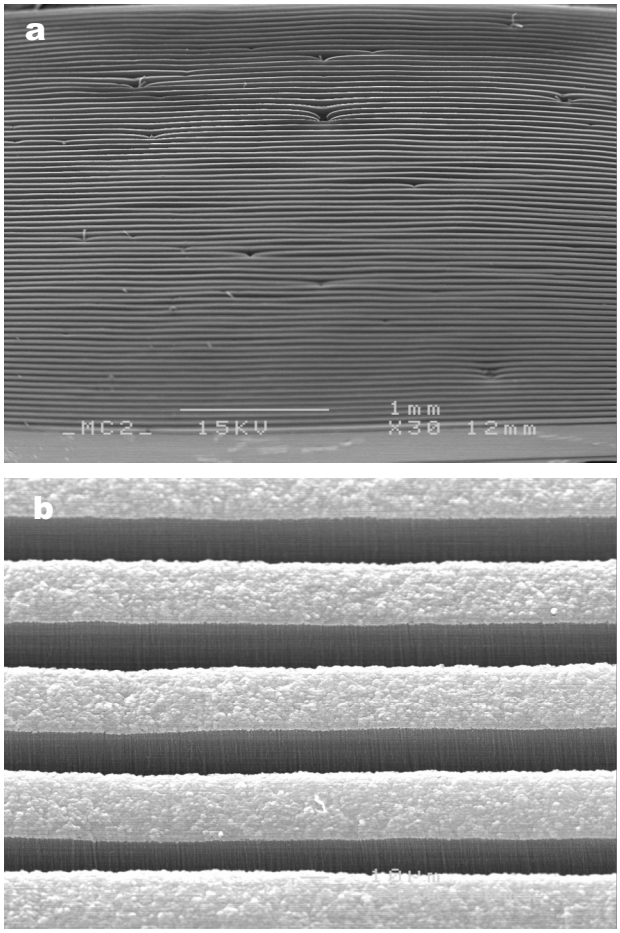

Figure 4: SEM images of 25µm wide CNT fins.

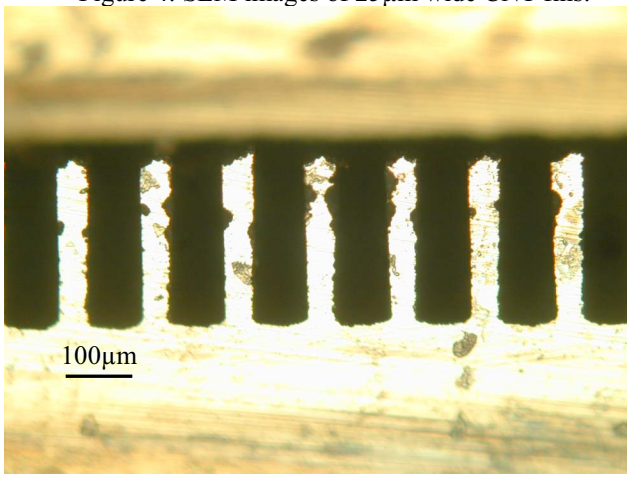

Figure 5: Cross section of a silicon microcooler.

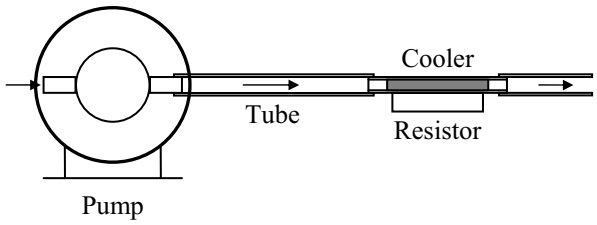

Figure 6: Schematic of measurement setup. The arrows represent the direction of water flow. The grey part of the cooler represents the fins. A thermocouple is placed between the resistor and the cooler to measure the temperature of the heat dissipation surface of the resistor.

Results and Discussions

The measurement results of three different coolers are listed in Table 1. Sample 1 is a CNT cooler with 50µm wide channels and fins. It should be noticed that sample 1 is not the one shown in Figure 4. The height and length of the fins are approximately 100µm and 10mm respectively. The entire cross section of the coolers is 0.3mm high and 4mm wide. Sample 2 is a silicon cooler with similar dimensions. The silicon fins are 50µm wide, 300µm high and 10mm long. The cross section area is the same as in sample 1. Sample 3 is a cooler with the same cross section as sample 1 and 2 but without any fins. All the measurements are taken under the room temperature of 23°C. The surface temperature of the power resistor is 56°C under natural air convection when it generates 1.85 watts power.

Table 1: Performance comparison of microcoolers.

Sample	1	2	3
Description	CNT cooler	Silicon Cooler with fins	Silicon cooler without fins
Power of resistor (W)	2.13	1.95	1.95
Flow rate (ml/min)	35.7	38.5	34.5
Temperature of resistor (°C)	42	42	50

Room temperature = 23°C

As shown in Table 1, the three coolers all show significant heat removal capability, in which sample 1 and 2 provide much better cooling performance than sample 3. This verifies that high heat transfer rate can be obtained by applying the microchannel structure. The measurement result of the CNT cooler is about 10-15% better than the silicon cooler. They both cool the resistor to 42°C while the CNT cooler achieve this temperature with a lower flow rate and higher power dissipation of the resistor. The results reveal the good cooling performance of CNT microcoolers. However, the potential of nanotubes has not been fully used in this case. First, the CNT fins of the measured cooler are much lower than the fins of the silicon cooler. Also, the base plate of the CNT cooler is around 400µm, which is much thicker than that of silicon cooler, which is around 200µm. This difference adds extra heat resistance to the CNT cooler. This difference also represents the two different methodologies of making microcoolers with CNTs and silicon. Nanotubes are grown on the silicon substrate, whereas the microchannels in the silicon cooler are made by etching into silicon. Therefore when there is not enough space at the back side of the silicon chips to make deep microchannels, it is a convenient alternative solution to make the channels by growing CNTs on silicon.

The CNT cooler has been kept running continuously for several hours and the CNT fins were examined using microscopy after the experiment. The fins all withstood the continuous water flow, but more and longer experiments are necessary to determine the reliability of CNT coolers.

Some possible improvements of the CNT microcoolers are proposed as follows. The nanotubes fabricated in this project are not high enough because of the limitations of the devices. Better cooling performance is expected by growing higher CNTs and making closed microchannels. In order to simplify and calibrate the measurements and perform accurate calculations, a power resistor can be integrated into the silicon substrate. It is also worthwhile to search other kinds of patterns and liquids used in the microcoolers.

Conclusions

In the present work, microchannel coolers with both carbon nanotube and silicon fins have been successfully manufactured. The performances of these microcoolers are then measured under the same conditions. The measurements show the better heat removal capability of the CNT cooler in comparison to the cooler with silicon fins and one with no fins.

Acknowledgements

The authors would like to thank Mr. Bengt Nilsson, Dr. Ulf Södervall, Dr. Göran Petersson, and Mr. Johan Andersson from the Nanofabrication Laboratory at Chalmers University of Technology for helping fabricating the mask and the silicon coolers. One of the authors (Johan Liu) is also grateful for the Intel Higher Education Program support to SMIT Center, Shanghai University, China

and to the Shanghai Science and Technology Commission with the Pu Jiang Program.

References

1. Sobhan C. B. and Garimella S. V., "A compatative Analysis of Studies on Heat Transfer and Fluid Flow in Microchannesls", *Microscale Thermophysical Engineering*, vol. 5 (2001), pp. 293-311.
2. Tuckerman D. B. and Pease R. F. W., "High-Performance Heat Sinking for VLSI", *IEEE Electron Device Letters*, vol. EDL-2 (1981), pp.126-129
3. Iijima S., "Helical Microtubules of Graphitic Carbon", *Nature*, Vol. 354 (1991), pp. 56-58.
4. Hone J., "Carbon Nanotubes: Thermal properties", *Dekker Encyclopedia of Nanoscience and nanotechnology*, pp. 603-610.
5. Berber S., Kwon Y. K., and Tomanek D., "Unusually High Thermal Conductivity of Carbon Nanotubes", *Physical Review Letters*, vol. 84 (2000), pp. 4613-4616.
6. Xie S., Li, W., Pan Z., Chang B. Sun L., "Mechanical and Physical Properties on Carbon Nanotube", *Journal of Physics and Chemistry of Solids*, vo. 61 (2000), pp. 1153-1158.
7. Kabir M. S., Morjan R. E.,Nerushev O. A., Lundgren P., Bengtsson S., Enokson P., Campbell E. E. B., "Plasma-enhanced chemical Vapour Deposition Growth of Carbon nanotubes on Different Metal underlayers", *Nanotechnology*, 16 (2005), pp. 458-466.
8. Mo Z., Anderson J., and Liu J., "Integrating Carbon Nanotubes with Microchannel cooler", *Proc. HDP'04*, Shanghai, China, June-July 2004, pp. 373-376.
9. Mo Z., Morjan R., Anderson J., Campbell E. E. B., and Liu J., "Integrated Nanotube Microcooler for Microelectronics Applications", *Porc. 55th Electronic Componenets and Technology conference*, Florida, USA, May-June 2005, pp. 51-54.
10. Ekstrand L., Mo Z., Zhang Yan., and Liu J., "Modelling of Carbon Nanotubes as Heat Sink Fins in Microelectronics Cooling", *Proc. IEEE CPMT Polytronic 05 Conference*, Wroclav, Poland, October 2005, pp. 185-187.